AFRL-AFOSR-UK-TR-2012-0034

Crack propagation in compressor rotor blade

Professor Romuald Rzadkowski

The Szewalski Institute of Fluid-Flow Machinery
Fiszera 14
Gdansk, Poland 80-952

EOARD Grant 10-3062

Report Date: August 2012

Final Report from 29 April 2010 to 28 April 2012

Air Force Research Laboratory
Air Force Office of Scientific Research
European Office of Aerospace Research and Development
Unit 4515 Box 14, APO AE 09421

REPORT DOCUMENTATION PAGE

Form Approved OMB No. 0704-0188

1. REPORT DATE *(DD-MM-YYYY)*	2. REPORT TYPE	3. DATES COVERED *(From – To)*
22 August 2012	Final Report	29 April 2010 – 28 April 2012

4. TITLE AND SUBTITLE

Crack propagation in compressor rotor blade

5a. CONTRACT NUMBER

FA8655-10-1-3062

5b. GRANT NUMBER

Grant 10-3062

5c. PROGRAM ELEMENT NUMBER

61102F

6. AUTHOR(S)

Professor Romuald Rzadkowski

5d. PROJECT NUMBER

5d. TASK NUMBER

5e. WORK UNIT NUMBER

7. PERFORMING ORGANIZATION NAME(S) AND ADDRESS(ES)

The Szewalski Institute of Fluid-Flow Machinery
Fiszera 14
Gdansk, Poland 80-952

8. PERFORMING ORGANIZATION REPORT NUMBER

N/A

9. SPONSORING/MONITORING AGENCY NAME(S) AND ADDRESS(ES)

EOARD
Unit 4515 BOX 14
APO AE 09421

10. SPONSOR/MONITOR'S ACRONYM(S)

AFRL/AFOSR/RSW (EOARD)

11. SPONSOR/MONITOR'S REPORT NUMBER(S)

AFRL-AFOSR-UK-TR-2012-0034

12. DISTRIBUTION/AVAILABILITY STATEMENT

Approved for public release; distribution is unlimited. (approval given by local Public Affairs Office)

13. SUPPLEMENTARY NOTES

14. ABSTRACT

Turbomachine blading crack propagation and initiations are one of the most important problems. Design, operation and modernization of the contemporary turbomachines are impossible without a detailed numerical and experimental analysis of vibrations on their most important structural elements, i.e. the blades. In addition to determining vibration characteristics, it is often necessary to find the distribution of vibration stresses and their localization.

This report is comprised of 4 progress reports for each 6 month period of this effort.

15. SUBJECT TERMS

EOARD, Damage Tolerance, Non-Destructive Evaluation, Turbomachinery

16. SECURITY CLASSIFICATION OF:			17. LIMITATION OF ABSTRACT	18, NUMBER OF PAGES	19a. NAME OF RESPONSIBLE PERSON
a. REPORT	b. ABSTRACT	c. THIS PAGE			Gregg Abate
UNCLAS	UNCLAS	UNCLAS	SAR	100	19b. TELEPHONE NUMBER *(Include area code)* +44 (0)1895 616021

Final Report

Crack Propagation in Compressor Rotor Blade

R. Rzadkowski

The Szewalski Institute of Fluid Flow Machinery, Gdansk, Poland

Grant: FA8655-10-1-3062

April 2010 – June 2012

This final report is a compilation of progress reports over the life of the grant. Those reports and their page numbers in this report are:

Crack Propagation in Compressor Rotor Blade

(Grant FA8655-10-1-3062)

Report for First Six Months

April-September 2010

R. Rzadkowski[1] J.S. Rao[2], Yu.S. Vorobiev[3]

[1]The Szewalski Institute of Fluid Flow Machinery, Gdansk, Poland

[2]Altair Engineering India Pvt Ltd, Bangalore

[3]National Ukrainian Academy of Sciences, Ukraine

Submitted to
European Office of Aerospace:
Research and Development
86 Blenheim Crescent
Ruislip, Middlesex HA4 7HB
United Kingdom

October 20, 2010

Table of Contents

Summary

In this report modal stress analysis was carried out on one compressor rotor blade of an SO-3 engine to locate the possible crack initiations. Various crack depths and lengths were created using a three-dimensional finite element model with the 3D prismatic quarter-point isoparametric elements and 20-node isoparametric elements to calculate the natural frequencies and mode shapes of the rotor blades.

1. Introduction

The initiation and propagation of cracks in turbo machine blades is a very serious problem. Military aircraft are subjected to the most extreme manoeuvres. On account of heavy transient loads, the engine, and particularly the blades are subjected to severe fatigue. These sudden, transient loads lead to high alternating stresses and thus initiate cracks. Once initiated, the cracks propagate to ultimately produce an unstable fracture.

Failures of cracked turbine blades were extensively studied in India, particularly for the Narora nuclear machine, see Rao (1995). This type of analysis has helped teams in India and Poland to develop life estimation technologies, see Rao (2009) and Rao et al., (2010).

In this project we examine crack propagation using new 3D solid crack elements. The two year plan of work is given in Annexure 1.

In this report the natural frequencies and mode shapes of a cantilever blade with a crack and without one were calculated and compared using an in-house code and the ABQUS code with 20-node (HEX20) elements and singularity elements.

For the numerical vibration analysis of cracked turbo machine blades, a three-dimensional finite element model with the 3D prismatic, quarter-point Isoparametric elements, Barsom (1997), was applied. These elements could be used for small scale yielding. Also analyzed was the influence of various crack depths and locations on the natural frequencies and mode shapes of an SO-3 engine first stage compressor blade. A comparison was made using either 20-node Isoparametric elements throughout the mesh or with 3D prismatic quarter-point Isoparametric elements just in the crack area.

2. Methods, Assumption and Procedures

The FE mesh in the crack region comprised either 3D Isoparametric 20-node elements or 3D Prismatic quarter-point Isoparametric $O(r^{-1/2})$ singularity elements, Barsom (1977), for stress and strain and $O(r^{1/2})$ for displacement where r is radius from crack front.

The 20-node Isoparametric element is defined upto the second order polynomial. So the displacement inside the element is a quadratic function. Deformations and stresses in the element are linear functions. The singularity element was obtained from a 20-node isoparametric element as follows: displacements towards the crack front change according to $\sqrt{r}$, see equation (3), where r is radius from the crack front, while deformations and stresses change according to $1/\sqrt{r}$ Barsom (1977). For this reason singularity elements describe stress and strain in the vicinity of a crack in a better way.

Figure 1 presents the transformation of 3D Isoparametric finite element into a Singular quarter-point element, Vorobiev et al., (2004) and Barsom (1977).

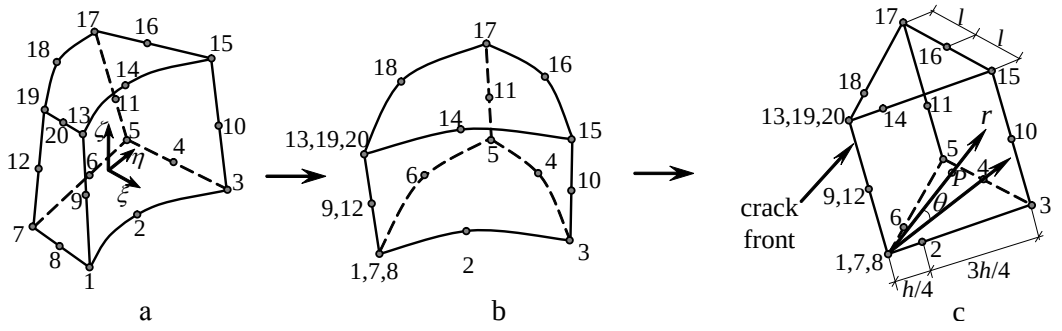

FIGURE 1 Transformation of isoparametric finite element into singular quarter-point element

The prismatic quadratic isoparametric elements are formed by collapsing one side and placing the mid-side node near the crack tip at the quarter point. The geometry of the 3D Prism element was mapped into normalized space through the following transformations:

$$x = \sum_i{}' N_i(\xi,\eta,\zeta)x_i\,,\ y = \sum_i{}' N_i(\xi,\eta,\zeta)y_i\,,\ z = \sum_i{}' N_i(\xi,\eta,\zeta)z_i\,,$$

$$N_i(\xi,\eta,\zeta) = \left[(1+\xi\xi_i)(1+\eta\eta_i)(1+\zeta\zeta_i)(\xi\xi_i+\eta\eta_i+\zeta\zeta_i-2)\right]\Big/8,\ i=1,3,5,7,13,15,17,19,$$

$$N_i(\xi,\eta,\zeta) = \left[(1-\xi^2)(1+\eta\eta_i)(1+\zeta\zeta_i)\right]\Big/4,\ i=2,6,14,18,$$

$$N_i(\xi,\eta,\zeta) = \left[(1-\eta^2)(1+\xi\xi_i)(1+\zeta\zeta_i)\right]\Big/4,\ i=4,8,16,20,$$

$$N_i(\xi,\eta,\zeta) = \left[(1-\zeta^2)(1+\xi\xi_i)(1+\eta\eta_i)\right]\Big/4,\ i=9,10,11,12, \qquad (1)$$

where $N_i(\xi,\eta,\zeta)$ are shape functions, ξ_i,η_i,ζ_i are local coordinates and x_i,y_i,z_i are global coordinates. For the element presented in Figure 1, the nodal coordinates were

$$x_1 = x_7 = x_8 = x_9 = x_{12} = x_{13} = x_{19} = x_{20} = 0,\ x_2 = x_6 = x_{14} = x_{18} = \frac{h}{4},$$

$$x_3 = x_4 = x_5 = x_{10} = x_{11} = x_{15} = x_{16} = x_{17} = h,$$

$$y_1 = y_4 = y_7 = y_8 = y_9 = y_{12} = y_{13} = y_{16} = y_{19} = y_{20} = 0,$$

$$y_2 = -y_6 = y_{14} = -y_{18} = -\frac{l}{4},\ y_3 = -y_5 = y_{10} = y_{11} = y_{15} = -y_{17} = -l,$$

$$z_1 = z_2 = \ldots = z_8 = 0,\ z_9 = z_{10} = z_{10} = z_{12} = b,\ z_{13} = z_{14} = \ldots = z_{20} = 2b. \qquad (2)$$

Substituting (2) in (1), we get

$$x = \frac{h}{8}\left\{\begin{matrix}(1-\xi^2)(1-\zeta)+(1-\xi^2)(1+\zeta)+(1+\xi)(1-\zeta)\left[\begin{matrix}(1-\eta)(\xi-\eta-\zeta-2)+\\(1+\eta)(\xi+\eta-\zeta-2)\end{matrix}\right]+\\(1+\xi)(1+\zeta)\left[\begin{matrix}(1-\eta)(\xi-\eta+\zeta-2)+\\(1+\eta)(\xi+\eta+\zeta-2)\end{matrix}\right]\end{matrix}\right\}+$$

$$+\frac{h}{4}(1+\xi)\left\{(1-\eta^2)(1-\zeta)+(1-\eta^2)(1+\zeta)+(1-\zeta^2)(1-\eta)+(1-\zeta^2)(1+\eta)\right\}$$

$$y = \frac{l}{8}\left\{\eta(1-\xi^2)(1-\zeta)+\eta(1-\xi^2)(1+\zeta)+(1+\xi)(1-\zeta)\left[\begin{matrix}(1+\eta)(\xi+\eta-\zeta-2)-\\(1-\eta)(\xi-\eta-\zeta-2)\end{matrix}\right]\right\}+$$

$$+\frac{l}{4}\left\{(1+\xi)(1+\eta)(1-\zeta^2)-(1+\xi)(1-\eta)(1-\zeta^2)\right\}$$

$$z=\frac{b}{2}\left\{\begin{array}{l}(1-\eta)(1-\zeta^2)+(1+\eta)(1-\zeta^2)+(1-\eta)(1-\zeta)(\xi^2-\eta+\zeta-2)+\\(1+\eta)(1+\zeta)(\xi^2+\eta+\zeta-2)\end{array}\right\}+$$
$$b\{(1-\xi^2)(1+\zeta)+(1-\eta^2)(1+\zeta)\}$$

From the above we get

$$x=\frac{h}{4}(1+\xi)^2,\ y=\frac{l}{4}\eta(1+\xi)^2,\ z=b(1+\zeta)$$

$$r=\sqrt{(x^2+y^2)}=\frac{l}{4}(1+\xi)^2\sqrt{\left(\frac{h}{l}\right)^2+\eta^2} \tag{3}$$

where

$$(1+\xi)=\frac{r^{1/2}}{\left[\frac{l}{4}\left(\left(\frac{h}{l}\right)^2+\eta^2\right)^{1/2}\right]^{1/2}}$$

Therefore, the singularity, quarter-point element ensured $O(r^{-1/2})$ singularity for stress and strain and $O(r^{1/2})$ for displacement. By using 3D finite-element models, an in-depth analysis of the vibration strength of a damaged blade can be carried out. Equation (3) implies a Jacobian matrix in the form

$$|J|=\begin{vmatrix}\frac{\partial x}{\partial\xi} & \frac{\partial y}{\partial\xi} & \frac{\partial z}{\partial\xi}\\ \frac{\partial x}{\partial\eta} & \frac{\partial y}{\partial\eta} & \frac{\partial z}{\partial\eta}\\ \frac{\partial x}{\partial\zeta} & \frac{\partial y}{\partial\zeta} & \frac{\partial z}{\partial\zeta}\end{vmatrix}=\begin{vmatrix}\frac{h}{2}(1+\xi) & \frac{l}{2}\eta(1+\xi) & 0\\ 0 & \frac{l}{4}(1+\xi)^2 & 0\\ 0 & 0 & b\end{vmatrix}$$

and its determinant

.
$$\det|J|=\frac{hlb}{8}(1+\xi)^3 \tag{4}$$

Displacements within the element were interpolated by

$$u=\sum_i N_i(\xi,\eta,\zeta)u_i\ ,\ v=\sum_i N_i(\xi,\eta,\zeta)v_i\ ,\ w=\sum_i N_i(\xi,\eta,\zeta)w_i$$

Thus the derivatives of *u, v, w* with respect to $\xi,\ \eta,\ \zeta$ are

$$\frac{\partial u}{\partial\xi}=\sum_i\frac{\partial N_i}{\partial\xi}u_i\ ,\ \frac{\partial u}{\partial\eta}=\sum_i\frac{\partial N_i}{\partial\eta}u_i\ ,\ \frac{\partial u}{\partial\zeta}=\sum_i\frac{\partial N_i}{\partial\zeta}u_i\ ,$$
$$\frac{\partial v}{\partial\xi}=\sum_i\frac{\partial N_i}{\partial\xi}v_i\ ,\ \frac{\partial v}{\partial\eta}=\sum_i\frac{\partial N_i}{\partial\eta}v_i\ ,\ \frac{\partial v}{\partial\zeta}=\sum_i\frac{\partial N_i}{\partial\zeta}v_i\ ,$$
$$\frac{\partial w}{\partial\xi}=\sum_i\frac{\partial N_i}{\partial\xi}w_i\ ,\ \frac{\partial w}{\partial\eta}=\sum_i\frac{\partial N_i}{\partial\eta}w_i\ ,\ \frac{\partial w}{\partial\zeta}=\sum_i\frac{\partial N_i}{\partial\zeta}w_i\ .$$

The potential energy in the vibrations of the blade or bladed disc is

$$\Pi = \frac{1}{2}\iiint_V \sigma_{ij}\varepsilon_{ij} dV$$

Taking into account (4), we have

$$dV = \det|J| d\xi d\eta d\zeta = \frac{hlb}{8}(1+\xi)^3 d\xi d\eta d\zeta$$

The potential energy represents features appropriate to the stresses in the crack tip, but is limited to *r* values. The finite element is derived following well known procedures using Energy methods.

3. Results and Discussions

The natural frequencies, mode shapes and modal stresses of the first stage SO-3 aircraft engine rotating compressor blade are calculated. The length of the blade is 0.106 m and is made of 18H2N2 steel with an Ultimate Tensile Strength of 800 MPa and Young's Modulus of 2.04 MPa. The rotor blade is modelled using 20-node, isoparametric, HEX20 elements, (Rao 1991). An FE mesh of a shell blade with root was prepared (Fig. 3a).

TABLE 1 Natural frequencies (Hz) of the cantilever blade at different speeds (rpm)

	0 rpm	6800 rpm	14500 rpm	15600 rpm
Mode 1	341.86	396.99	547.62	572.85
Mode 2	1342.0	1389.9	1541.5	1568.9
Mode 3	1847.5	1860.6	1909.1	1919.4
Mode 4	3114.7	3138.1	3213.8	3227.9
Mode 5	3917.7	3962.2	4119.8	4151.2

The natural frequencies of the blade at different speeds from Abaqus are given in Table 1. Campbell diagram of the rotor blade is presented in Figure 2. This shows that 2EO (2×) could cause a high level of vibration at a speed of 15000 rpm.

A free vibration analysis of the blade, [see Rao (1965), Rao and Rieger (1981), Rao (1992), Janecki and Krawczuk (1998)], is carried out to predict the positions of the crack initiation for particular mode shapes, Rzadkowski (1998). Figure 3b presents the modal stresses in the first two mode shapes. They show that maximum modal stresses occur near the root area of the suction side of the blade in the first and second mode and also on the leading edge on the pressure side of the first mode, though not the second.

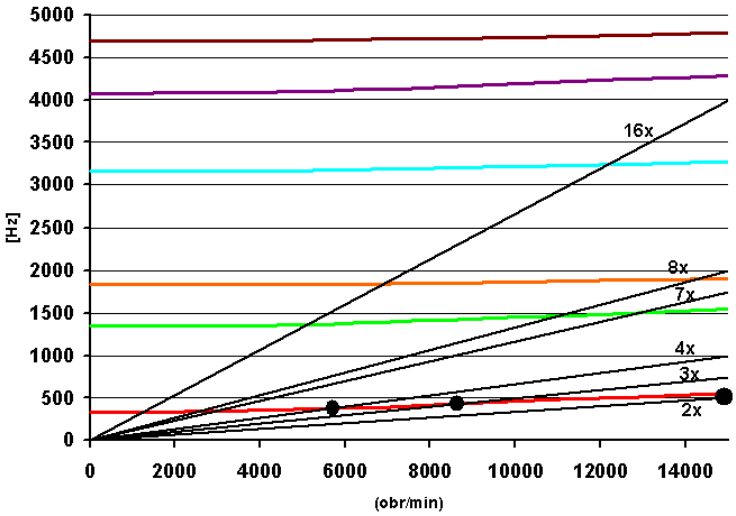

FIGURE 2 Campbell diagram of first stage of SO-3 engine rotor blade

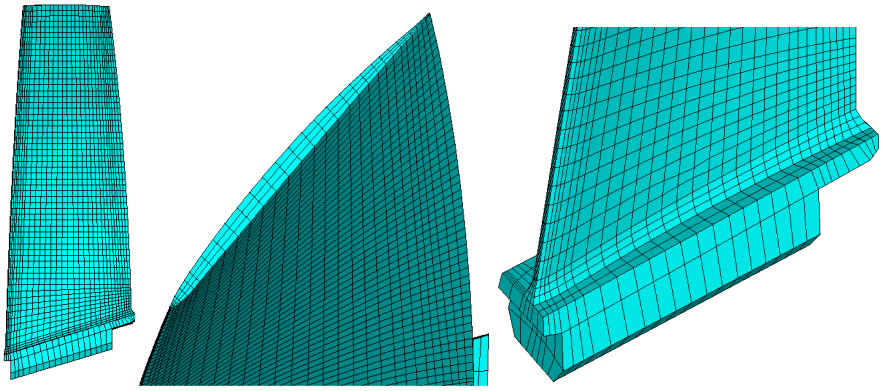

FIGURE 3a FE mesh of rotor blade

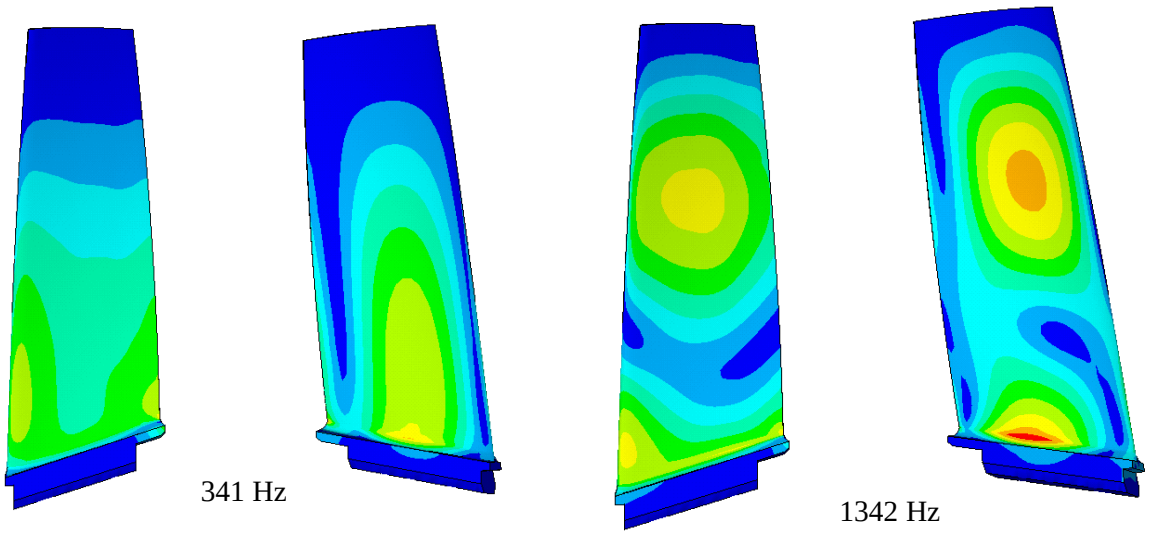

FIGURE 3b Modal stresses at 341 Hz and 1342 Hz (pressure side and suction side)

The natural frequencies of the rotor blades are calculated for various crack lengths L (1.9 to 21.9 mm) and crack areas S, see Figure 4. Table 2 presents the natural blade frequencies for crack lengths L with the blade chord measuring 50 mm. These crack values were equivalent to the crack area on the blade cross-section S, see Figure 4, where S_o was the blade cross-section without the crack.

FIGURE 4 Induced crack areas on the blade cross-section where Peak Stress Occurs

TABLE 2 Natural blade frequency changes for different crack lengths L and areas S/S_o.

L (mm)	1.9	3.8	5.7	7.6	11.4	14.9	18.4	21.9
S/S_0	0.007	0.014	0.042	0.062	0.133	0.192	0.297	0.368
f1	341.86	341.66	340.86	340.37	338.12	332.24	327.11	315.19
f2	1342	1341.1	1337.6	1335.5	1325.9	1302	1282.7	1241.9
f3	1847.5	1847.5	1847.5	1847.4	1846.9	1845.5	1843	1838.6
f4	3114.7	3113.8	3111.6	3110.3	3104.2	3087.7	3073.2	3041.9
f5	3917.7	3918.2	3914	3911.6	3900.2	3873.9	3850.4	3807.1
f6	4623.3	4623.3	4623.1	4623	4621.9	4619	4614.1	4605.5
f7	6862.4	6861.8	6852.8	6847.7	6824.1	6769.3	6725.6	6643.7
f8	7482.9	7483.2	7482.3	7481.7	7478.4	7470.5	7458.9	7439.6
f9	10049	10048	10044	10042	10032	10008	9987.5	9946.7
f10	10357	10357	10357	10357	10032	10008	9987.5	9946.7

Figure 5 gives the % [illegible] As a typical case, figure 6 shows the stress

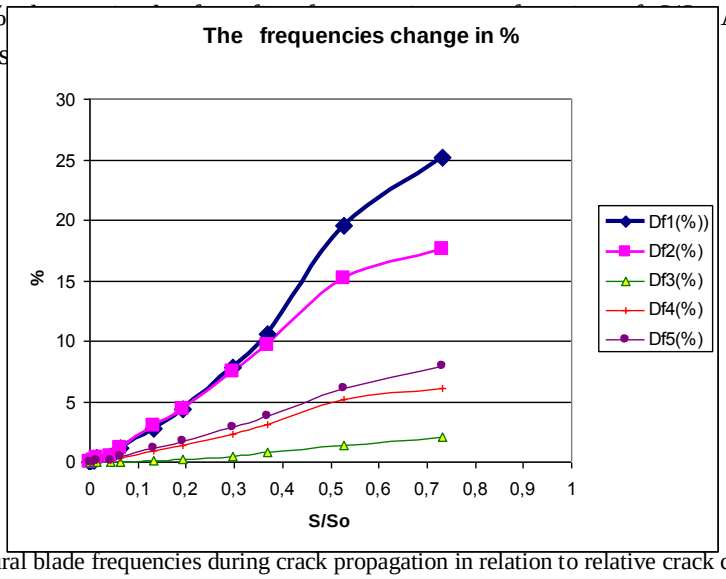

FIGURE 5 Relative change of natural blade frequencies during crack propagation in relation to relative crack cross-sections

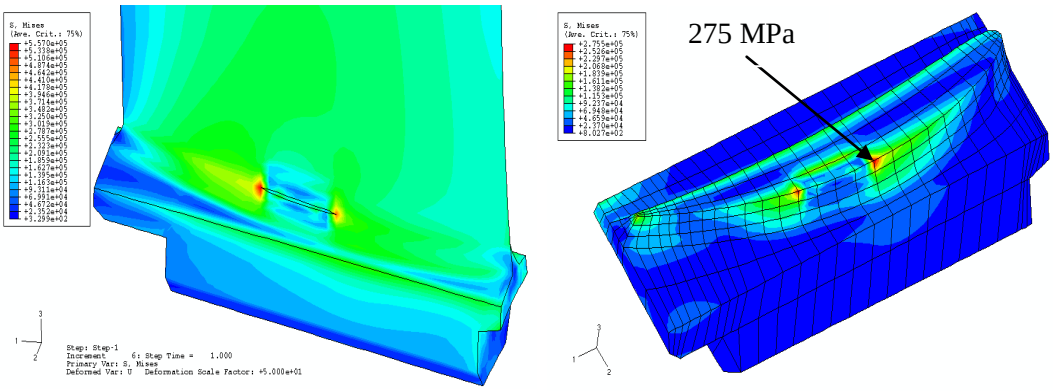

FIGURE 6 Centrifugal stresses in the blade with a 7.6 mm crack at 15000 rpm

There were only very minor changes in natural frequencies when a small crack extended slightly, see Table 3. For example, a blade with a crack of 1.9 mm (S/S_o= 0,007) had virtually the same natural frequencies as a blade without a crack. With a crack of 3.8 mm (S/S_o= 0.014) the first natural frequency changed by 0.2 Hz and the second by 0.9 Hz. With a crack of 5.7 mm (S/S_o= 0.04) the first frequency changed by 1 Hz and the second by 4.4 Hz. The frequency changes were higher when the S/S_o was greater than 0.1 (see Figure 5). Figure 6 presents the stress distribution of the rotor blade with a 7.6 mm crack. Maximum stress concentration is seen on the edges of the crack.

An in-house code was developed at the Ukrainian Academy of Sciences to calculate the natural frequencies and modes of rotor blades using 3D 20-node isoparametric elements and 3D, prismatic, quarter-point, isoparametric elements. Tables 3, 4 and 5 compare the natural frequencies of the S0-3 engine I stage compressor blade using the in-house code and ABAQUS code with 20-node isoparametric elements. The results are similar. Figures 7-12 present the mode shapes of a blade without a crack as calculated by the in-house code. Figures 13-18 present the in-house code calculation results for the mode shapes of a blade with a 11.4 mm crack. The mode shapes were the same as those calculated in ABAQUS.

Table 6 presents the natural frequencies of a I stage compressor blade with a 11.4 mm crack as calculated by the in-house code using singularity elements in the crack area and the ABAQUS code with 20-node, isoparametric elements. The natural frequencies obtained by the 3D prismatic quarter-point isoparametric element model are slightly lower. The main difference is in the modal stress results of the crack area.

TABLE 3 Natural frequencies (Hz) of the cantilever blade L = 0.106 m for 0 rpm without crack

FE Element	f1	f2	f3	f4	f5	f6	f7	f8
in-house code	340.71	1337.9	1846.2	3060	3874	4616,7	6844	7478
ABAQUS	337.86	1338.1	1835.5	3170.7	4074.7			

TABLE 4 Natural frequencies (Hz) of the cantilever blade L = 0.106 m for 15600 rpm without crack

FE Element	f1	f2	f3	f4	f5	f6	f7	f8
in-house code	571.87	1564.6	1917.8	3165.9	4115.6	4722.4	7112.7	7652
ABAQUS	572.85	1568.9	1919.4	3227.9	4151.2			

TABLE 5 Natural frequencies (Hz) of L = 0.106 m cantilever blade for 0 rpm with 11.4mm crack

.

FE Element	f1	f2	f3	f4	f5	f6	f7	f8
HEX 20-in-house code	330.52	1300.2	1841.3	2983.3	3759.0	4599.1	6728.9	7466
ABAQUS	338.12	1325.9	1846.9	3104.2	3900	4621.9	6824	7478

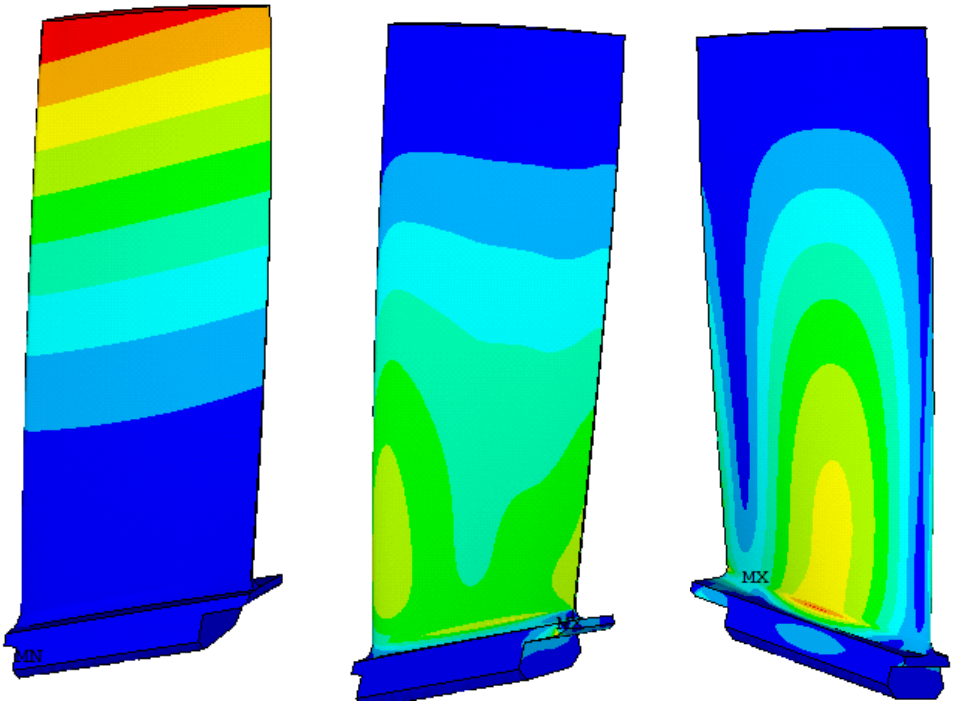

FIGURE 7 Modal displacement and stress at 340.7 Hz (pressure side and suction side)

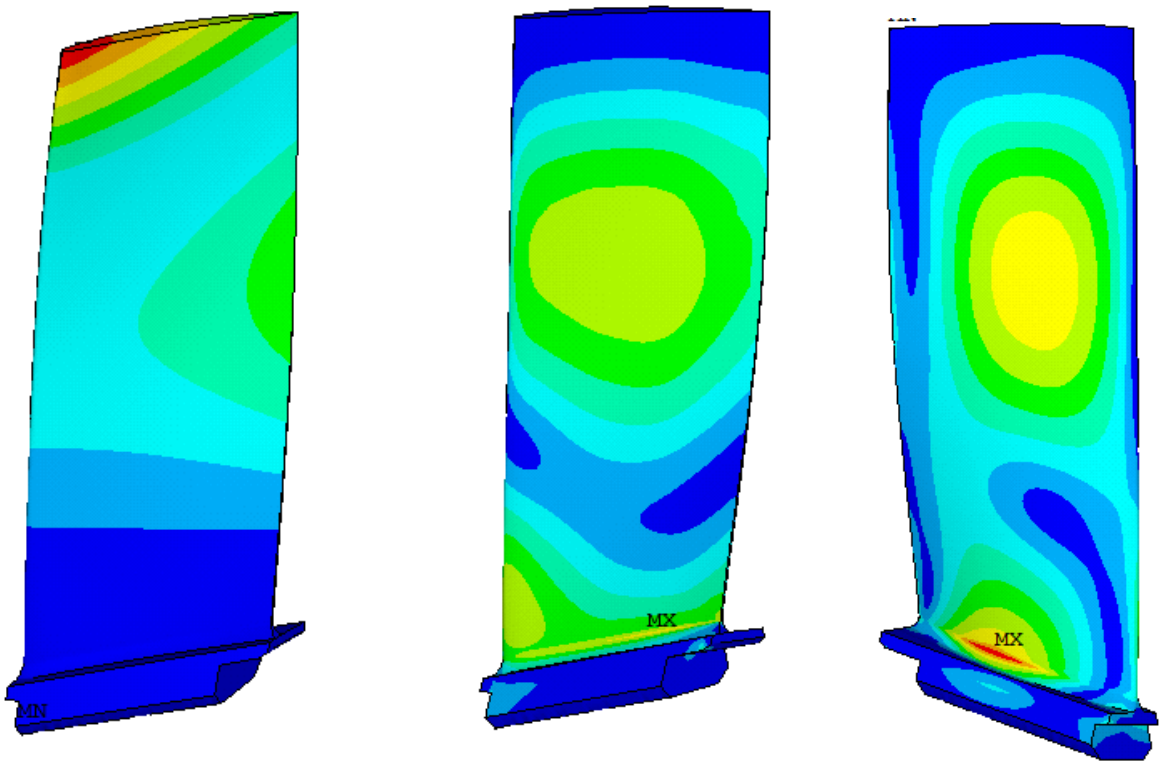

FIGURE 8 Modal displacement and stress at 1338 Hz (pressure side and suction side)

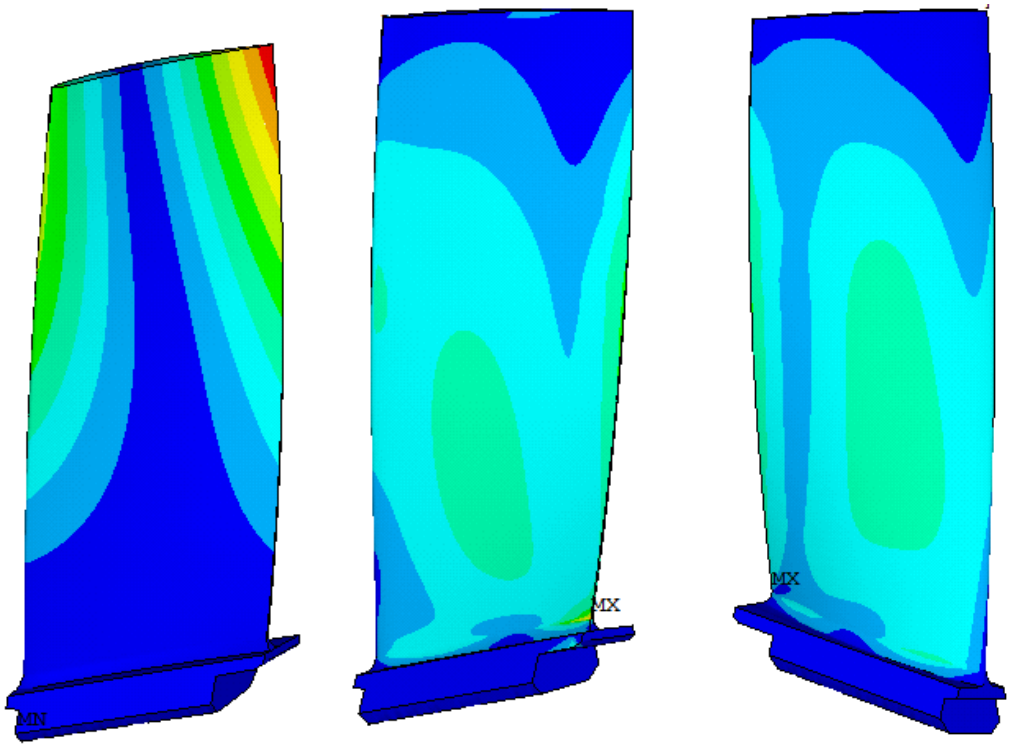

FIGURE 9 Modal displacement and stress at 1846 Hz (pressure side and suction side)

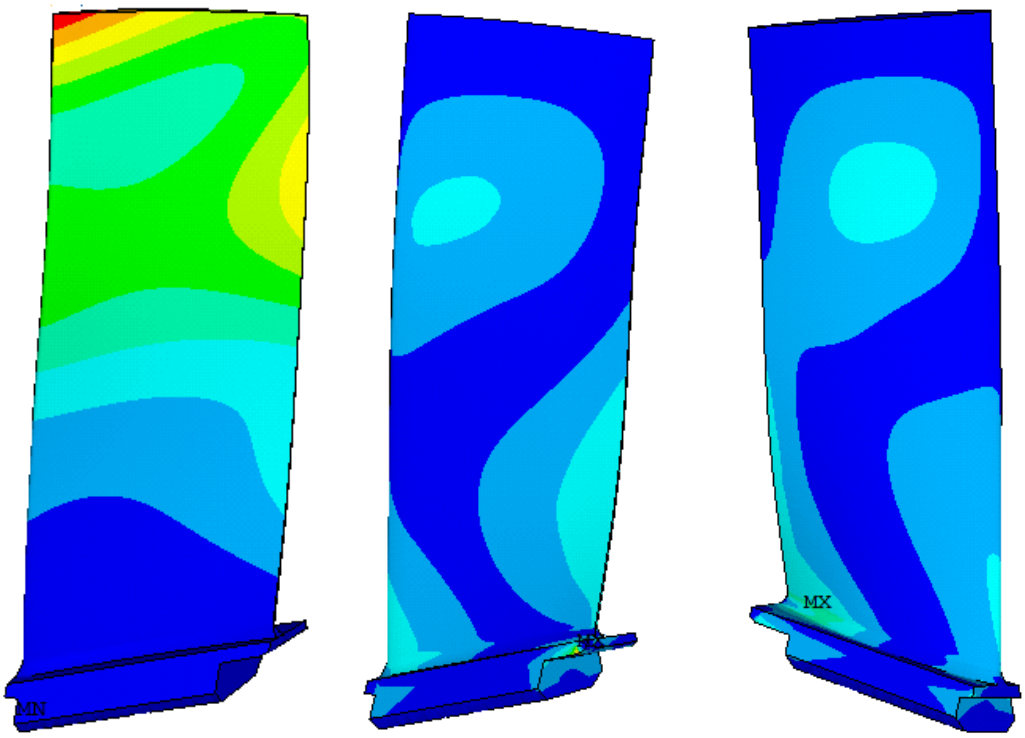

FIGURE 10 Modal displacement and stress at 3060 Hz (pressure side and suction side)

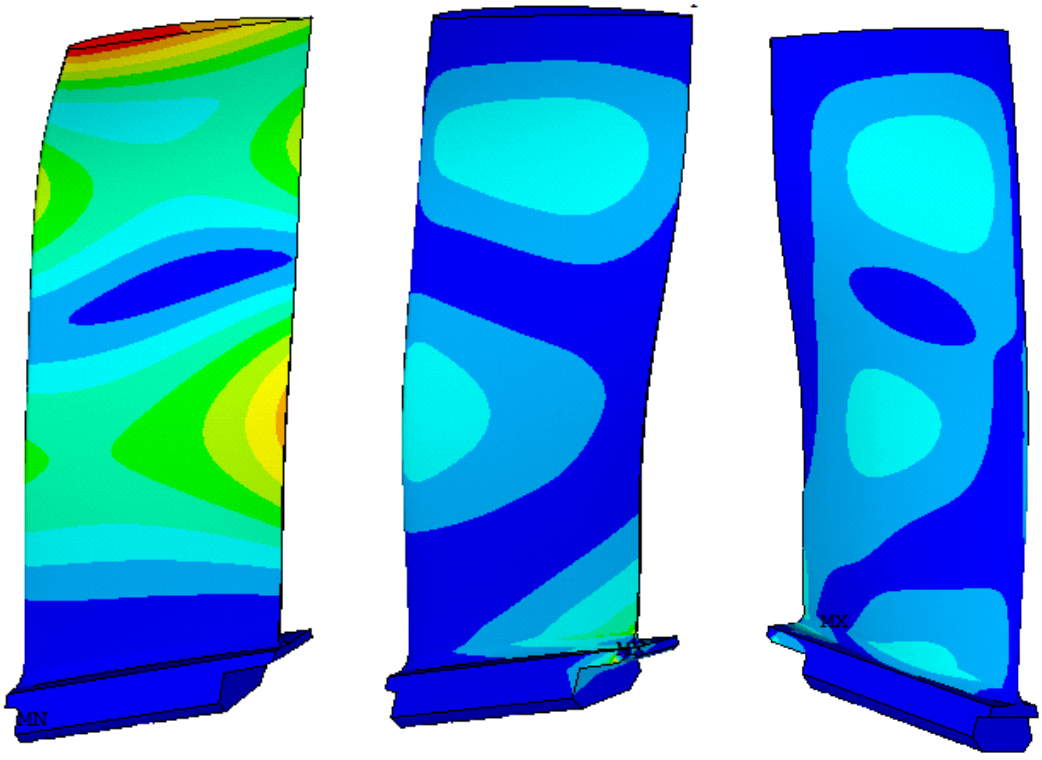

FIGURE 11 Modal displacement and stress at 3874 Hz (pressure side and suction side)

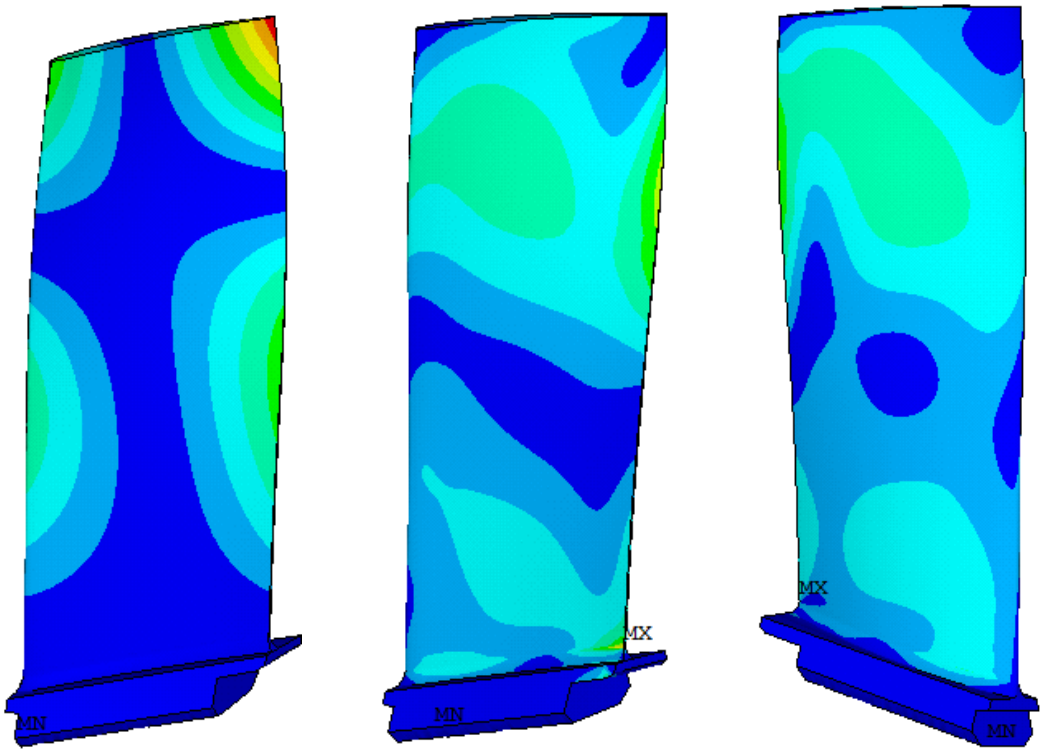

FIGURE 12 Modal displacement and stress at 4617 Hz (pressure side and suction side)

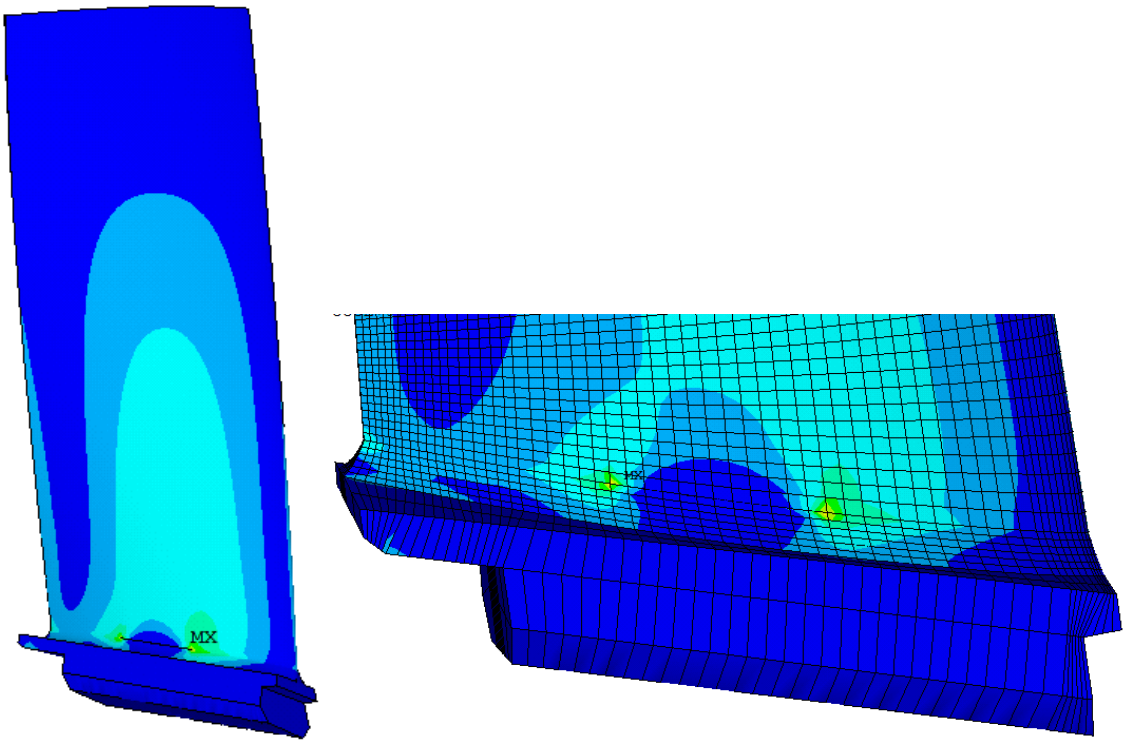

FIGURE 13 Modal stress at 330.52 Hz of compressor blade with 11.4 mm crack, 20-node isoparametric elements

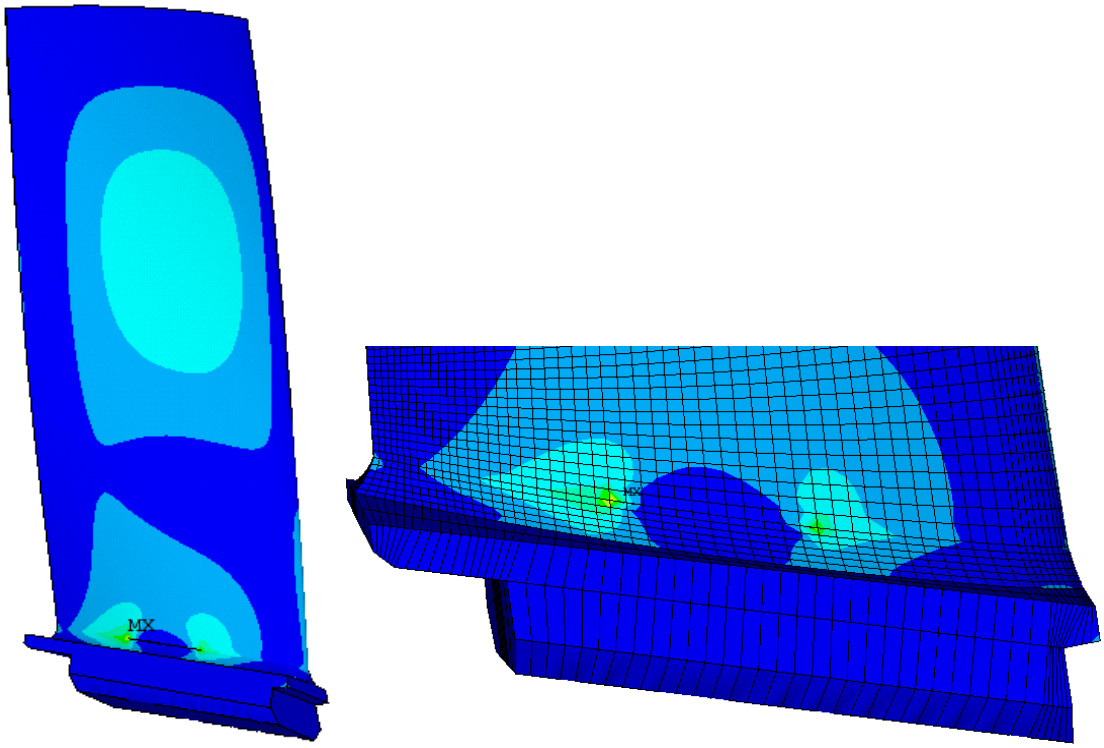

FIGURE 14 Modal stress at 1300.2 Hz of compressor blade with a crack of 11.4 mm, 20-node isoparametric elements

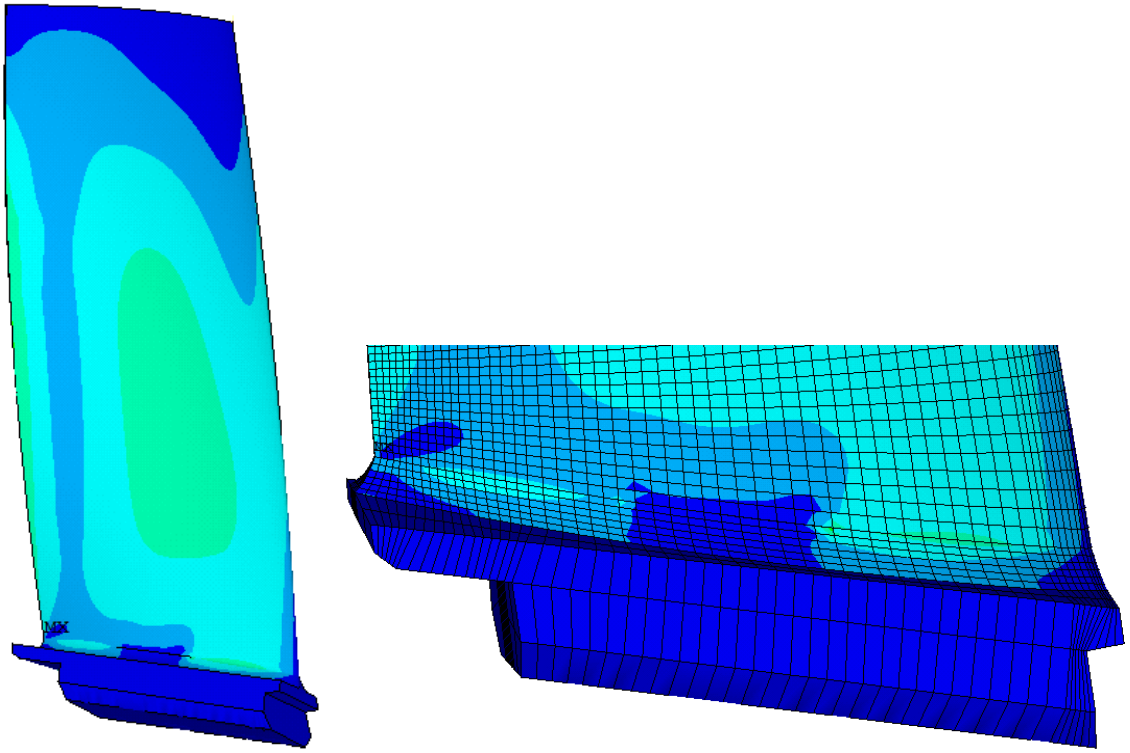

FIGURE 15 Modal stress at 1841.3 Hz of compressor blade with a crack of 11.4 mm, 20-nodes isoparametric elements

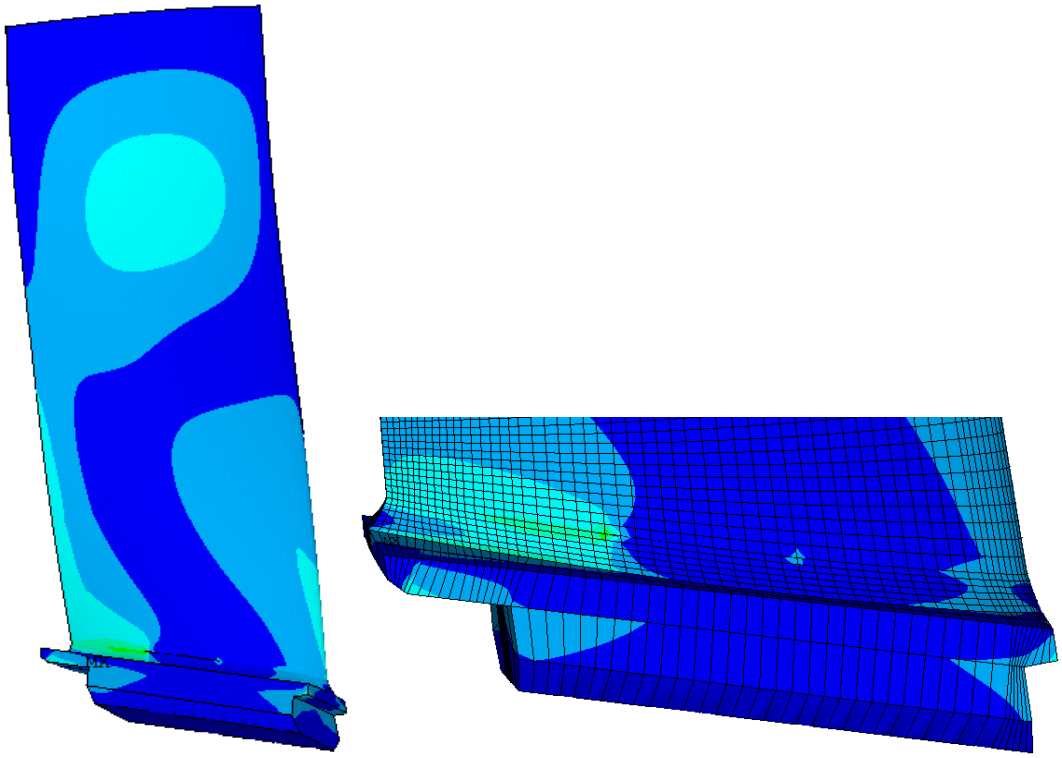

FIGURE 16 Modal stress at 2983.3 Hz of compressor blade with a crack of 11.4 mm, 20-nodes isoparametric elements

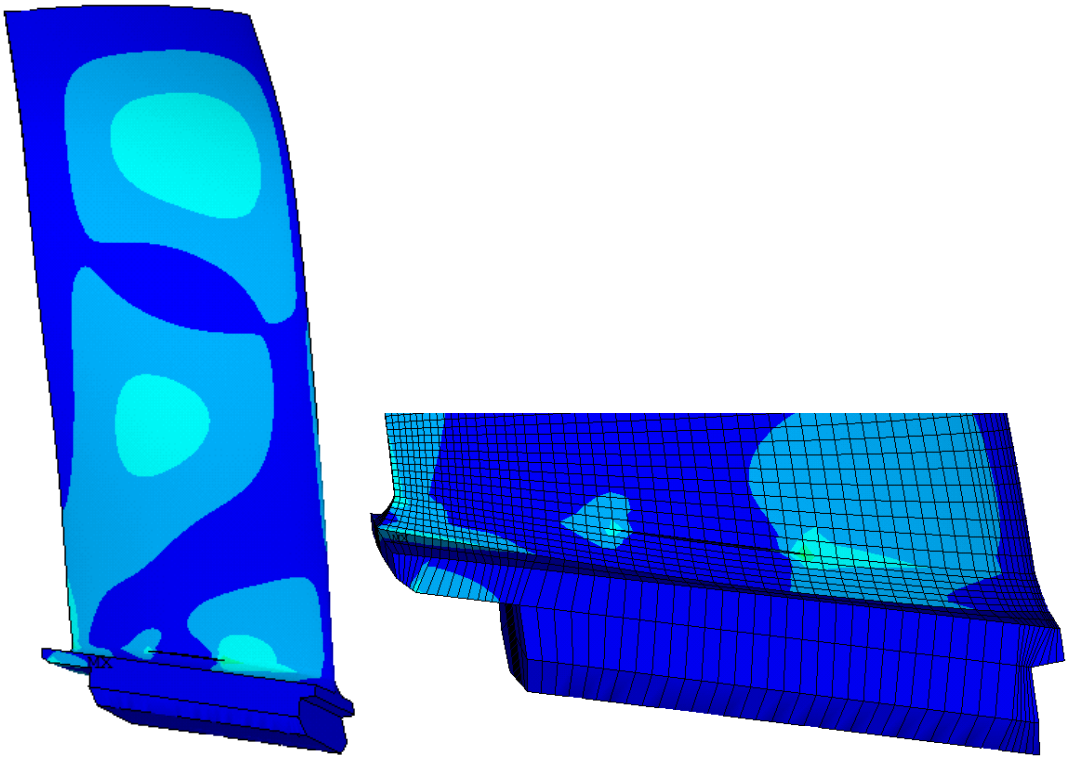

FIGURE 17 Modal stress at 3759 Hz of compressor blade with a crack of 11.4 mm, 20-node isoparametric elements

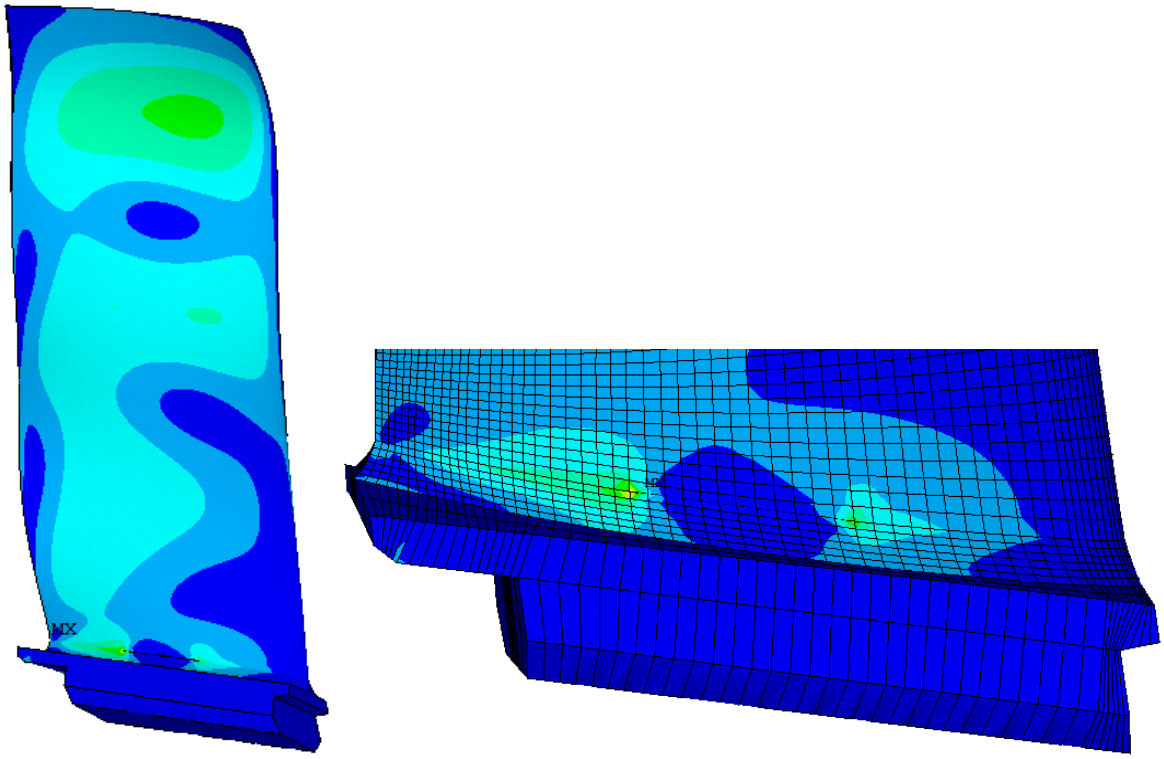

FIGURE 18 Modal stress at 6728.9 Hz of compressor blade with a crack of 11.4 mm, 20-node isoparametric elements

Figures 19-20 present a FE mesh for rotor blades with a 11.4 mm crack, using singularity elements in the crack region. Figure 20 is subdivided in the crack region as follows: on the outside, area 1.1 (green) comprising 20-node isoparametric elements; closer to the crack, area 1.2 (blue) comprising 20-node isoparametric elements, gradually turning into singularity, quarter-point elements in the next area; nearest to the crack, area 2 (yellow), comprising singular quarter-point elements, and finally the actual crack, area 3 (green dark).

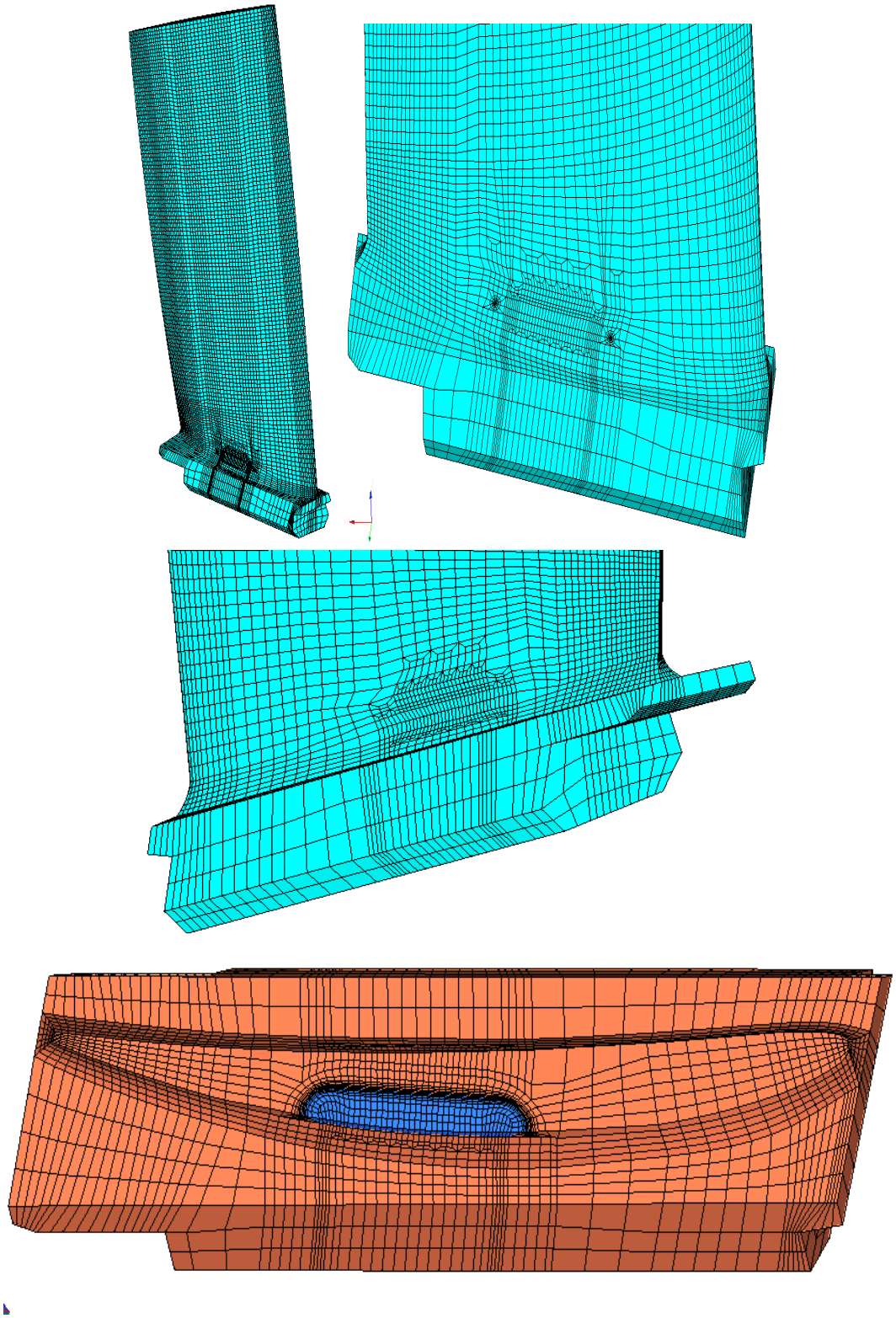

FIGURE 19 FE Mesh of compressor blade with a crack of 11.4 mm, using singularity quarter-point elements

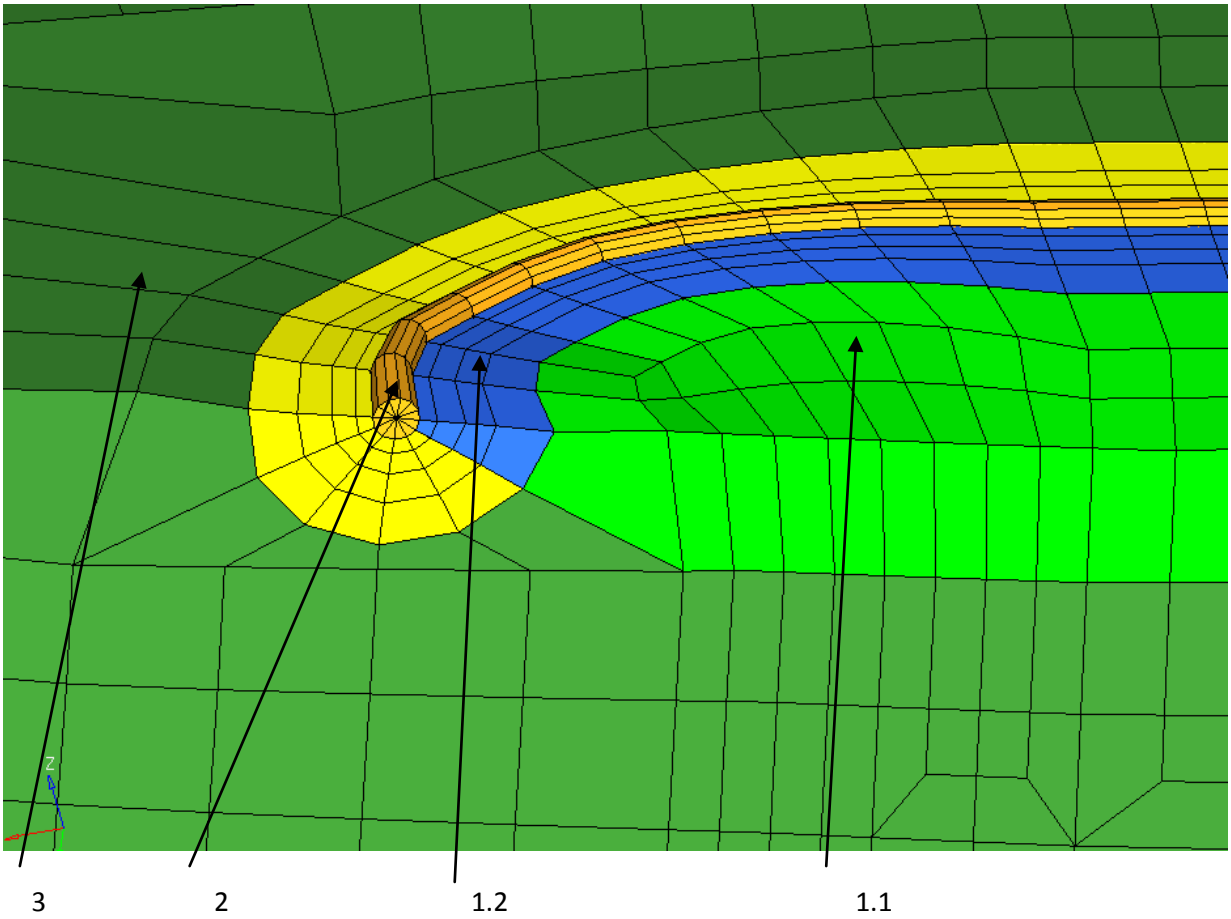

Area 1.1 (green) – 20-node isoparametric elements, Area 1.2 (blue) 20-node isoparametric elements turning into singular quarter-point elements, Area 2 (yellow) – the crack surrounded by singular quarter-point elements Area 3 (green dark) – blade crack area

FIGURE 20 FE Mesh of a 11.4 mm crack

TABLE 6 Natural frequencies (Hz) of L = 0.106 m cantilever blade for 0 rpm with 11.4 mm crack, using the singularity and HEX20 elements

FE Element	f1	f2	f3	f4	f5	f6	f7	f8
singular quarter-point element	327.79	1271.8	1819.0	2974.9	3699.4	4534.3	6584.7	7349.7
HEX 20-in-house code	330.52	1300.2	1841.3	2983.3	3759.0	4599.1	6728.9	7466

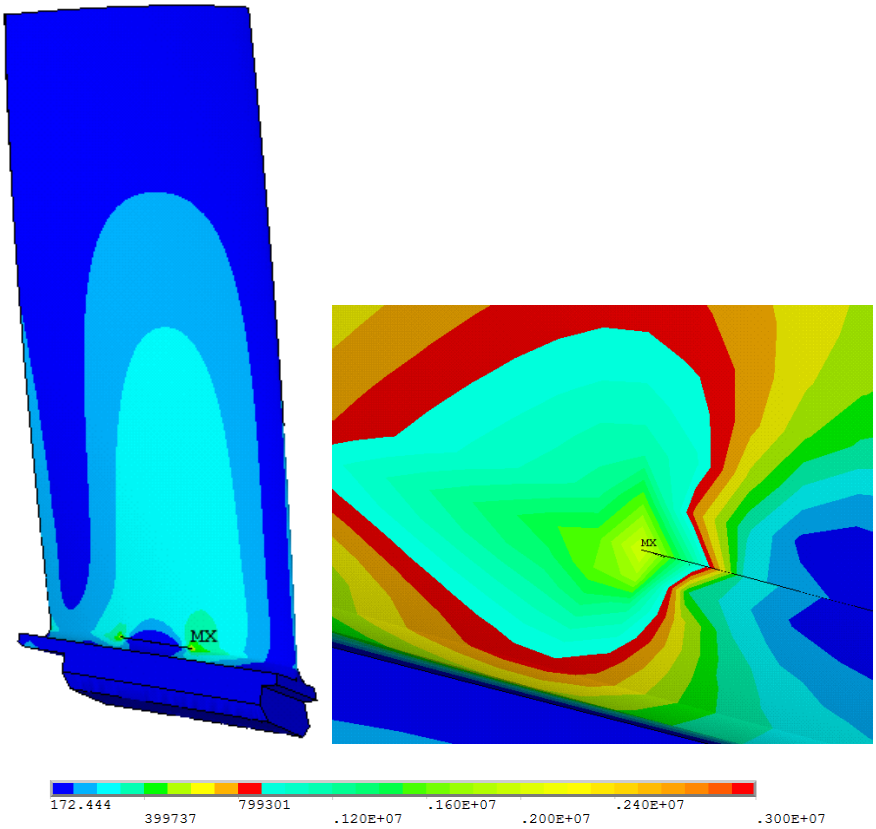

FIGURE 21 Modal stress at 330.52 Hz of compressor blade with a crack of 11.4 mm, 20-node isoparametric elements

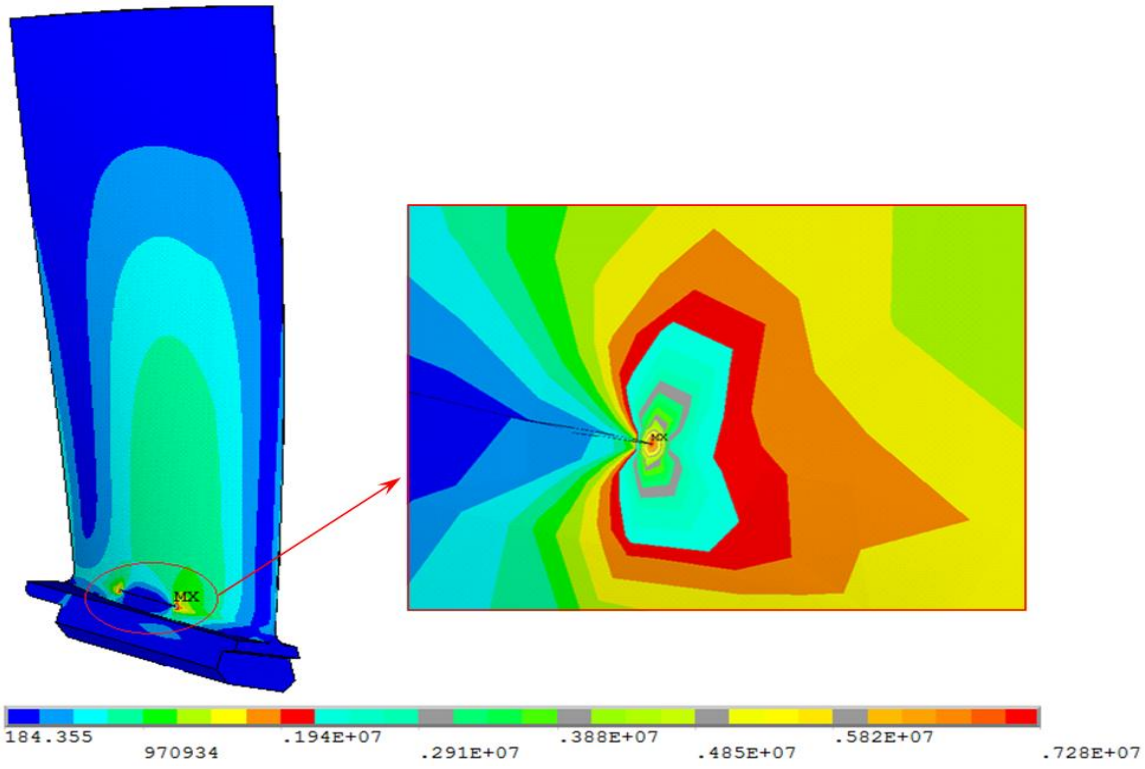

FIGURE 22 Modal stress at 327.79 Hz of compressor blade with a crack of 11.4 mm (singular quarter-point element)

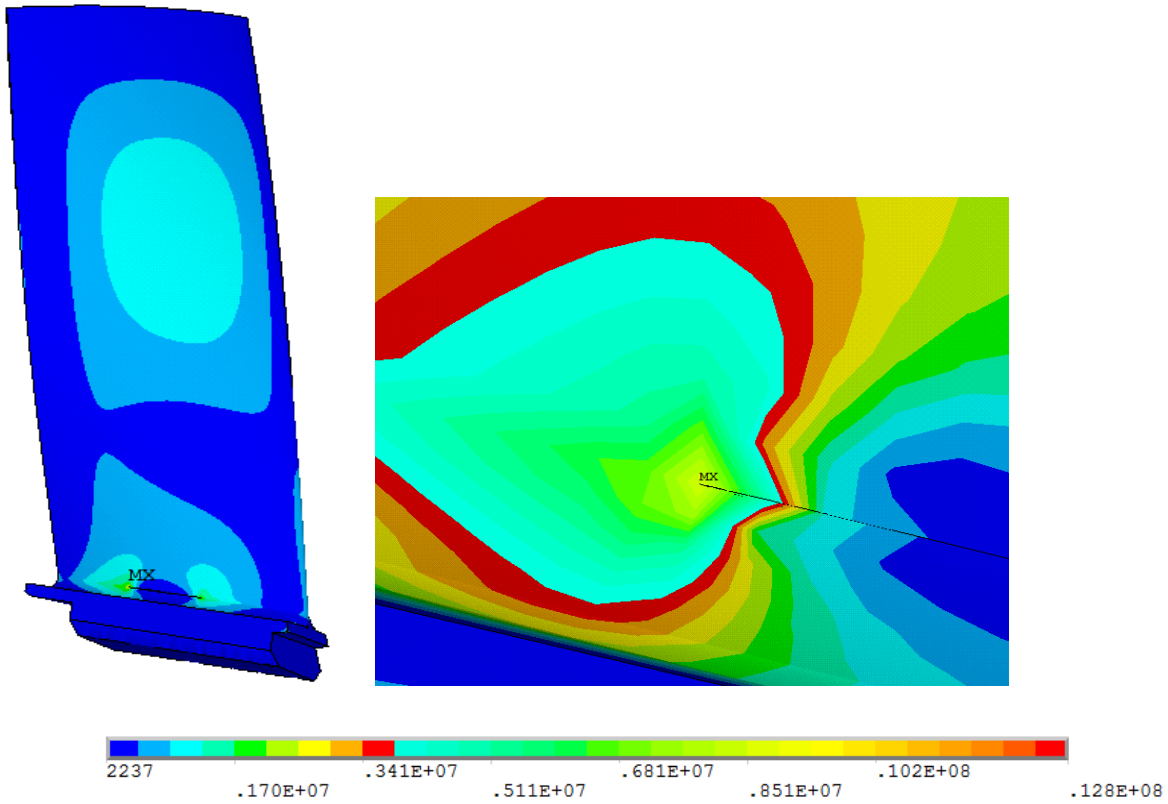

FIGURE 23 Modal stress at 1300.2 Hz of compressor blade with a crack of 11.4 mm (HEX 20)

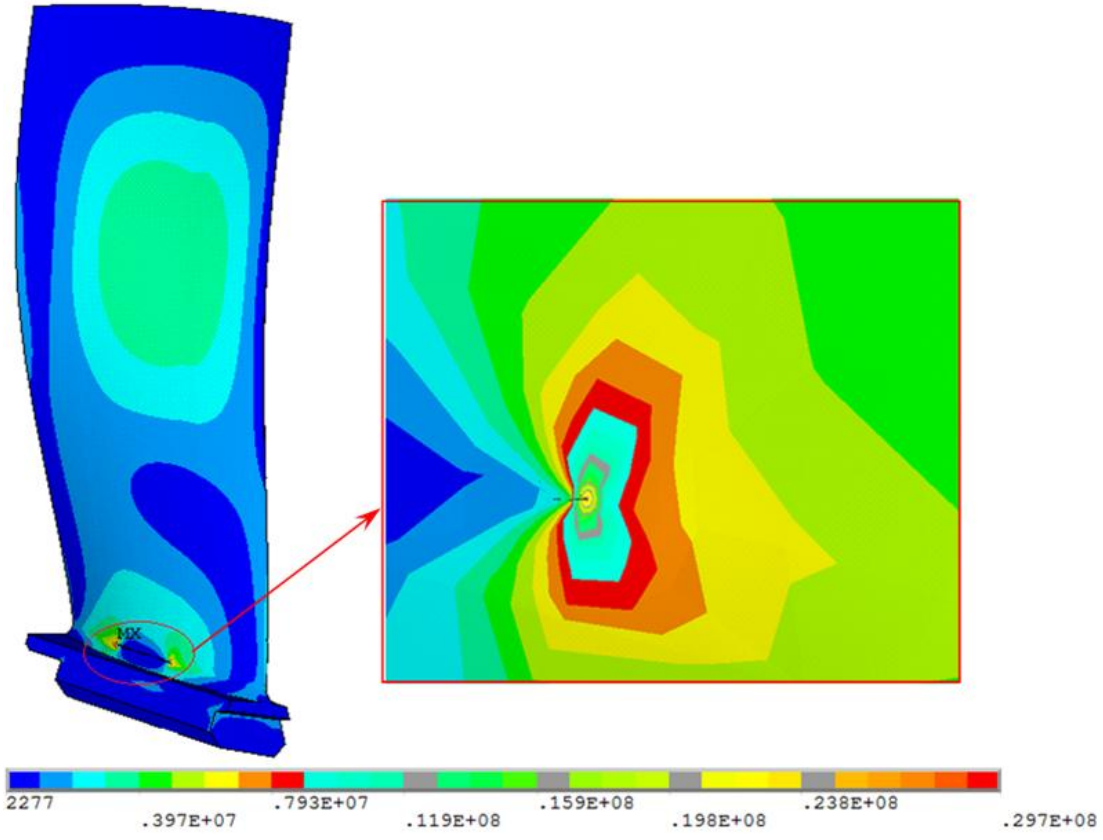

FIGURE 24 Modal stress at 1271.8 Hz of compressor blade with a crack of 11.4 mm (singular quarter-point element)

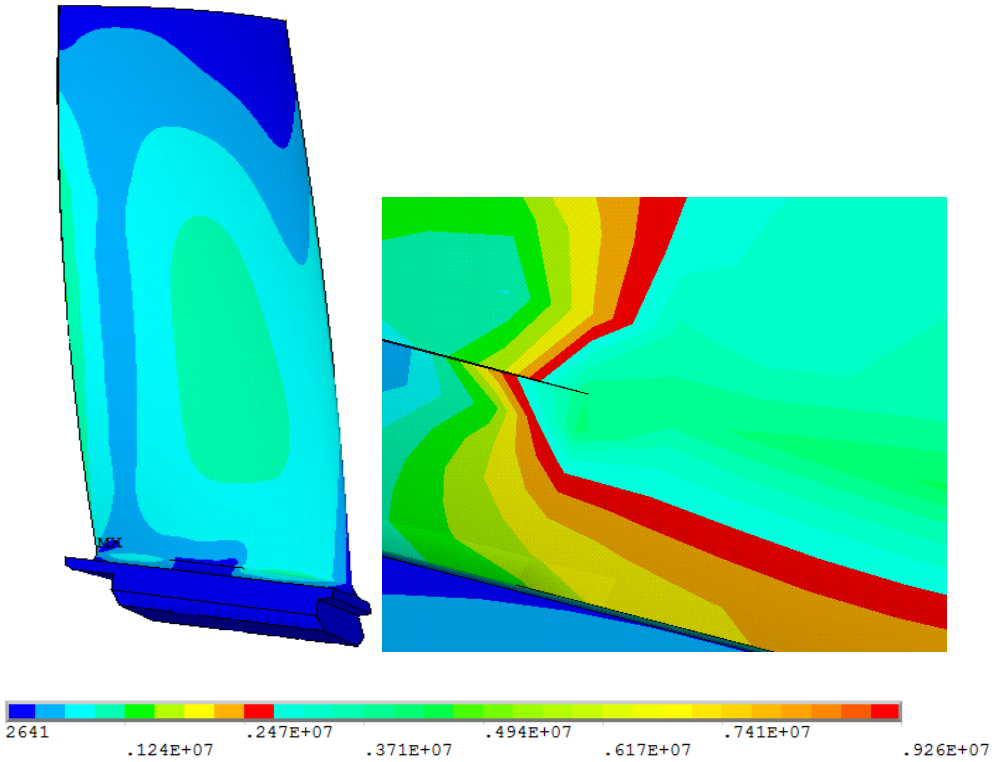

FIGURE 25 Modal stress at 1841.3 Hz of compressor blade with a crack of 11.4 mm (HEX 20)

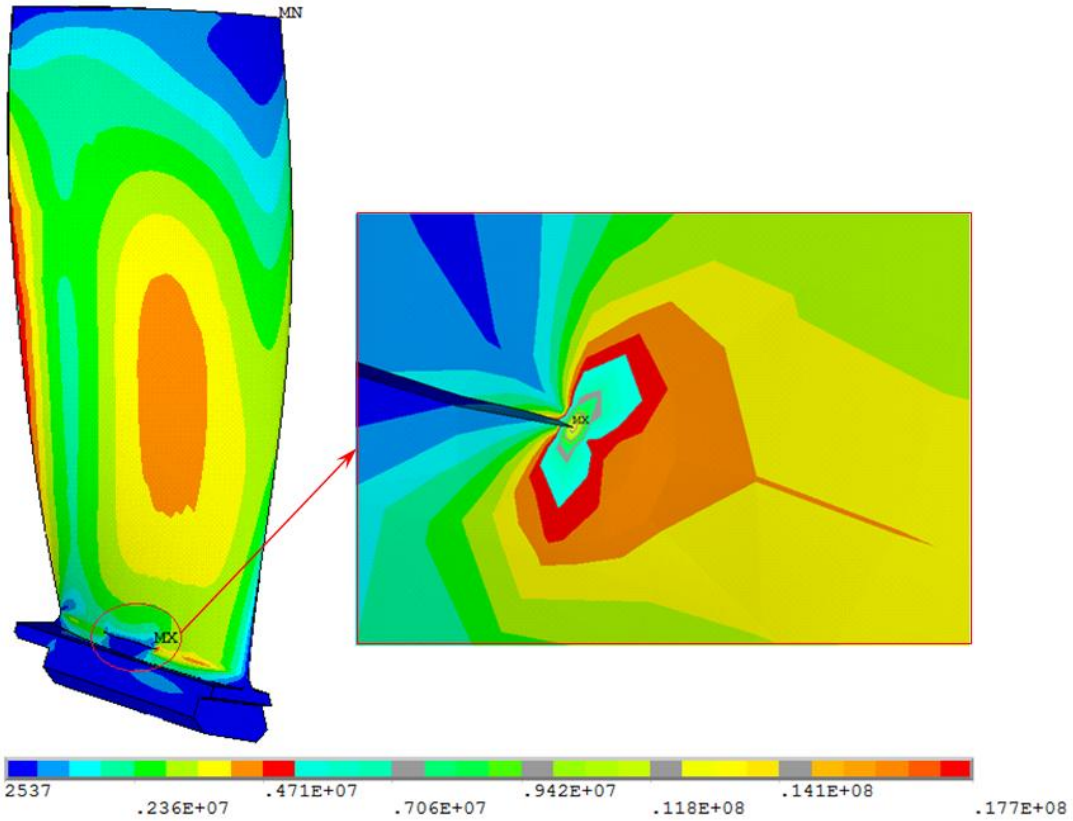

FIGURE 26 Modal stress at 1819 Hz of compressor blade with a crack of 11.4 mm (singular quarter-point element)

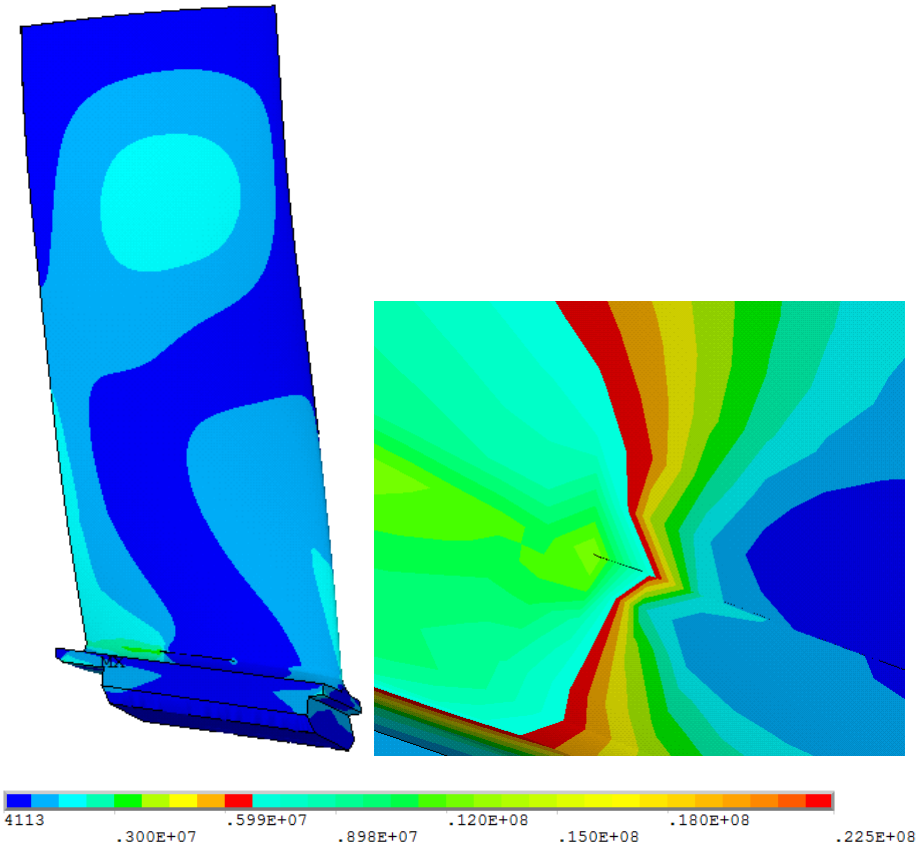

FIGURE 27 Modal stress at 2983.3 Hz of compressor blade with a crack of 11.4 mm (HEX 20)

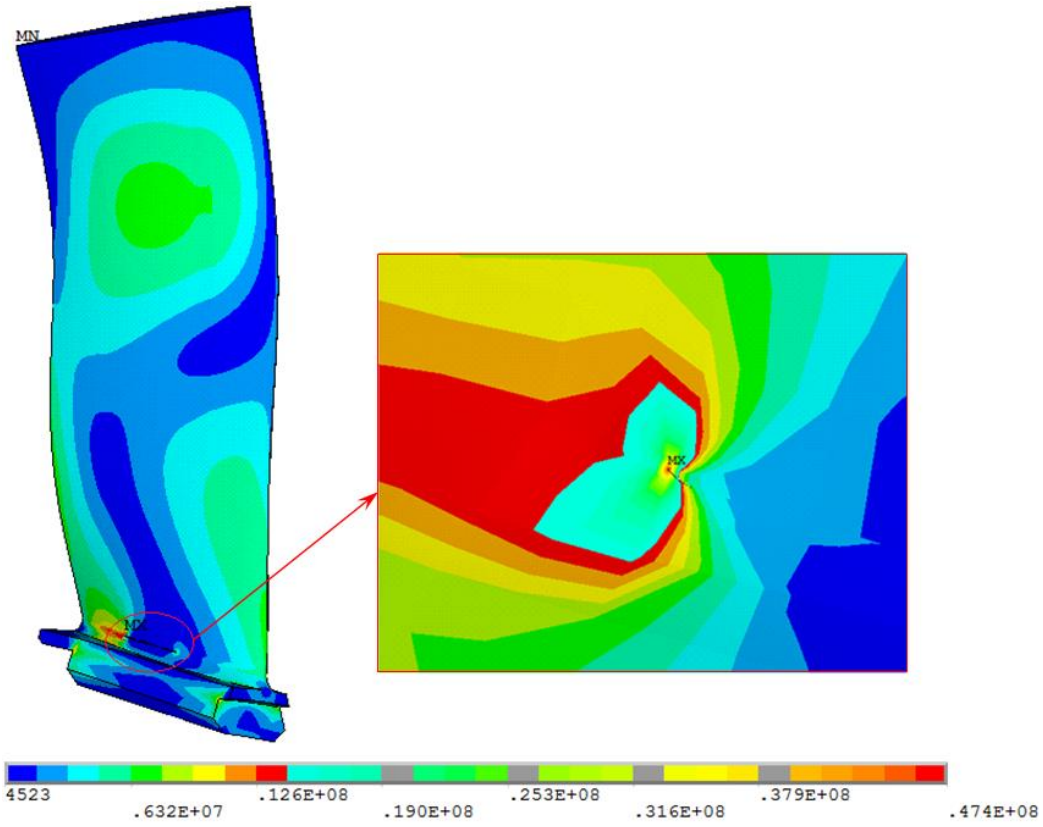

FIGURE 28 Modal stress at 2974.9 Hz of compressor blade with a crack of 11.4 mm (singular quarter-point element)

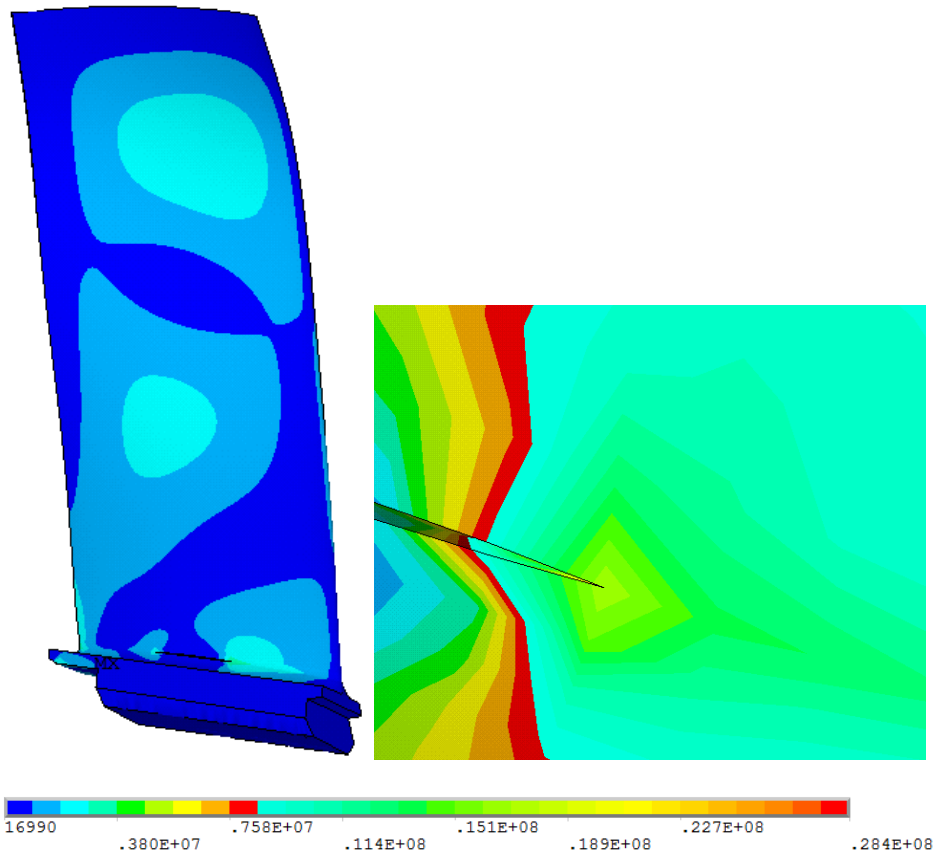

FIGURE 29 Modal stress at 3759 Hz of compressor blade with a crack of 11.4 mm (HEX 20)

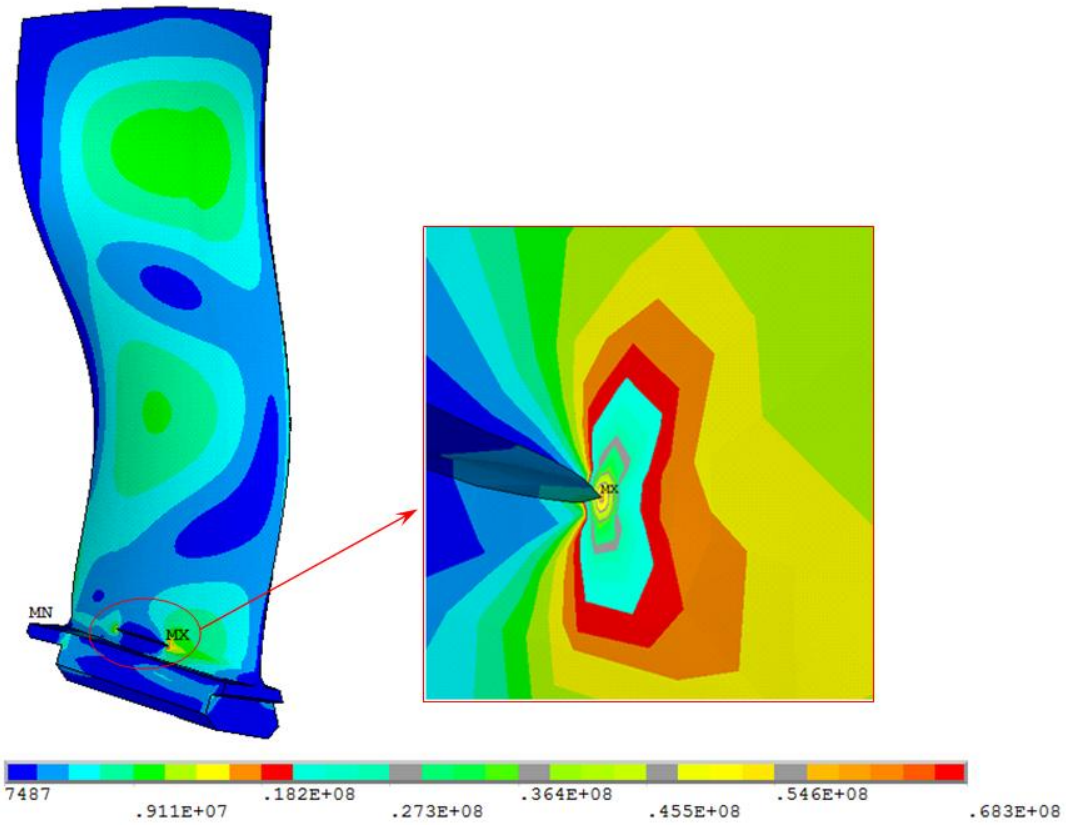

FIGURE 30 Modal stress at 3699.4 Hz of compressor blade with a crack of 11.4 mm (singularity quarter-point element)

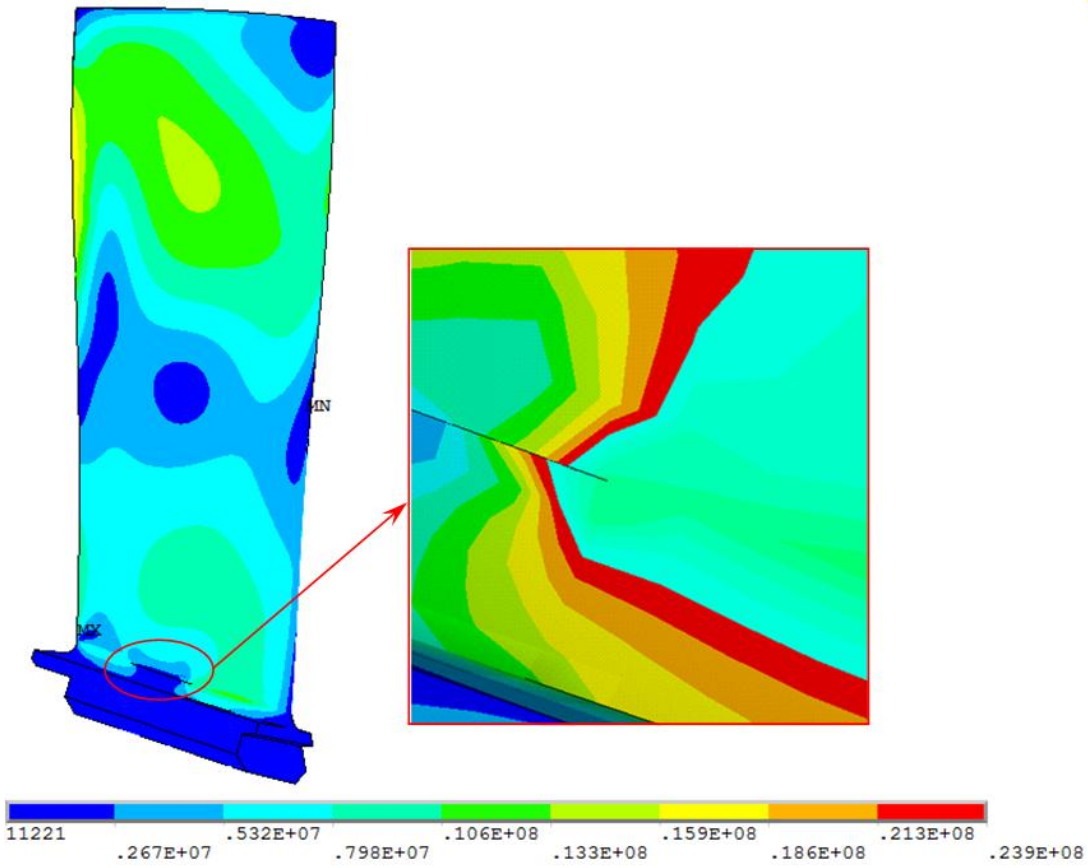

FIGURE 31 Modal stress at 4599 Hz of compressor blade with a crack of 11.4 mm (HEX 20)

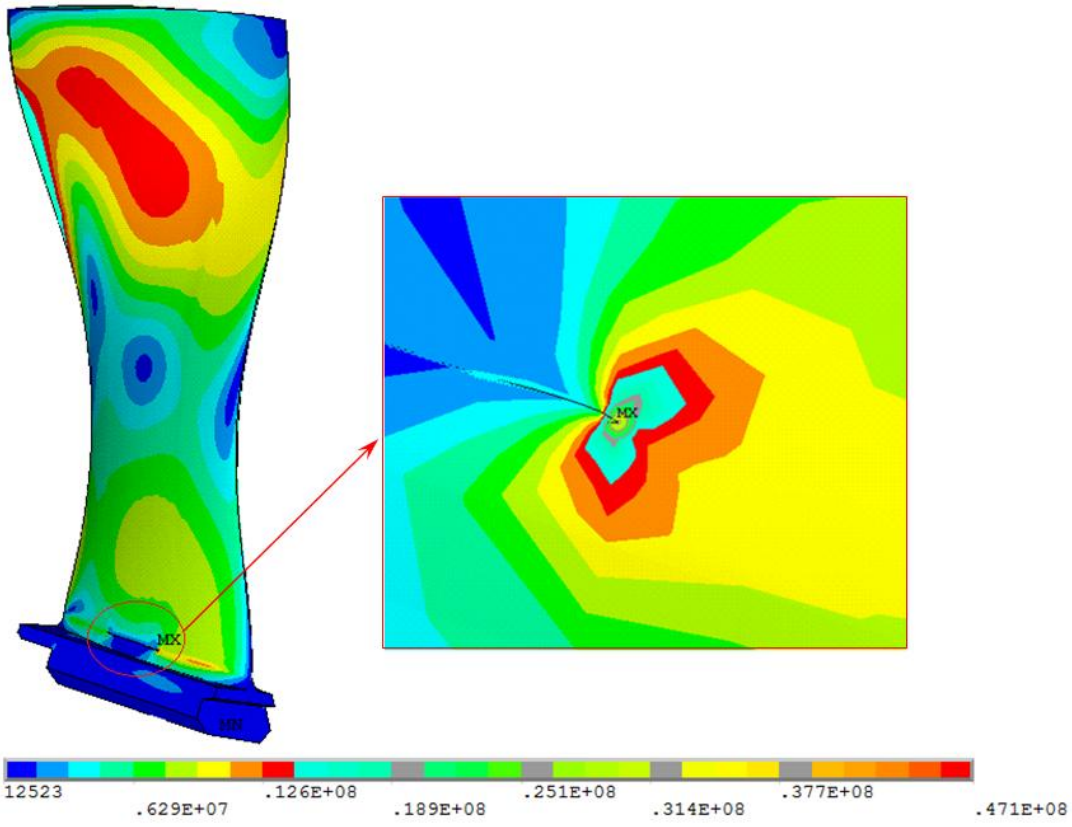

FIGURE 32 Modal stress at 4534.3 Hz of compressor blade with a crack of 11.4 mm (singularity quarter-point element)

A higher modal stress gradient was noted in the crack region when using the singularity, quarter-point elements, see Figures 21-32. Maximal stress was observed in the crack front, and this caused the crack to spread. Another advantage of using a singularity, quarter-point element mesh in the crack area is that it reduces the total number of HEX20 elements.

4. Conclusions

The natural frequencies and mode shapes of a cantilever blade with a crack and without one were calculated and compared using an in-house code and the ABQUS code with 20-node (HEX20) elements and singularity elements. Frequency changes became more noticeable when the crack was above 10 mm long.

The natural frequencies obtained using the 3D, prismatic, quarter-point, isoparametric element model were lower. But the main difference was seen in the modal stresses of the crack region.

A higher stress gradient in the crack region was observed when singularity, quarter-point elements were used. Maximal stress was noted in the crack front, from where the crack spread. Using a singularity, quarter-point element mesh in the crack region reduced the total number of degrees of freedom in the model.

5. List of Symbols

EO	engine order excitation
HEX20	isoparametric 20-node element
h	length of singular quarter-point element edge from crack front, see Figure 1
J	Jacobian
L	crack length
l	semi-width of singular quarter-point element, see Figure 1
$N_i(\xi,\eta,\zeta)$	shape functions
r	radius from crack front
S_o	blade cross-section area without the crack
S	crack areas
V	volume
x_i, y_i, z_i	global coordinates
ξ_i, η_i, ζ_i	local coordinates
Π	potential energy
σ, ε	stress and strain

References

Barsom, R.S., Triangular quarter-point elements as elastic and perfectly-plastic crack tip elements, *Int J for Num Meth in Engineering*, V. 11, N 1, 85-98, (1977)

Chandwani, R., and Timbrell, C., Simulation of 3D Non-Planar Crack Propagation, *NAFEMS World Congress* 2007, Vancouver, Canada, (2007)

Janecki, S. and Krawczuk, M., *Dynamics of steam turbine rotor blading, Part I. Single blades and packets*, Ossolineum, Wroclaw (1998)

Rao, J. S., The Fundamental Flexural Frequency of A Cantilever Beam of Rectangular Cross-section with Uniform Taper, *Aero Qly*, v.16, p.139 (1965)

Rao, J. S., Fracture Mechanics Analysis of A Steam Turbine Blade Failure, *Proc. 1995 Design Engng Technical Conferences*, DE-Vol. 84-2, ASME, p. 1173, September 17-21, (1995), Boston.

Rao, J. S., Fracture Mechanics in TurboManager Quickens Blade Failure Investigations, *International Review of Aerospace Engineering (I.RE.AS.E)*, vol. 2, No. 6, p. 329, (2009)

Rao, J. S., *Turbine Blade Life Estimation*, Narosa Publishing House, (2000).

Rao, J. S., Narayan, R. and Ranjith, M. C., Lifing of Turbomachine Blades – A Process Driven Approach, *Advances in Vibration Engineering*, The Vibration Institute of India, vol. 9, No. 1, (2010)

Rao, J. S. and Rieger, N. F., *Vibrations of Rotating Machinery, Part 2: Blading and Torsional Vibrations*, The Vibration Institute, Clarendon Hills, Illinois, USA, (1981)

Rao, J. S., Turbomachine Blade Vibration, John Wiley and Sons, (1991)

Rao, J. S., Advanced Theory of Vibration John Wiley and Sons, (1992)

Rao, J. S., Turbomachine Unsteady Aerodynamics - New Age International, (1994)

Rzadkowski, R., *Dynamics of Steam Turbine Rotor Blading, Part.2 Bladed Discs*, Ossolineum, Wroclaw (1998)

Vorobiev, Yu. S., Romanenko, V. N., Tishkovets, E. V and Storozhenko, M. A., Turbomachine Blades Vibration with Damage, *Vibraciya v technike i technologii*, No. 5(37), 47-51 (2004) (in Rus.).

List of Figures

List of Tables

Annexure 1
Plan of Work

First year

1. Model and perform Modal stress analysis of one compressor rotor blade of SO-3 to find the possible crack initiation locations.

2. Modelling of different crack depths using a three-dimensional finite element model with the 3D prismatic quarter point Isoparametric elements of Vorobiev et al. (2004) and 20 noded Isoparametric elements.

3. Calculating natural frequencies of blades for different crack lengths.

4. Calculation of unsteady pressures acting on compressor rotor blade in a stage – using transient analysis in Fluent.

5. Determine material and friction damping values as a function of strain amplitude in each mode of vibration interest using Process Driven Approach codes developed on HyperWorks platform by Rao et al, (2010).

Second year

7. Determine resonant stresses at critical speeds.

8. Stress Intensity Factor approach will be used for fatigue crack initiation studies.

9. Stress Intensity Factor approach will be used for fatigue crack propagation studies with the help of Paris law.

10. Determine crack propagation using finite element model under the alternating stress

11. Compare Paris values, FE model values and experiments

Crack Propagation in Compressor Rotor Blade

(Grant FA8655-10-1-3062)

Report for Second Six Months

October 2010 – March 2011

R. Rzadkowski[1] J.S. Rao[2], Yu.S. Vorobiev[3]

[1]The Szewalski Institute of Fluid Flow Machinery, Gdansk, Poland

[2]Altair Engineering India Pvt Ltd, Bangalore

[3]National Ukrainian Academy of Sciences, Ukraine

Submitted to
European Office of Aerospace:
Research and Development
86 Blenheim Crescent
Ruislip, Middlesex HA4 7HB
United Kingdom

April 20, 2011

Investigators

1. Principal Investigator: Professor Romuald Rzadkowski
The Szewalski Institute of Fluid Flow Machinery,
Fiszera 14, 80-952 Gdansk, Poland
Tel: +48502975518
E-mail: z3@imp.gda.pl

2. Senior Investigator and Mentor: Prof. J.S Rao
Chief Science Officer, Altair Engineering (India)
Mercury 2B Block, 5th Floor, Prestige Tech Park
Sarjapur Marathhalli Outer Ring Road
Bangalore 560 103
Tel: +91 80 66294742 +91 98453 46503 Fax: +91 80 66294700
E-mail: js.rao@altair.com

3. Investigator: Professor Iurii Vorobiov
Department of Non-stationary Mechanical Processes,
Podgorny Institute for Mechanical Engineering Problems,
National Ukrainian Academy of Sciences, Ukraine
E-mail:vorobiev@ipmach.kharkov.ua

4. Investigator: Dr Marina Chugay
Department of Non-stationary Mechanical Processes,
Podgorny Institute for Mechanical Engineering Problems,
National Ukrainian Academy of Sciences, Ukraine
E-mail: chugay@ipmach.kharkov.ua

5. Investigator: Dr Marcin Drewczyński
Assistant Professor
The Szewalski Institute of Fluid Flow Machinery,
Fiszera 14, 80-952 Gdansk, Poland
E-mail: mdrew@imp.gda.pl

6. Investigator: Dr. Ryszard Szczepanik
Assistant Professor
Air Force Institute of Technology
01-494 Warszawa, Poland
E-mail: ryszard.szczepanik@itwl.pl

7. Investigator: Mr. Narayan Rangarajan
Lead Engineer, Altair Engineering (India)
Tel: +91 80 6629 4500/ 4700 (Fax)
E-mail: narayan.rangarajan@altair.com

8. Investigator: Mr. Rejin Ratnakar
General Motors (India) Bangalore
Tel: +91 99860 15670
E-mail: rejin.ratnakar@gm.com

Table of Contents

Summary

In the first six months report (*April-September 2010*) *modal stress analysis was carried out on one compressor rotor blade of an SO-3 engine to locate the possible crack initiations. Various crack depths and lengths were created using a three-dimensional finite element model with the 3D prismatic quarter-point isoparametric elements and 20-node isoparametric elements to calculate the natural frequencies and mode shapes of the rotor blades.*

This is the second report (October 2010 - March 2011).

The Stage is modelled in CFD using Fluent. Different types of blockage are simulated and the results for frequency harmonics due to flow path excitation are identified. Important critical speeds are determined where life estimation will be made.

The methodology to analytically determine a nonlinear damping model as a function of strain amplitude at a reference point in a given mode of vibration at a given speed of rotation of bladed-disk is described. Both material and friction damping are included. The friction damping is considered for both macro (Coulomb) and micro (fretting) slip conditions. For the blade under consideration, these damping values are determined and presented.

The damping estimation process is developed on HyperWorks platform "TurboManager" by calling suitable solvers for determining the mode shapes. The pre-processing is done by using HyperMesh and post-processing is carried out by using HyperView.

The excitation pressure field and the stress response at critical speeds will be determined in the second year. The stress based and strain based lifing algorithms and fracture mechanics algorithm will also be carried out in the second year leading to estimation of life for each critical speed crossing. These methods will all be included in the template under development to enable life estimation in a comprehensive manner under one platform using appropriate solvers. This work is in progress.

1. Introduction

In the determination of life of a turbomachine blade, unsteady forces acting on rotor blades and damping play the most significant role in accurately assessing the peak stress and strain levels at a critical speed while starting the engine or shutting down. Yet, the design engineer depends on an approximate linearized value obtained from tests which are expensive and time consuming. The damping mechanism is known to be highly nonlinear and dependent on the state of stress condition in the rotating blade.

Damping in resonant conditions without flutter consists essentially of

1. Material Damping
2. Friction Damping

Both these damping mechanisms are highly nonlinear; material damping is dependent on the state of stress and there is a hysteresis loss of energy in vibration. Under resonant conditions it is purely dependent on the stress mode shape; each element is subjected to the state of stress that depends on the mode of vibration at a given speed of rotation. Hysteresis is known to be highly nonlinear.

Friction is also highly nonlinear that depends on the normal contact force and may be governed by Coulomb friction if there is a sufficient clearance beyond asperity level contact or by micro friction (fretting) tribological laws governed by Hertzian contacts with asperity level contacts.

In this report we will consider the procedure of setting up nonlinear damping as an equivalent viscous damping given by a function of strain amplitude of a rotating turbomachine blade at one of the natural frequencies on the Campbell diagram for a given speed of rotation.

We will also demonstrate an iterative procedure for determining the resonant stress at a critical speed using the nonlinear damping model. This resonant stress together with the mean stress allows an accurate determination of damage suffered by a blade while crossing a critical speed.

2. Unsteady forces acting on rotor blades

Experiments were carried out on a first stage rotor blade in the compressor of an SO-3 engine at the Air Force Institute of Technology in Warsaw to measure the blade amplitude.

The rotor blade and disc of the first stage was made of 18H2N2 steel. Young's modulus of the blade is 204 GPa, density is 7850 kg/m^3, Poisson's ratio 0.3. The blade length is 0.1063 m, the radius of blade attachment in the disc is 0.2077 m, the number of rotor blades in the stage is $N_2 = 28$ and the number of stator blades is $N_1 = 34$.

In the experiment a crack was initiated in the first compressor stage by placing rectangular blocks (125×100 mm) on the stator blades (Fig. 1), which in real life could be caused by birds engulfed in the engine.

FIGURE 1 Test rig of an SO-3 jet engine

The unsteady forces acting on the rotor blades were calculated for the 3D non-viscous flow of ideal gas (15000 rpm) through the stator-rotor-stator stage using the FLUENT code.

A 3D model of the first stage of an SO-3 jet engine compressor is shown in Fig. 2. The model, created using the Gambit program, consists of 44 blades in the Inlet Stator Cascade, 28 blades in the Rotor Cascade (only one of which is seen in the picture) and 34 blades in the Stator Cascade of the first stage. The reference rotor blade in Fig. 2 is divided into 10 cross-sections.

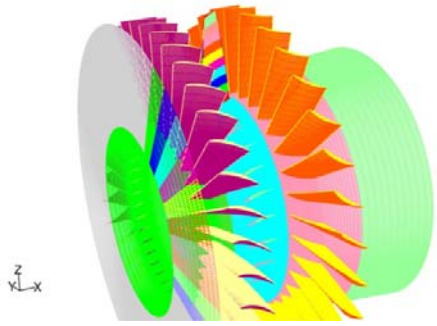

FIGURE 2 CFD model of an SO-3 engine first stage compressor

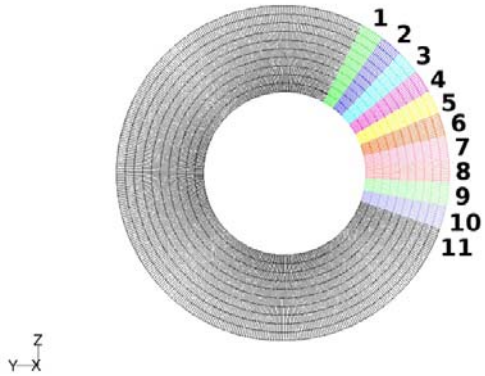

FIGURE 3 View of Inlet's segments

In order to model the block (125×100 mm Fig. 1) in the inlet of the engine, ¼ of the area was divided into 11 segments. During the simulations three operating states were analysed. The first was the nominal state (fully-opened inlet) the second was the state in which one of these segments was blocked (Fig. 3) and the third was the state in which four of these segments were blocked.

The fourth partially blocked inlet caused a local disturbance of the flow. Fig. 4 presents the contour Mach number in the stage around the blocked area.

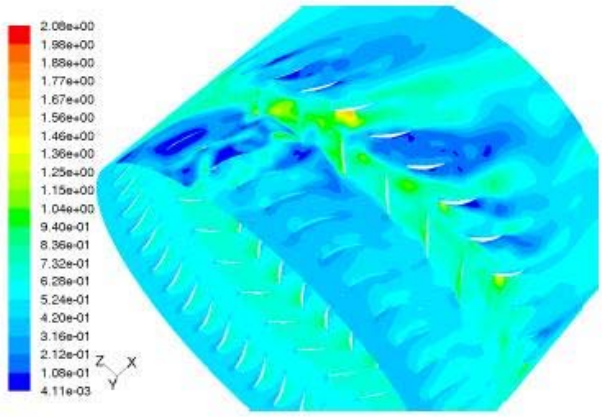

FIGURE 4 Contours of Mach number – blocked area

Fig. 5 presents a comparison of results for an unblocked inlet (red), a single blocked inlet segment (green) and four blocked inlet segments (blue). It is clearly visible that the blocked inlet segment has a strong local influence on the amplitude. The red line in Fig. 5 shows the axial force in operating conditions (with unblocked inlet), whereas the green and blue lines represent the results in the off-design case (with one and four blocked inlet segment).

The graph clearly shows that the four blocked inlet segments have a stronger local influence than the single blocked inlet segment. The local maximum for the four segments was slightly above 100 N, while for the single segment it was 50 N.

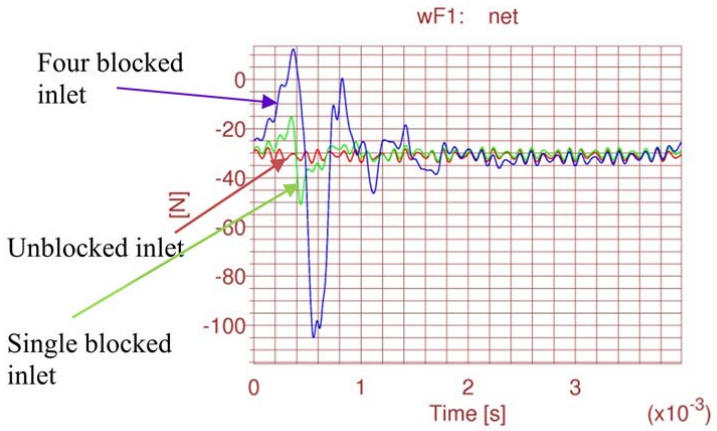

FIGURE 5 The average force for unblocked inlet, for a single blocked inlet segment and for a four blocked inlet segments

The four blocked inlet segments (blue) caused low-frequency harmonics of a higher amplitude (30% of the steady part) than the single blocked inlet (green) with just 7% of the steady part (Fig. 6).

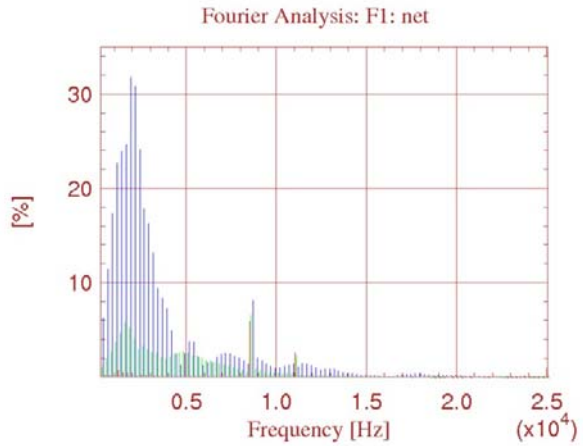

FIGURE 6 Unsteady axial force harmonics (comparison of blocked and unblocked inlet)

The magnitudes of unsteady forces on the reference rotor blade for different harmonics (from FFT) in axial and circumferential directions on the blade are given in Tables 1 and 2 respectively.

TABLE 1 Axial Unsteady Force N

Harmonic	Frequency Hz	No Block	One Block	Four Block
1	250.75	0.0722	0.3245	1.9518
2	501.51	0.0703	0.5676	3.5187
3	752.26	0.0639	0.8235	5.3595
4	1003.01	0.1336	1.0938	6.9932
5	1253.76	0.2419	1.4101	7.3761
6	1504.51	0.1601	1.7421	7.6080
7	1755.27	0.1413	1.5929	9.8222
8	2006.02	0.0650	1.2178	9.5135
9	2256.77	0.0404	0.8960	7.4678
10	2507.52	0.0798	1.0020	5.5012
34	8525.58	1.8223	1.9794	2.5256
44	11033.1	0.8118	0.6889	0.3299

TABLE 2 Circumferential Unsteady Force N

Harmonic	Frequency Hz	No Block	One Block	Four Block
1	250.75	0.0638	0.5369	3.2108
2	501.51	0.0684	0.7601	7.6735
3	752.26	0.0526	1.0287	10.3333
4	1003.01	0.1598	1.4220	11.8097
5	1253.76	0.2471	1.8324	11.2942
6	1504.51	0.1903	2.4363	9.0390
7	1755.27	0.1493	2.5192	12.4782
8	2006.02	0.0841	2.2132	13.4424
9	2256.77	0.0607	1.5821	11.8532
10	2507.52	0.2536	1.3225	10.5429
34	8525.58	2.6664	2.9217	3.7234
44	11033.1	0.8402	0.7461	0.2149

We notice that the magnitude of force increases with blockage. The worst case will be when maximum blockage occurs when a bird hit occurs. The NPF 44× from the upstream component decreases with blockage, whereas 34× component due to downstream stage increases with blockage. Higher harmonics become predominant with increased blockage.

1. Results from Original Stage Calculations without any blockage:

The fundamental excitation is NPF at 44×250 = 11000 Hz; the time period is 0.90909×10^{-4} sec. This is the main component as can be seen in Figs. 5 and 6; the excitation magnitude is small. Also the Campbell diagram in Fig. 7 does not show a blade mode at this high frequency.

From the Campbell diagram of the first stage compressor tuned bladed disc (Fig. 7), one can see that 2EO excitation at 15000 rpm can cause blade resonance stress. The critical speed is marked by a circle. Usually this component of excitation can be predominant because of misalignment arising out of operation hours.

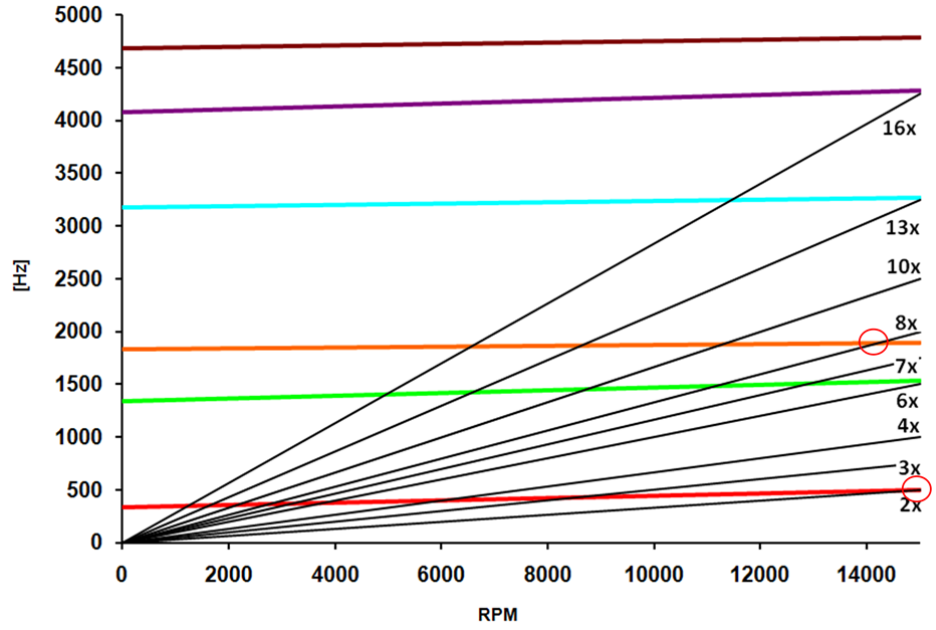

FIGURE 7 Campbell diagram for first compressor stage of SO-3 engine

2. Results from One Block and Four Block Segment Closure Calculations:

We note here from Table 2 that 8× component becomes predominant from CFD analysis; this means that at a speed slightly below 15000 rpm, we have resonance with 1919 rpm third mode frequency as indicated in Fig. 7.

We notice that a block simulated (as in a bird strike) produces resonance at 1919 rpm 3rd mode natural frequency. We can consider the worst case pressure field and estimate the resonant stress.

In determining the resonant stress, it is just not the magnitude of pressure load, but also te damping that is more important. This is usually weak link in all lifing exercises. Now we develop a procedure to determine analytically a nonlinear damping model that gives more accurate lifing results.

Damping arises mainly from hysteresis and friction in bladed disks. These are considered in the next section.

3. Material (Hysteresis) Damping

Lazan (1968) at Wright Patterson Air Force Base conducted systematic and extensive measurements on hysteresis in simple tension and defined the loss of energy per cycle D under a stress amplitude σ by

$$D = J\left(\frac{\sigma}{\sigma_e}\right)^n \tag{1}$$

where J and n are material properties and σ_e is endurance limit.

The idea of determining hysteresis damping using Lazan's law was conceived recently by Rao and Saldanha (2003). A bladed-disk can be modelled to have a given number of finite elements. At a given speed of rotation we can extract the desired number of modes that appear in the Campbell diagram. The mode shapes at these critical speeds give the state of stress. Because they are modal properties we can choose a suitable reference point and define the deflected proportional shape with the stress field. For a chosen proportional shape, say orthonormal condition, with reference amplitude defined we can consider each of the finite elements in the total mesh as a test specimen and apply the Lazan's law for the stress condition of the element under consideration. The loss of energy in all the elements can be determined and summed up to give the total loss of energy per cycle. This loss of energy can be compared with the strain energy in the mode shape under consideration and obtain the loss factor and thus equivalent viscous damping. The approach is summarized below.

Total damping energy D_0 (Nm) in entire volume of the body:

$$D_0 = \int_0^v D dv \tag{2}$$

Loss factor η:

$$\eta = \frac{D_0}{2\pi W_0} \tag{3}$$

where W_0 is the total strain energy (Nm).

Equivalent Viscous Damping C (N-s/m):

$$C = \frac{\eta K}{\omega} \tag{4}$$

where ω the natural frequency (rad/s) and K is the modal stiffness (N/m).

The exact state of stress under resonant condition is not known apriori. We therefore construct a relation for equivalent viscous damping as a function of strain amplitude at the chosen reference point. This relationship defines the nonlinear nature of hysteresis damping.

For increased (or decreased) strain amplitudes, the orthonormal reference strain amplitudes, stress and strain energy are multiplied by a factor F to obtain the equivalent viscous damping C_e at various strain amplitudes as given below.

$$\begin{aligned}
\varepsilon' &= \varepsilon F \\
W_0' &= W_0 \times F^2 \\
\eta' &= \frac{D_0'}{2\pi W_0'} \\
C_e' &= \frac{\eta' K}{\omega_n} F^2 \\
\xi &= \frac{C_e}{2\sqrt{Km}} F^2
\end{aligned} \tag{5}$$

A plot of equivalent viscous damping ratio as function of reference strain amplitude in the chosen mode of vibration defines the nonlinear damping model. Typical material friction characteristics obtained, Rao (2011), using such a process above are given in Fig. 8.

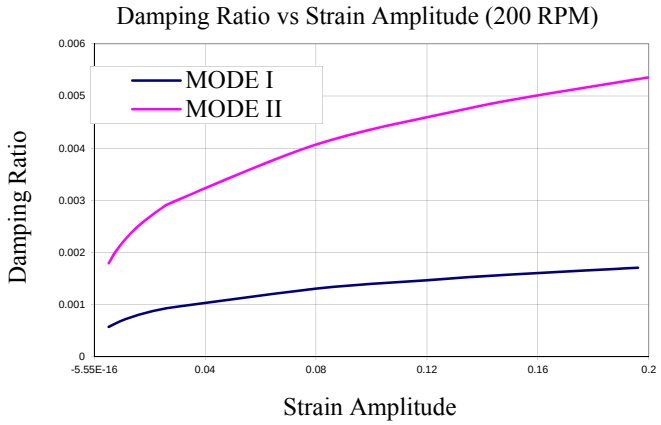

FIGURE 8 Material Friction Characteristics

This process is captured in a template *TurboManager* described in section 5

4. Macro-slip or Coulomb Damping

As mentioned, friction damping between interfacial slip surfaces, here the dovetail and blade roots, takes place as macro-slip with clear gap more than asperity level contact or micro-slip with contact taking place at asperity level (that occurs with high normal loads at high speeds). The case of macro-slip condition is fairly straight forward as today's solvers can be used to simulate the free vibration decay curve of a rotating blade under an impact (like a hammer hitting the tip of the blade in a damping test). The decay curve may then be filtered to pass through the required natural frequencies and the resulting decay curve can be used to determine the damping as a function of strain amplitude at a reference point (choose preferably the same point as in hysteresis damping case discussed in section 2) in the filtered mode of vibration at the given speed of rotation.

A typical decay curve given in Rao (2011) is given in Fig. 9.

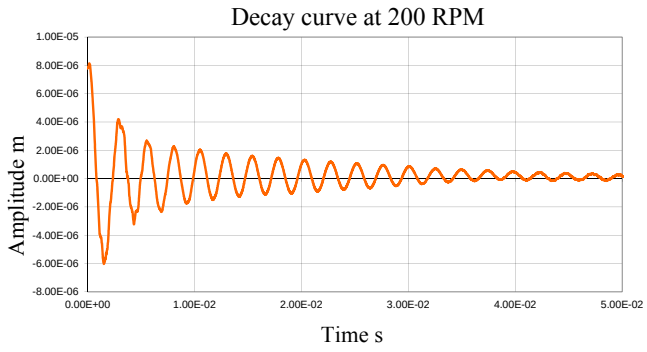

FIGURE 9 Decay from Macro-slip

The damping characteristic from the decay curve as a function of strain amplitude is given in Fig. 10. Note that the relation obtained shows the dependence on the nonlinear characteristic of friction and

unlike the material damping characteristic in Fig. 8 the analytical derivation displays an experimental test looking like phenomenon.

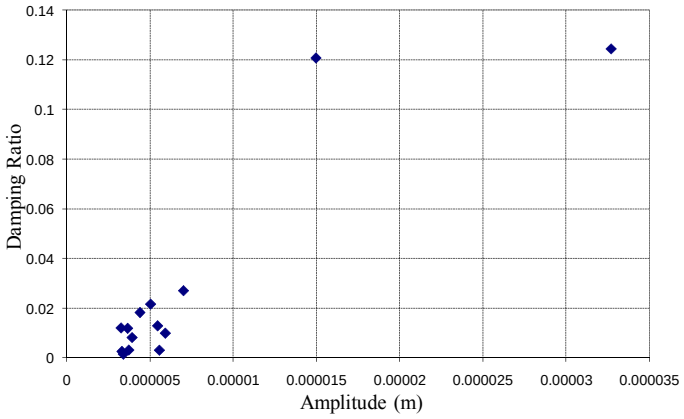

FIGURE 10 Damping from Macro-slip

5. Micro-slip or Fretting Damping

Olofsson and Hagman (1997) gave most promising analytical derivation for fretting fatigue. After a lapse of more than a decade this theory is experimentally put to test by Asai et al (2009). These tests have shown that the tribological derivation from Hertzian contact theory is valid and is therefore adopted here in deriving a nonlinear damping model similar to hysteresis and Coulomb damping considered in sections 2 and 3. Briefly the theory is explained here.

Consider a flat smooth surface in contact with a rough flat surface shown in Fig. 11. The frictional load is parallel to the x axis.

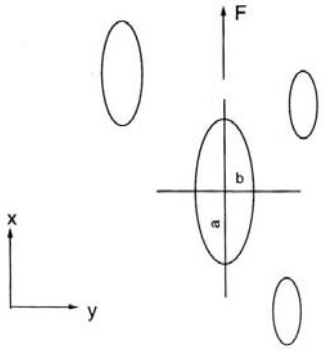

FIGURE 11 Schematic of Contact

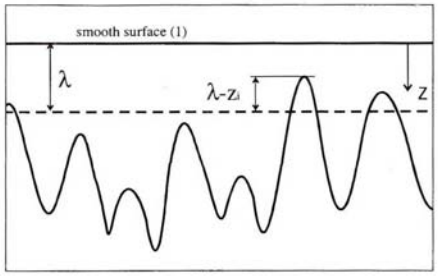

FIGURE 12 Flat Surface in Contact with Rough Surface

The following assumptions are made:

1. Shape of asperities is ellipsoidal
2. Height distribution of asperities is uniform
3. Surface contact is elastic and the behaviour of an individual asperity follows Hertz theory for elliptical contacts
4. All asperities have their semi-axes *a* and *b* in the same global *x*- and *y*- directions, respectively
5. Contacting asperities have the same constant ovality ratio $k = a/b$, $a<b$ and $k = b/a$, $b<a$

The surface is brought into contact with a normal approach λ □□see Fig. 12. □□The normal load, P_i, for an asperity at depth z_i and the major semi-axis c for that asperity is expressed as

$$P_i = \frac{2\pi E'}{k\left(\frac{9}{2\varepsilon R}\right)^{\frac{1}{2}}}\left(\frac{\lambda - z_i}{\kappa}\right)^{\frac{3}{2}} \tag{6}$$

$$c = \left(\frac{3\varepsilon P_i R}{k^2 \pi E'}\right)^{\frac{1}{3}} \tag{7}$$

In the above

E' is the composite modulus of elasticity given by $\frac{1}{E'} = \frac{1-\nu_1^{\,2}}{E_1} + \frac{1-\nu_2^{\,2}}{E_2}$

R is the curvature sum of elliptical contact given by $\frac{1}{R} = \frac{1}{r_{2x}} + \frac{1}{r_{2y}}$ with r as radius of curvature and κ, ε are complete elliptic integrals of the first and second kind with argument $e = \sqrt{1-k^2}$.

The number of asperities in contact, N, is assumed to increase linearly with the approach of the two surfaces. Thus

$$N = Cz \tag{8}$$

where C is a surface parameter which relates the number of contacts per unit area and z the approach of the surfaces. The normal load for the approach λ can be expressed as

$$P = CA\int_0^{\lambda} P_i dz = \frac{4CA\kappa\pi E'}{5k\left(\frac{9}{2\varepsilon R}\right)^{\frac{1}{2}}}\left(\frac{\lambda}{\kappa}\right)^{\frac{5}{2}} \tag{9}$$

where A is the apparent area of contact.

The force-displacement relationship for an individual asperity, i, can be expressed as

$$F_i = \mu P_i\left(1 - \left(1 - \frac{16cG'}{3\mu P_i}\frac{\delta_d}{\phi}\right)^{\frac{5}{2}}\right) \tag{10}$$

where G' is the composite shear modulus given by $\frac{1}{G'} = \frac{2-\nu_1}{G_1} + \frac{2-\nu_2}{G_2}$ and

$$\phi = \left[\frac{4}{\pi(2-\nu_2)}\right]\left[\left(1-\frac{\nu_2}{e^2}\right)\kappa + \frac{\nu_2\varepsilon}{e^2}\right], \quad a < b$$
$$\phi = \left[\frac{4}{\pi(2-\nu_2)}\right]\left[\left(1-\nu_2+\frac{\nu_2}{e^2}\right)\kappa - \frac{\nu_2\varepsilon}{e^2}\right], \quad b < a \tag{11}$$

F_i will deflect upto $F_i = \mu P_i$. Equation (10) gives the limit deflection δ_{Li}

$$\delta_{Li} = \frac{3\mu P_i}{16cG'}\phi = \frac{\pi\mu E'\phi}{8G'}\left(\frac{\lambda - z_i}{\kappa}\right) \tag{12}$$

Equation (12) gives the limit height of the asperities, z_{Li}. Asperities higher than z_{Li} will stick and asperities lower than z_{Li} will slip.

$$z_{Li} = \lambda - \frac{8G'\delta}{\pi\mu E'\phi} \tag{13}$$

The total frictional load becomes

$$F = F_{\text{spring}} + F_{\text{slip}} = \int_0^{z_{Li}} F_i CA dz + \int_{z_{Li}}^{\lambda} \mu P_i CA dz \tag{14}$$

where F_{spring} is the frictional load from the active asperities which have not reached their limiting tangential deflection and F_{slip} is the contribution from asperities which have reached their limiting tangential deflection.

The total frictional load is obtained from using equations (6), (10) and (13) in equation (14)

$$F = \frac{4}{5}\mu CA\kappa\frac{\pi E'}{k\left(\frac{9}{2\varepsilon R}\right)^{\frac{1}{2}}}\left[\left(\frac{\lambda}{\kappa}\right)^{\frac{5}{2}} - \left(\frac{\lambda}{\kappa} - \frac{8G'\delta}{\mu\pi E'\phi}\right)^{\frac{5}{2}}\right]$$
$$= \mu P\left[1 - \left(1 - \frac{8G'\delta\kappa}{\mu\pi E'\phi\lambda}\right)^{\frac{5}{2}}\right] \tag{15}$$

Equation (15) is valid until

$$\delta_{\max} = \frac{\lambda\mu\pi E'\phi}{8\kappa G'} \tag{16}$$

Suppose that after reaching a value F^*, the frictional load F is reduced; the force displacement relationship under unloading for an individual asperity I can be expressed as, see Fig. 13.

$$F_{di} = 2\mu P_i\left[1 - \left(1 - \frac{16cG'\delta_{di}}{2\times 3\mu P_i\phi}\right)^{\frac{3}{2}}\right] \tag{17}$$

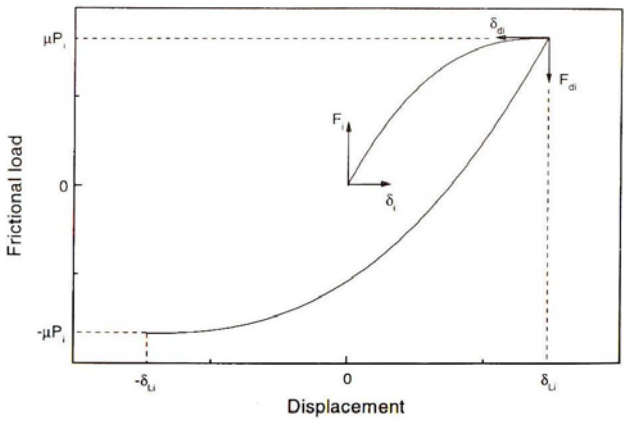

FIGURE 13 Frictional Load vs. Displacement for an Individual Ellipsoidal Body

The corresponding limit deflection for unloading is twice that for loading. The maximum height of the asperities z_{dli} for which they will slip is

$$z_{dLi} = \lambda - \frac{4G'\delta}{\pi\mu E'\phi} \tag{18}$$

The sense of slip must be reversed, but its absolute magnitude is not altered during unloading. Then the slip part of the tangential load during unloading is twice that for loading. The equation for the frictional load during unloading is

$$F_d = \int_0^{z_{dLi}} F_{di} CA dz + \int_{z_{dLi}}^{\lambda} 2\mu P_i CA dz$$

$$= 2\mu P\left[1 - \left(1 - \frac{4G'\delta_d\kappa}{\mu\pi E'\phi\lambda}\right)^{\frac{5}{2}}\right] \tag{19}$$

where δ_d is the reduction in the initially loaded displacement, δ^*, and F_d is the reduction in the initially applied load, F^*.

The equation for frictional load transformed to the original co-ordinate system is

$$F_r = F^* - 2\mu P\left[1 - \left(1 - \frac{4G'\kappa\left(\delta^* - \delta\right)}{\mu\pi E'\phi\lambda}\right)^{\frac{5}{2}}\right] \tag{20}$$

Suppose now that the frictional load is oscillating between F^* and $-F^*$. The situation at $F = -F^*$ is identical with that at $F = F^*$, except for the reversal of sign. Hence the frictional load becomes

$$F_s = -F_r\left(-\delta\right) = -F^* + 2\mu P\left[1 - \left(1 - \frac{4G'\kappa\left(\delta^* + \delta\right)}{\mu\pi E'\phi\lambda}\right)^{\frac{5}{2}}\right] \tag{21}$$

Now consider when $\phi = 1$, $a = b$ (asperities modelled as spheres), then $\kappa = \varepsilon = \frac{1}{2}\pi$, equations (15), (19) become

$$F = \mu P\left[1 - \left(1 - \frac{4G'\delta}{\mu E'\lambda}\right)^{\frac{5}{2}}\right] \tag{15a}$$

$$F_d = 2\mu P\left[1-\left(1-\frac{2G'\delta_d}{\mu E'\lambda}\right)^{\frac{5}{2}}\right] \tag{19a}$$

Asai et al (2009) adapted the formulation above in such a way as to verify Olofsson's formulation for blades. Their microslip damping model of two surfaces under contact with F_t and F_n as tangential and normal forces is given in Fig. 7; the tangential contact stiffness is

$$K_{tc} = \frac{F_t}{d_{stick}} \tag{22}$$

For the linear model without hysteresis, the material property is Imaginary Tangential Contact Stiffness $K_{tc,im}$ given by

$$K_{tc,im} = \frac{F_t}{d_{total}} \tag{23}$$

In Fig. 14, the total displacement is stick and slip as shown and given by

$$\begin{aligned} d_{total} &= d_{stick} + d_{slip} \\ &= \frac{F_t}{K_{tc}} + d_{slip} \end{aligned} \tag{24}$$

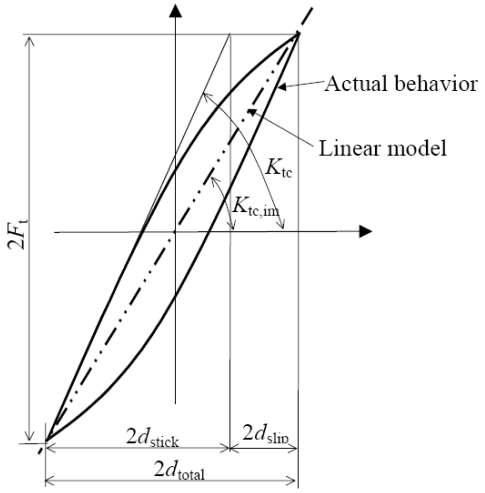

FIGURE 14 Micro-Slip Damping Model

If δ_{slip} is the displacement due to the normal force F_n (slip per unit normal force) and tangential stiffness k_{tc}, we define a parameter

$$\frac{d_{slip}K_{tc}}{F_n} = \frac{d_{slip}}{\delta_{slip}} \tag{25}$$

Under constant normal load, as the displacements are increasing, in Oloffson's model for oscillating displacements, the asperities are replaced by spheres with the same radius. It is assumed that the height distribution of the asperities is uniform and the behaviour of an individual asperity follows Hertz theory. The resulting contact model is

$$\frac{F_t}{F_n} = m\left[1-\left\{1-\left(\frac{K_{tc}d_{total}}{nmF_n}\right)\right\}^n\right] \tag{26}$$

where n and m are constants. Using (24) the above becomes

$$\frac{F_t}{F_n} = m\left[1-\left\{1-\frac{1}{nm}\left(\frac{F_t}{F_n}-\frac{d_{slip}K_{tc}}{F_n}\right)\right\}^n\right] \tag{27}$$

Asai et al (2009) verified the above experimentally for the parameter $\frac{d_{slip}K_{tc}}{F_n}$ as shown in Fig. 15 for three different test specimens. Microslip occurs for large values of F_n ($F_t < F_n$) as shown and d_{slip} values are in the range of 0.1 to 5 microns. m and n are obtained from the mean curve of experimental results.

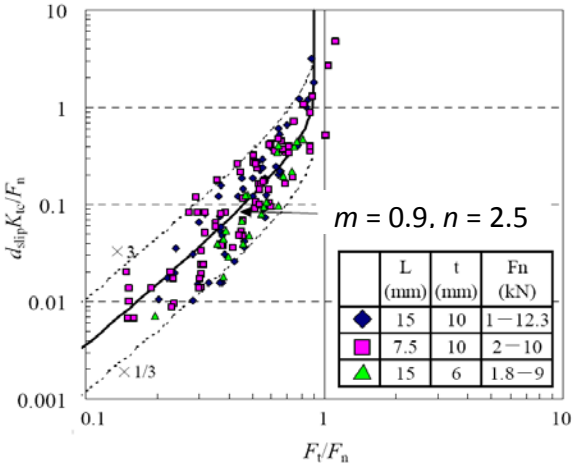

FIGURE 15 Asai et al Experimental Result for Micro-Slip

Asai's experiments have shown that the Hagman and Olofsson elasto-plastic theory of contact provides a workable model for blades given by (15a). The problem however is highly nonlinear and not simple.

$$F = \mu P\left[1-\left(1-\frac{4G'\delta}{\mu E'\lambda}\right)^{\frac{5}{2}}\right] \tag{15a}$$

1. First of all the coefficient of friction μ at asperity level is not known and as given in Olofsson's relation it is dependent on tangential displacement δ.
2. Secondly the steady state condition for the penetration λ is not known.

Otherwise the penetration λ is left to be determined. The penetration can often be achieved directly from the finite element code. If the penalty method is used to simulate contact stiffness, the penetration values can be unreliable. Instead a more reliable variable in finite element simulations, the contact pressure, can be used to calculate the penetration. An empirical relationship between the penetration and the contact pressure, P, can be adequately described by the following equation, see Reshetov and Levina (1965)

$$\lambda = cP^m \tag{28}$$

where c = 0.0014 for ground/ground steel surfaces and m = 0.5 for most metallic materials and for normal contact pressures encountered in joints.

In this report the present status upto the determination of damping in Process Template developed to determine life is described.

6. Process Template TurboManager

Lifing is a multifaceted technology using CFD to determine unsteady forces, structural mechanics to determine natural frequencies for different speeds and obtain Campbell diagram, damping estimate, resonant stress and/or strain, cumulative damage for crossing critical speeds, stress based (HCF) and strain based (LCF) life estimation and fracture mechanics for crack initiation, propagation and unstable fracture conditions determination. There is no single code to achieve this set of calculations. The main goal of this project is to establish such a unified procedure.

There are few standard calculations well established, e.g., CFD of a blade stage and determining unsteady pressure field, structural dynamics codes to determine natural frequencies … Here a process template approach is used to call such of those established methods and perform those calculations that are not available under one platform. TurboManager is a template developed using Altair HyperWorks Process Manager (2011).

Process Manager is a programmable personal workflow manager that guides users through standard work processes, see Ousterhout (1994); Tcl and the Tk Toolkit are used for developing the core and Graphical user interface (GUI) respectively. The Process Manager features are:

1. Process Manager Client is integrated with the HyperWorks desktop.
2. The "Process Tree" displays a series of steps the user executes.
3. A simple checkbox is used to mark completed steps.
4. The GUI provides the ability to re-execute an individual or series of steps automatically.
5. Each process can be run in an interactive mode.
6. Break-points can be set to stop at any step for user-input if/when appropriate.
7. The state of the project can be saved to a persistent file.
8. Process Studio is available for authoring Process Manager Templates.

In HyperWorks, the process *TurboManager* developed has three windows, Process Tree, Process Task and Animation Client as given in chart 1 below.

Chart 1

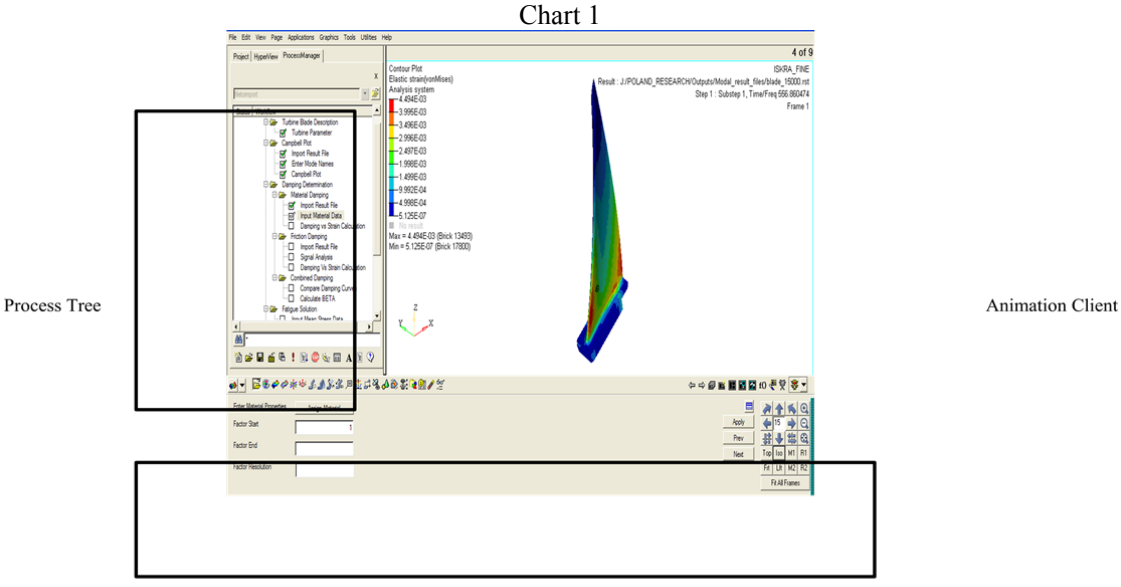

Various steps involved in estimating life of Turbine Blade are captured as tasks in Hyper Works Process Manager Tree, see chart 2.

Chart 2 describes the complete life estimation process to the user. The panel also describes the various inputs and technologies involved in this package. The user can browse and understand the input and theory behind the individual panel.

Turbine parameter panel shown in chart 3 has only one task “Turbine Details”. No of nozzles and Operating speed range are taken in as user inputs. These inputs will be used for making Campbell plot.

Chart 2

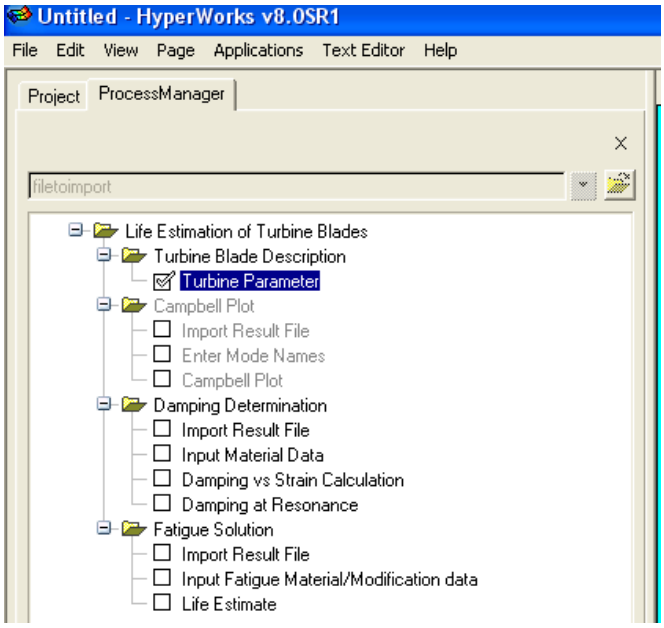

Chart 3

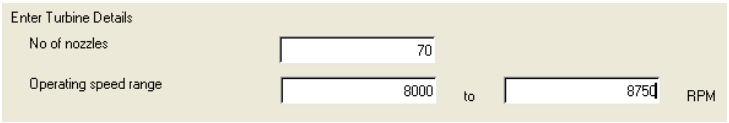

The blade under consideration is from the first report, Rao, Rzadkowski and Vorobievv (2010) given in Fig. 16. It belongs to first stage SO-3 aircraft engine rotating compressor blade. The length of the blade is 0.106 m and is made of 18H2N2 steel with an Ultimate Tensile Strength of 800 MPa and Young’s Modulus of 2.04 MPa. The rotor blade is modelled using 20-node, isoparametric, HEX20 elements.

In the Campbell plot module, the panel in chart 4 invokes HyperWorks post processor Hyperview which is an open platform where results files of various commercially available solvers can be viewed. It provides for importing the modal results (frequencies in Hz of orthonormal modes) of the turbine blade determined by an appropriate code. The user can import results files to capture natural frequencies for different speeds taking into account stress stiffening and spin softening effects. The Campbell plot module will be provided with the capability to prepare deck and launch a suitable solver to obtain these modal results directly in future applications.

Chart 4

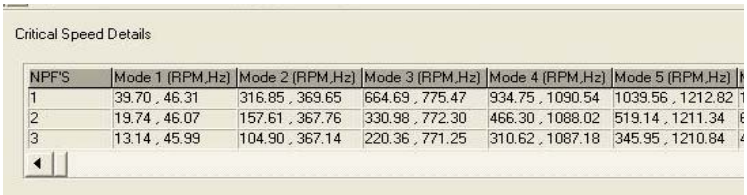

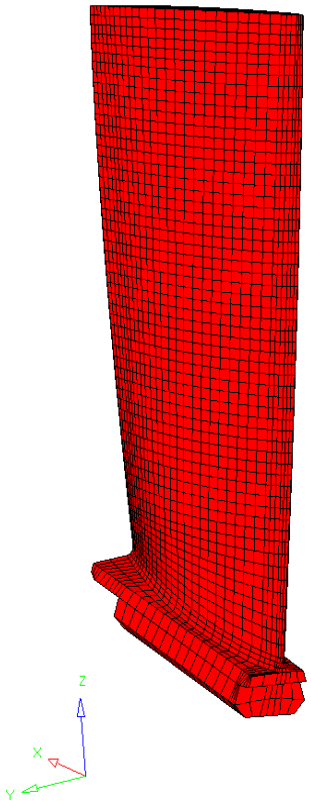

FIGURE 16 First stage of SO-3 engine compressor rotor blade

In Enter Mode Names panel, chart 5 displays all modal frequencies in the imported result file. The user can associate Mode Names for the modes imported. The names defined would be used in the Campbell plot diagram.

Chart 5

Modal Frequency Details

Sl_No	Mode No	Frequency at first Speed	Frequency at second Speed	Mode Name
1	1	45.830276	148.923279	I Bending
2	2	365.890839	466.871124	II Bending
3	3	769.150696	849.952637	I Torsion
4	4	1085.513184	1131.254150	Coupled I Torsion

Campbell Plot panel invokes HyperWorks plot client Hypergraph which is an open platform where results files of various commercially available solver can be plotted. This tool is used to plot the Campbell Diagram. The panel, chart 6 also displays typically the critical speeds (rpm) and corresponding natural frequency (Hz) with a scroll action, to be used by the Life Estimation Module.

Chart 6

Critical Speed Details

NPF'S	Mode 1 (RPM,Hz)	Mode 2 (RPM,Hz)	Mode 3 (RPM,Hz)	Mode 4 (RPM,Hz)	Mode 5 (RPM,Hz)
1	39.70 , 46.31	316.85 , 369.65	664.69 , 775.47	934.75 , 1090.54	1039.56 , 1212.82
2	19.74 , 46.07	157.61 , 367.76	330.98 , 772.30	466.30 , 1088.02	519.14 , 1211.34
3	13.14 , 45.99	104.90 , 367.14	220.36 , 771.25	310.62 , 1087.18	345.95 , 1210.84

Table 3 gives the first five natural frequencies for four different speeds. The results reported in the first six months report, Rao, Rzadkowski and Vorobievv (2010) are also given for a comparison in Table 4; they are in good agree with the present results.

TABLE 3 Natural frequency (Hz) of the cantilever blade obtained at different speed

Mode No.	0 rpm	5000 rpm	10000 rpm	15000 rpm	20000 rpm	25000 rpm
1	339.45	370.42	450.11	556.86	676.96	803.75
2	1336.89	1363.13	1437.59	1548.81	1680.10	1810.14
3	1842.29	1849.28	1870.63	1907.87	1965.17	2051.54
4	2998.33	3008.67	3038.66	3086.10	3149.32	3228.31
5	3805.73	3832.14	3910.69	4038.77	4210.66	4416.31

TABLE 4 Natural frequency (Hz) of the cantilever blade from Rao et al (2010)

Mode No.	**Natural Frequency (Hz)**			
	0 rpm	6800rpm	14500 rpm	15600rpm
1	341.86	396.99	547.62	572.85
2	1342	1389.9	1541.5	1568.9
3	1847.5	1860.6	1909.1	1919.4
4	3114.7	3138.1	3213.8	3227.9
5	3917.7	3962.2	4119.8	4151.2

The Campbell diagram of this blade is given in Fig. 17.

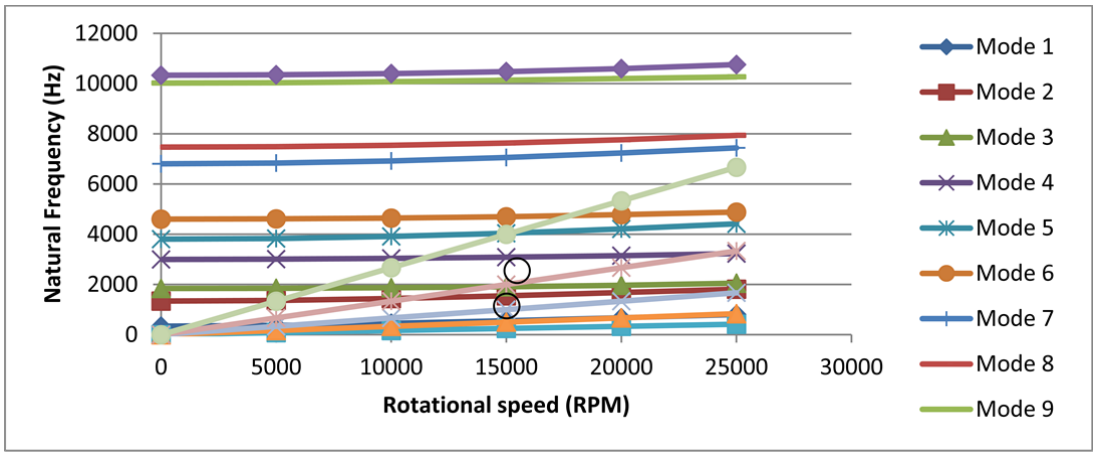

FIGURE 17 Campbell diagram of first stage of SO-3 engine rotor blade

6.1 Damping Estimation (Hysteresis)

In this panel, damping is quantified as a function of strain amplitude at a reference point in the blade as described in section 2. Total damping energy and strain energy are calculated by integrating them over the entire volume of the blade. Then the loss factor is obtained and damping ratio as a function of reference strain amplitude is plotted for the given mode of vibration and speed of operation. Fig. 18 shows the reference element chosen.

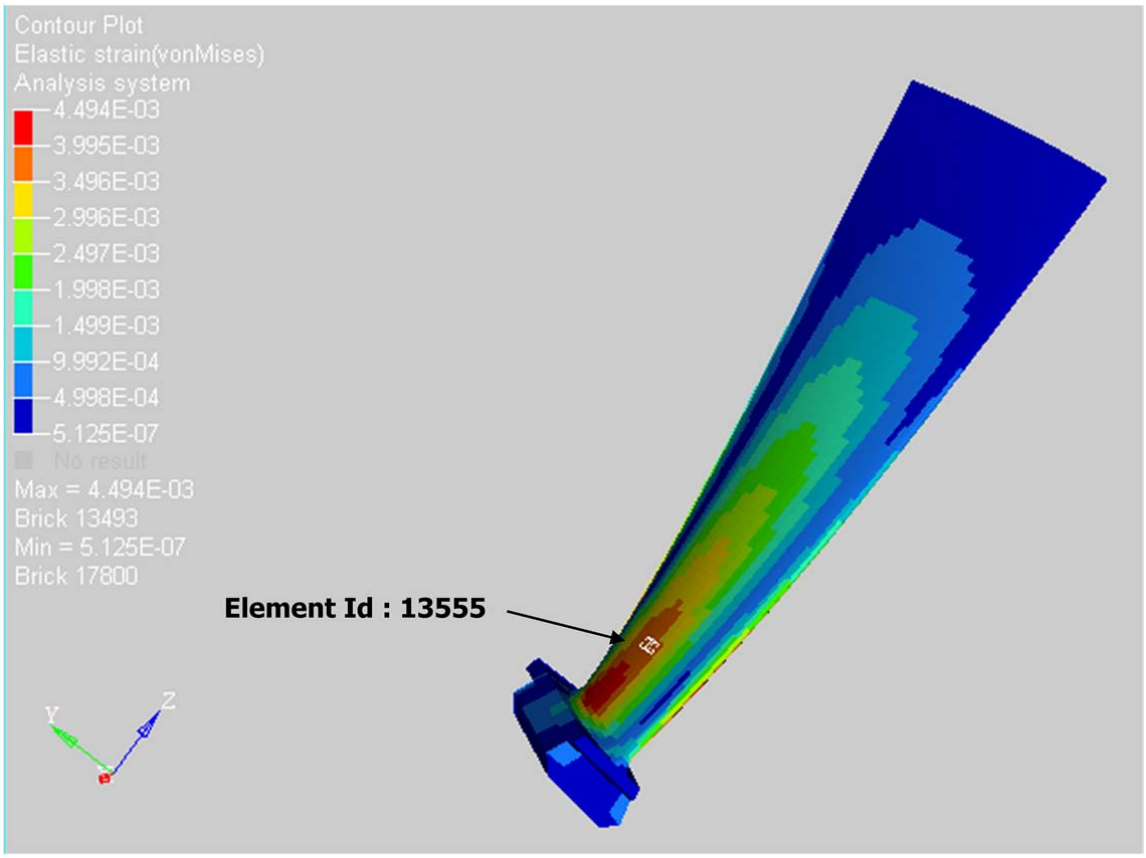

FIGURE 18 Reference Element

The material property used is given by

- Damping Coefficient $J = 16$
- Damping Exponent $n = 2.3$
- Endurance Limit $\sigma_e = 63000$ N/cm^2

Figs. 19 to 21 show the damping in the first three modes of the blade.

These damping values are highly nonlinear depending on the strain amplitude in a given mode shape at an operating speed. The actual condition of strain and damping have to be matched at a resonant condition and thus resonant stress field is to be determined. This will yield the peak stress condition which governs the fatigue. This work is in progress.

6.2 Damping Estimation (Friction)

As discussed, the blade is given an impact at the tip, point A as shown in Fig. 22. In this case 60 N load at $t = 0$ is applied. Poisson's ratio is taken as 0.3. The contact element used is Target 170, Contact 174 and a Friction Coefficient = 0.2 is used.

Fig. 23 shows the decay response obtained captured upto 0.01 sec. In time domain we can see that periodic time of 0.004, 0.0018 and 0.00065 s that correspond to 250 Hz - 1×, 550 Hz, first mode and 1540 Hz, second mode respectively.

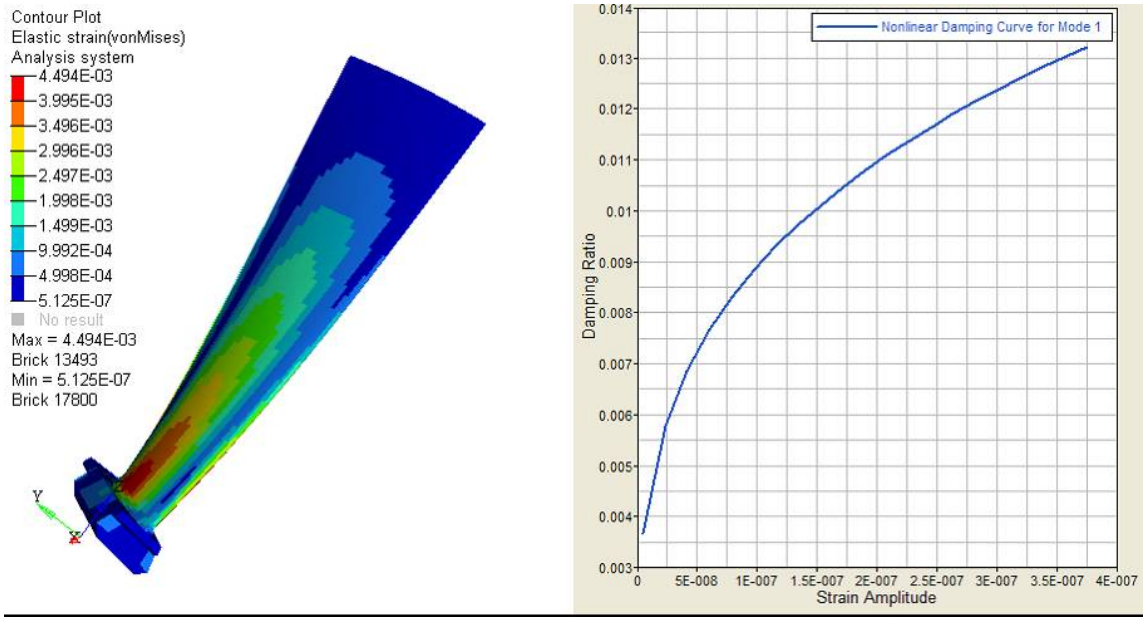

FIGURE 19 First Mode Damping

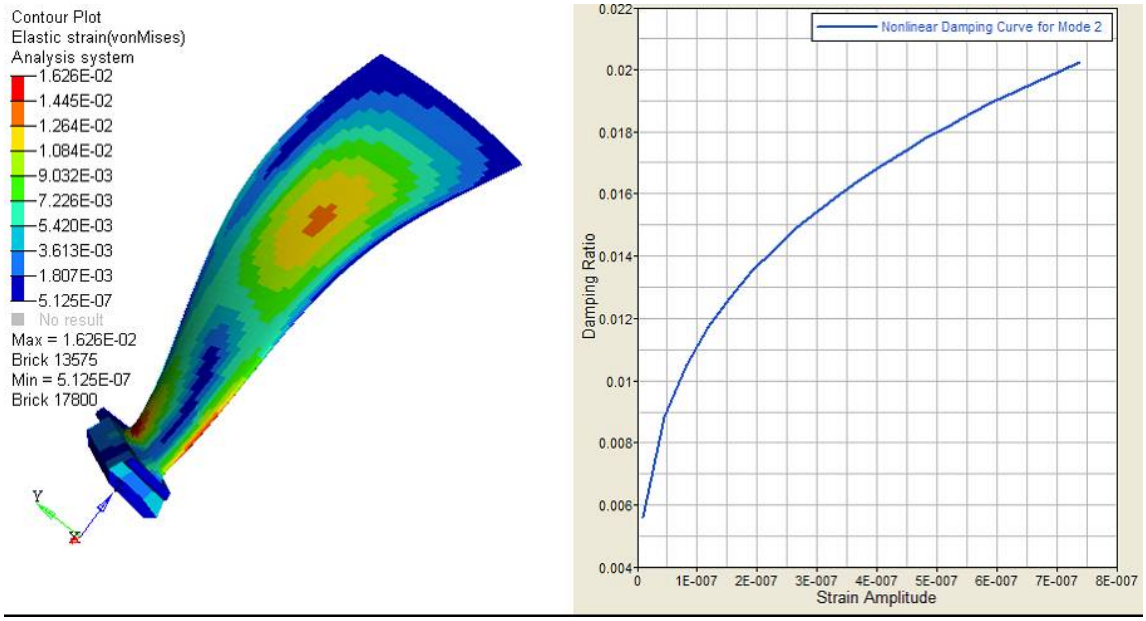

FIGURE 20 Second Mode Damping

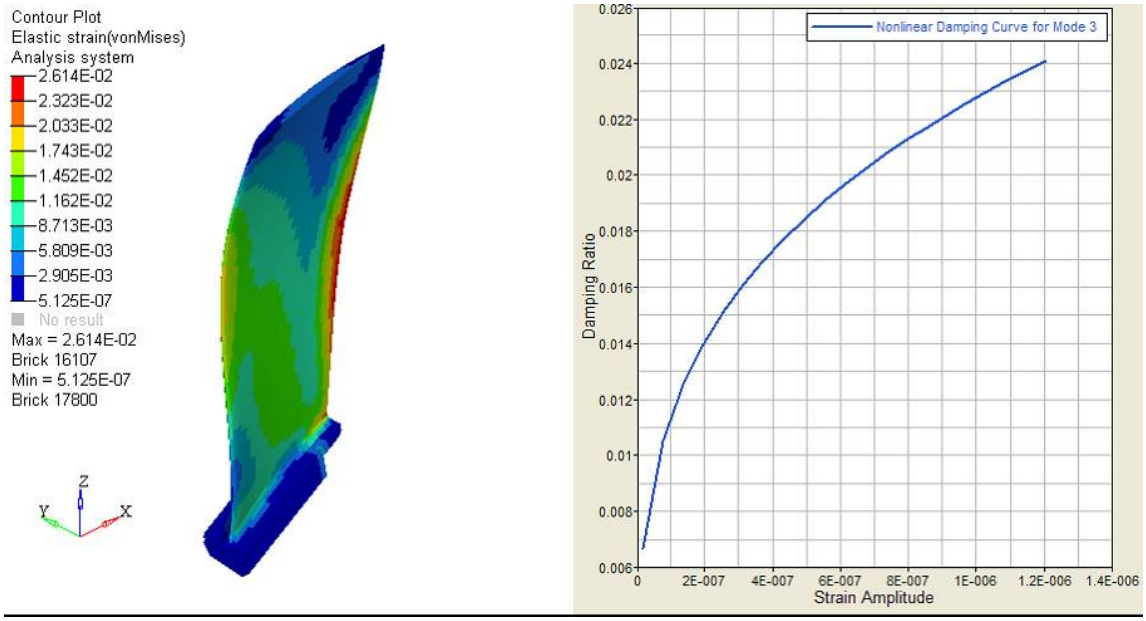

FIGURE 21 Third Mode Damping

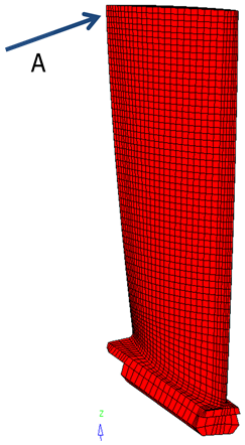

FIGURE 22 Impact Load

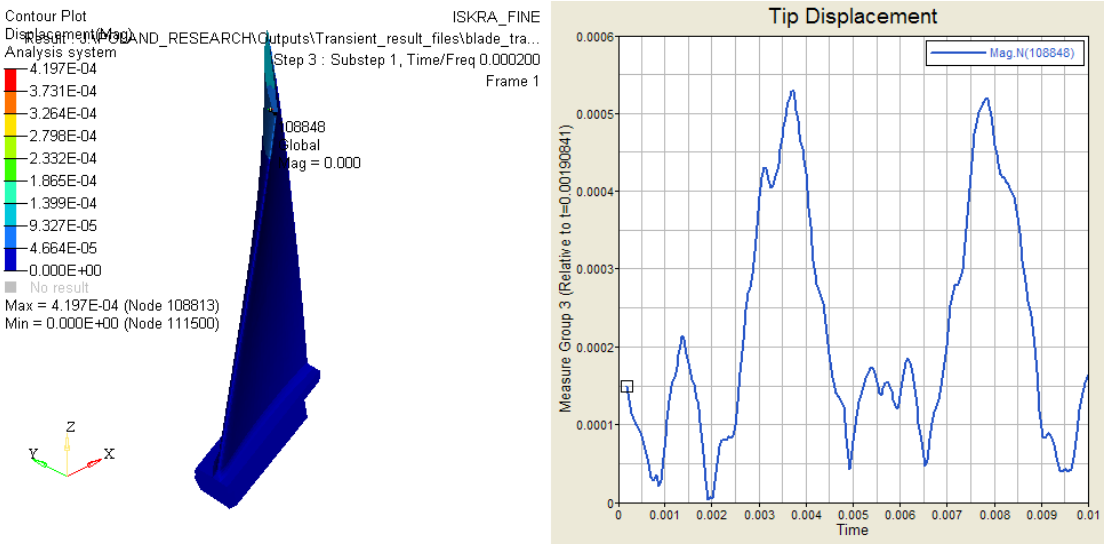

FIGURE 23 Tip Displacement Decay Response

The response decays very slowly. This means friction offers very low damping. This is because the rotational speed is very high 15000 rpm and the resulting centrifugal load makes the blade disk interfaces to be almost closed. We are extracting the response for a longer period and take FFT to get the modal decay curves and equivalent viscous damping in these modes. This will be reported in the next report.

6.3 Damping Estimation (Fretting Friction)

Fretting fatigue study was conducted according to the theory given before and no convergence obtained; indicating that there is Coulomb damping still possible. Fretting regime may be still further away in this case.

Finally the damping in the entire possible strain amplitude for the blade will be defined for each mode at the corresponding critical speed. An iteration procedure to determine the stress response due to this nonlinear damping will be described in the next report.

7. Conclusions

1. The possible resonant conditions that can lead to the failure of first stage compressor rotor blade are identified
2. The excitation force and harmonics are identified from a CFD analysis
3. Classical resonance and possible blockages similar to a bird strike are identified
4. FFT has been done to get the specific frequencies of excitation
5. Detailed CFD analysis is being made to obtain the pressure distribution of possible excitation harmonics leading to resonance. Since the inertia terms at high speed conditions dominate nonviscous flow conditions are assumed to reduce computational time
6. Damping is the main uncertainty in the lifing exercises and an analytical determination procedure for hysteresis and slip damping is developed. Both macro (Coulomb) and micro (Fretting) slip conditions are considered.
7. A template is developed to determine the nonlinear damping model; damping that depends on strain amplitude in a given mode of vibration for a given speed of rotation corresponding to a resonant condition.
8. A method of using this nonlinear damping model to determine the resonant stress is to be completed after having the pressure distribution from CFD analysis.
9. Stress based and Strain based lifing algorithms through a template are under development using the resonant stresses or strains depending on the applicability of HCF or LCF for the specific condition of resonance
10. A cumulative damage calculation is under development to pass through a critical speed with a given acceleration of the rotor
11. Fracture mechanics for propagation life is also under development using crack elements described in the first report

List of Symbols

A apparent area of contact
a, b semi-axes in x and y directions
C surface parameter, viscous damping coefficient
C_e equivalent viscous damping coefficient
c major semi-axis
D loss of energy per cycle
D_0 total loss of energy in the body
d_{slip} slip displacement
d_{stick} stick displacement
d_{total} total slip and stick displacement
E' composite modulus of elasticity given by

$$\frac{1}{E'} = \frac{1-\nu_1^2}{E_1} + \frac{1-\nu_2^2}{E_2}$$

F friction load, factor
F_t tangential (friction) load
F_n normal load
F^* initially applied load
G' composite shear modulus given by

$$\frac{1}{G'} = \frac{2-\nu_1}{G_1} + \frac{2-\nu_2}{G_2}$$

J material property
k ovality ratio a/b, $a<b$ and b/a, $b<a$.
K modal stiffness
K_t shear (tangential) stiffness
K_{tc} tangential contact stiffness
$K_{tc,im}$ imaginary tangential contact stiffness
M modal mass
N number of asperities in contact
n exponent in friction equation, material property
P normal load
P_i normal load for an asperity at depth z_i
R curvature sum of elliptical contact $\frac{1}{R} = \frac{1}{r_{2x}} + \frac{1}{r_{2y}}$
r radius of curvature
v volume
W_0 modal strain energy
z_i depth of an asperity
δ displacement
ε strain
η loss factor
κ,ε complete elliptic integrals of the first and second kind with argument $e = \sqrt{1-k^2}$
ϕ see equation (11)
λ normal approach or penetration
σ stress
μ friction coefficient
ν Poisson's ratio
ξ viscous damping ratio
ω natural frequency

References

Altair HyperWorks 11.0 suite manuals, 2011

Asai K, Sakurai S, Kudo T and Ozawa N, Evaluation of Friction Damping in Dovetail Root Joints based on Dissipation Energy on Contact Surfaces, ASME Turbo Expo, GT2009-59508, 2009

Lazan, B. J., *Damping of Materials and Members in Structural Mechanics*, Pergammon, 1968

Olofsson U and Hagman L, (1997) A model for microslip between flat surfaces based on deformation of ellipsoidal elastic bodies, *Tribology International*, 30, 8, p. 599.

Ousterhout, J. K., *Tcl and the Tk Toolkit*, Addison Wesley, Reading, Massachusetts, May 1994

Rao, J. S., *History of Rotating machinery Dynamics*, History of Mechanism and Machine Science Series 20, Springer, 2011

Rao, J. S., Rzadkowski, R and Vorobievv, Yu, S., Crack Propagation in Compressor Rotor Blade – Report for first six months, April – September 2010, (Grant FA8655-10-1-3062), European Office of Aerospace: Research and Development, 86 Blenheim Crescent, Ruislip, Middlesex HA4 7HB, United Kingdom, October 2010

Rao, J. S and Saldanha A, Turbomachine Blade Damping, *Journal of Sound and Vibration*, v. 262, Issue 3, 2003 p. 731

Reshetov D. N and Levina Z. M., Machine Design for Contact Stiffness, *Machines and Tooling*, vol. 36, 1965, p. 15

Rao, J. S., Fracture Mechanics Analysis of A Steam Turbine Blade Failure, *Proc. 1995 Design Engng Technical Conferences*, DE-Vol. 84-2, ASME, p. 1173, September 17-21, (1995), Boston.

Rao, J. S., Fracture Mechanics in TurboManager Quickens Blade Failure Investigations, *International Review of Aerospace Engineering (I.RE.AS.E)*, vol. 2, No. 6, p. 329, (2009)

Rao, J. S., *Turbine Blade Life Estimation*, Narosa Publishing House, (2000).

Rao, J. S., Narayan, R. and Ranjith, M. C., Lifing of Turbomachine Blades – A Process Driven Approach, *Advances in Vibration Engineering*, The Vibration Institute of India, vol. 9, No. 1, (2010)

List of Figures

List of Tables

Annexure 1
Plan of Work

First year

1. Model and perform Modal stress analysis of one compressor rotor blade of SO-3 to find the possible crack initiation locations.

2. Modelling of different crack depths using a three-dimensional finite element model with the 3D prismatic quarter point Isoparametric elements of Vorobiev et al. (2004) and 20 noded Isoparametric elements.

3. Calculating natural frequencies of blades for different crack lengths.

4. Calculation of unsteady pressures acting on compressor rotor blade in a stage – using transient analysis in Fluent.

5. Determine material and friction damping values as a function of strain amplitude in each mode of vibration interest using Process Driven Approach codes developed on HyperWorks platform by Rao et al, (2010).

Second year

7. Determine resonant stresses at critical speeds.

8. Stress Intensity Factor approach will be used for fatigue crack initiation studies.

9. Stress Intensity Factor approach will be used for fatigue crack propagation studies with the help of Paris law.

10. Determine crack propagation using finite element model under the alternating stress

11. Compare Paris values, FE model values and experiments

Crack Propagation in Compressor Rotor Blade

(Grant FA8655-10-1-3062)

Report for Third Six Months

April – September 2011

R. Rzadkowski[1] J.S. Rao[2], Yu.S. Vorobiev[3]

[1]The Szewalski Institute of Fluid Flow Machinery, Gdansk, Poland

[2]K L University, Green Fields, Vaddeswaram, India

[3]National Ukrainian Academy of Sciences, Ukraine

Submitted to
European Office of Aerospace:
Research and Development
86 Blenheim Crescent
Ruislip, Middlesex HA4 7HB
United Kingdom

November 20, 2011

Investigators

1. Principal Investigator: Professor Romuald Rzadkowski
The Szewalski Institute of Fluid Flow Machinery,
Fiszera 14, 80-952 Gdansk, Poland
Tel: +48502975518
E-mail: z3@imp.gda.pl

2. Senior Investigator and Mentor: Prof. J.S Rao
Protem Chancellor
K L University, Green Fields
Vaddeswaram, India 522502
Tel: +91 98453 46503
E-mail: jsrao@kluniversity.in

3. Investigator: Professor Iurii Vorobiov
Department of Non-stationary Mechanical Processes,
Podgorny Institute for Mechanical Engineering Problems,
National Ukrainian Academy of Sciences, Ukraine
E-mail:vorobiev@ipmach.kharkov.ua

4. Investigator: Dr Marina Chugay
Department of Non-stationary Mechanical Processes,
Podgorny Institute for Mechanical Engineering Problems,
National Ukrainian Academy of Sciences, Ukraine
E-mail: chugay@ipmach.kharkov.ua

5. Investigator: Dr Marcin Drewczyński
Assistant Professor
The Szewalski Institute of Fluid Flow Machinery,
Fiszera 14, 80-952 Gdansk, Poland
E-mail: mdrew@imp.gda.pl

6. Investigator: Dr. Ryszard Szczepanik
Assistant Professor
Air Force Institute of Technology
01-494 Warszawa, Poland
E-mail: ryszard.szczepanik@itwl.pl

7. Investigator: Mr. Narayan Rangarajan
Lead Engineer, Altair Engineering (India)
Tel: +91 80 6629 4500/ 4700 (Fax)
E-mail: narayan.rangarajan@altair.com

8. Investigator: Mr. Rejin Ratnakar
General Motors (India) Bangalore
Tel: +91 99860 15670
E-mail: rejin.ratnakar@gm.com

Table of Contents

Summary

In the first six months report (*April-September 2010*) *modal stress analysis was carried out on one compressor rotor blade of an jet engine to locate the possible crack initiations. Various crack depths and lengths were created using a three-dimensional finite element model with the 3D prismatic quarter-point isoparametric elements and 20-node isoparametric elements to calculate the natural frequencies and mode shapes of the rotor blades.*

In the second six months report (October 2010 - March 2011), the methodology to analytically determine a nonlinear damping model as a function of strain amplitude at a reference point in a given mode of vibration at a given speed of rotation of bladed-disk is described. Both material and friction damping are included. The friction damping is considered for both macro (Coulomb) and micro (fretting) slip conditions. For the blade under consideration, these damping values are determined and presented. The damping estimation process is developed on HyperWorks platform by calling suitable solvers for determining the mode shapes. The pre-processing is done by using HyperMesh and post-processing is carried out by using HyperView.

In this report for the six months April – September 2011, the excitation pressure field due to a bird hit is simulated using CFD and unsteady pressure field is determined on the rotor blade pressure and suction surfaces. A bird strike is simulated by two or three blade passage blocks in the incoming flow and the pressure field is obtained from a CFD code. For the blade the Campbell diagram is prepared and the critical speeds are identified. The alternating pressures corresponding to the critical speed are obtained from an FFT. A nonlinear damping model is estimated using Lazan's hysteresis law using previously developed model; the equivalent viscous damping model is determined as a function of reference strain amplitude in the given mode of vibration at the rotational speed. An iterative solution is developed with the nonlinear damping model and the resonant stress and location is determined. The life at this critical speed is determined using a cumulative damage criterion developed.

1. Introduction

In the determination of life of a turbomachine blade, unsteady forces acting on rotor blades and damping plays the most significant role in accurately assessing the peak stress and strain levels at a critical speed while starting the engine or shutting down. The previous reports [1,2] discussed and presented the procedures used in developing a nonlinear model for damping and dependent on the state of stress condition in the rotating blade for a given mode of vibration at an operating speed or critical speed.

In this third report we will consider the unsteady pressure field on the rotor blade due to a bird strike simulated as a blockage in the inlet struts. FFT analysis is conducted to identify all possible excitations arising out of the transient response. Based on the Campbell diagram the critical speeds are identified. The severe conditions of blade loading, the magnitude and frequency of the unsteady forces are identified. The excitation is an impulse type or shock type loading lasting few milliseconds. Two different cases are identified one with an operation at a critical speed before reaching the full speed during coast-up of the engine in the take-off period and the other at full operating speed. In this report the 8× harmonic at operating speed is considered for demonstrating the lifing process.

The nonlinear damping is modelled as an equivalent viscous damping given by a function of strain amplitude of a rotating turbomachine blade at one of the natural frequencies on the Campbell diagram for a given speed of rotation.

An iterative procedure for determining the resonant stress at a critical speed using the nonlinear damping model is presented. This resonant stress together with the mean stress allows an accurate determination of damage suffered by a blade while crossing a critical speed. The expected life due to a bird strike is thus determined.

2. Unsteady forces acting on rotor blades

The 3D model of the first stage of the jet engine compressor under consideration is shown in Fig. 1. The model is created using Gambit program and consists of 44 blades in the Inlet Stator Cascade, 28 blades in the Rotor Cascade (only one is shown) and 34 blades in the Stator Cascade of the first stage. The reference rotor blade in Fig. 1 is divided into 10 cross-sections.

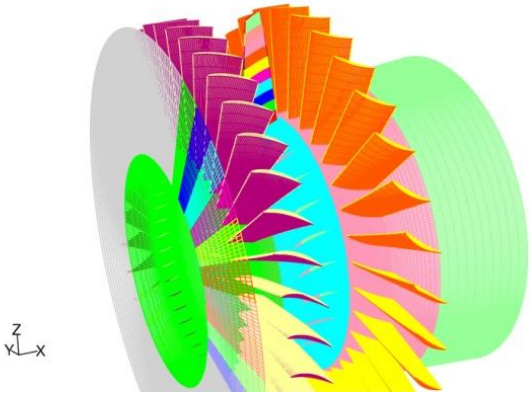

Fig. 1 CFD model of an SO-3 engine first stage compressor

A quarter of the area of the inlet of the engine is divided into 11 segments as shown in Fig. 2. During the simulations three operating states were analysed;

1. Nominal state (fully-opened inlet)
2. One segment blocked and
3. Four segments blocked.

The fourth partially blocked inlet caused a local disturbance of the flow. Fig. 3 presents the contours of Mach number in the stage around the blocked area.

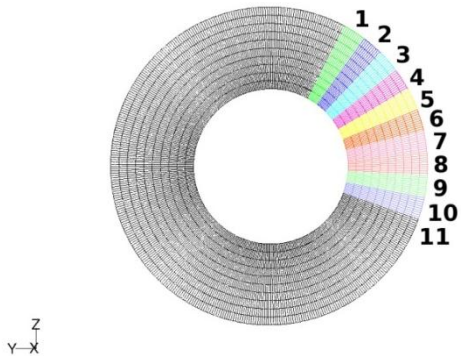

Fig. 2 View of Inlet's segments

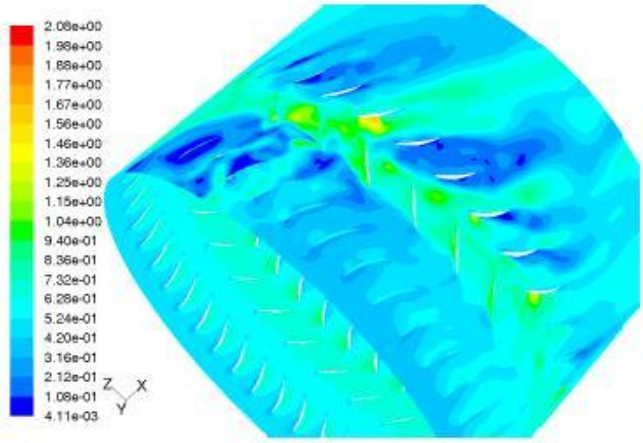

Fig. 3 Contours of Mach number – blocked area

Fig. 4 presents a comparison of results for an unblocked inlet (red), a single blocked inlet segment (green) and four blocked inlet segments (blue). It is clearly visible that the blocked inlet segment has a strong local influence on the amplitude. The red line in Fig. 4 shows the axial force in operating conditions (with unblocked inlet) with time period = 0.90909×10^{-4} sec corresponding to NPF 44×250 = 11000 cps. The green and blue lines represent the results in the off-design case (with one and four blocked inlet segments). The four blocked inlet segments have a stronger local influence than the single blocked inlet segment. The local maximum for the four segments was slightly above 100 N, while for the single segment it was 50 N.

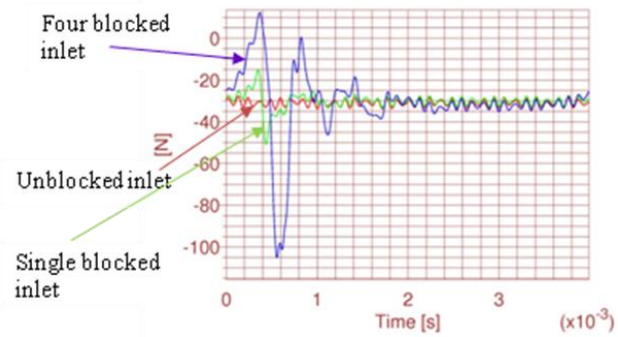

Fig. 4 The average force for different cases of blocking inlet segments

The FFT of time domain signals in Fig. 4 are given in Fig. 5. The four blocked inlet segments (blue) caused low-frequency harmonics of higher amplitude (30% of the steady part) than the single blocked inlet (green) with just 7% of the steady part, see Fig. 5. The peak value occurred at a frequency 2006.02 Hz i.e., 120361.2 RPM. This is 8× component of 15000 RPM operating speed, which is not close to natural frequency of rotor blade (see Table 1). Life estimation is made assuming that the blade responds at this resonance with the flow blockage from a bird hit.

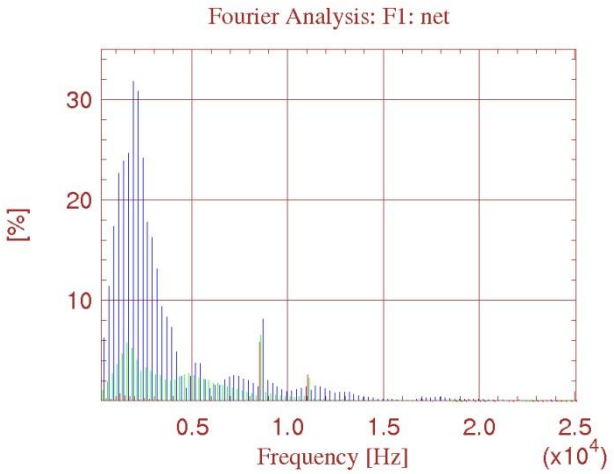

Fig. 5 Unsteady axial force harmonics of blocked and unblocked inlet

3. Campbell diagram

The CAD model of the blade for structural analysis is shown in Fig. 6. The natural frequencies determined for different speeds are reported in Table 1. Campbell diagram obtained from *TurboManager* is shown in Fig. 7.

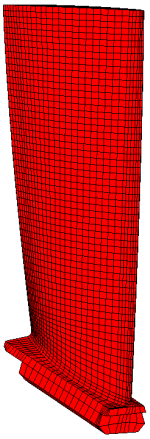

Fig. 6 CAD Model of Blade

Table 1 Natural Frequencies in Hz

Mode	0	5000	10000	15000	20000	25000
1	339	370	450	556	677	804
2	1336	1363	1437	1548	1680	1810
3	1842	1849	1870	1907	1965	2051
4	2998	3008	3038	3086	3149	3228
5	3805	3832	3910	4038	4210	4416

3.1 Results from Stage Calculations without any blockage

The fundamental excitation is NPF at 44×250 = 11000 Hz; the time period is 0.90909×10^{-4} sec. This is the main component as can be seen in Figs. 4 and 5; the excitation magnitude is small. Also the Campbell diagram in Fig. 7 does not show a blade mode at this high frequency. From the Campbell diagram of the first stage compressor tuned bladed disc (Fig. 7), one can see that 2EO excitation at 15000 rpm can cause blade resonance stress. Usually this component of excitation can be predominant because of misalignment arising out of operation hours.

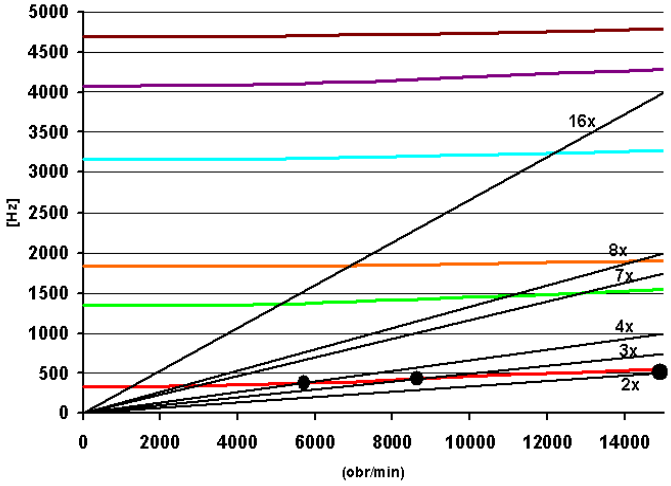

Fig. 7 Campbell diagram for first compressor stage of jet engine

3.2 Results from Four Block Segment Closure Calculations

For four block segment closure, the time period is $4\times0.90909\times10^{-4} = 3.6363\times10^{-4}$ sec. The corresponding frequency is 2750 Hz (11×). Therefore at a speed of $\frac{1919}{2750}\times15000 = 10467$ rpm, resonance occurs with the third mode.

We should note here that the time period cannot be calculated as above, because it all depends on how the wakes shed by the upstream blade with this four block segment work; Fig. 5 shows the major component is at 2000 Hz rather than 2750 Hz. This means that at a speed slightly below 15000 rpm, we have resonance with 1907 Hz third mode frequency.

The pressure field at this excitation can be determined from CFD analysis and apply it on a structure code to find the resonant stress.

3.3 Results from One Block Segment Closure Calculations

Fig. 5 shows that the frequencies are similar, the major component is slightly lower in frequency than case 2, but the magnitude is significantly less.

We notice that a block simulated (as in a bird strike) produces resonance at 1919 rpm 3rd mode natural frequency. We can consider the worst case pressure field and estimate the resonant stress.

In determining the resonant stress, it is just not the magnitude of pressure load, but also the damping that is more important. This is usually weak link in all lifing exercises. The procedure to determine analytically a nonlinear damping model that gives more accurate lifing results has been described in the previous report for the second six month period. Table 2 gives the worst case (highlighted) of loading to estimate life.

Table 2 Worst case of loading

Harmonic	Frequency	No	One	Four
1	250.75	0.0638	0.5369	3.2108
2	501.51	0.0684	0.7601	7.6735
3	752.26	0.0526	1.0287	10.3333
4	1003.01	0.1598	1.4220	11.8097
5	1253.76	0.2471	1.8324	11.2942
6	1504.51	0.1903	2.4363	9.0390
7	1755.27	0.1493	2.5192	12.4782
8	2006.02	0.0841	2.2132	13.4424
9	2256.77	0.0607	1.5821	11.8532
10	2507.52	0.2536	1.3225	10.5429
34	8525.58	2.6664	2.9217	3.7234
44	11033.1	0.8402	0.7461	0.2149

4. Material (Hysteresis) Damping

A plot of equivalent viscous damping ratio as function of reference strain amplitude in the chosen mode of vibration defines the nonlinear damping model. This process is captured in TurboManager.

For the third mode of vibration identified in Table 2 the hysteresis damping is determined. The reference element ID chosen is 13555 as shown in Fig. 8. The material properties are taken as J = 16, n = 2.3 and σ_e = 63000 N/cm^2

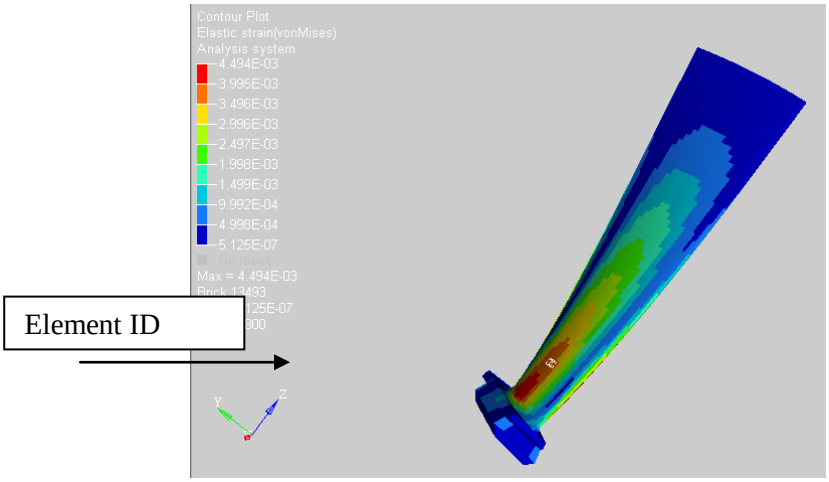

Fig. 8 Reference Element

For the third mode under consideration, the hysteresis damping is obtained as equivalent viscous damping ratio as a function of strain amplitude at the reference point at the operating speed and shown in Fig. 9.

This damping model is used in evaluating the resonant stress for making a life estimate.

The Coulomb friction damping and fretting damping are neglected here because of very high speed of operation.

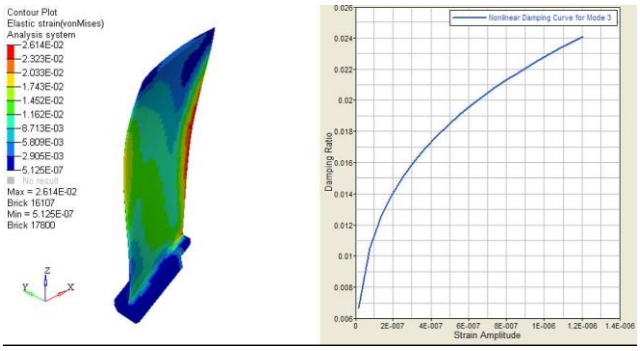

Fig. 9 Nonlinear Damping in third mode of the blade

5. Mean Stress on the Blade

The material Young's modulus *E* is taken as 203000 MPa. At the operating speed 15000 rpm the peak value of mean stress is obtained as 100 MPa given in Fig. 10. This peak stress and peak alternating stress occurred at the same location.

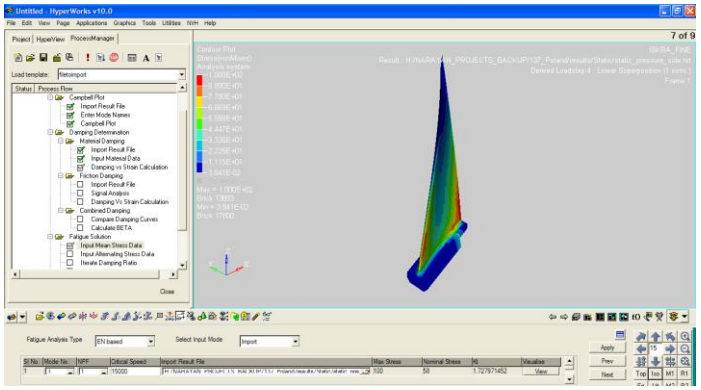

Fig. 10 Mean stress at the operating speed

6. Alternating Stress

The average force on the blade for the worst case of loading is taken from Table 2 for the purpose of estimating the alternating stress. This force is divided by the area of the blade and it is assumed as average alternating pressure at the critical speed. To estimate the resonant stress the alternating load is first considered as steady pressure and the stress distribution is obtained. The peak value obtained is 9.17 MPa.

The resonant stress is then determined by multiplying with the quality factor $\frac{1}{2\xi}$. However, the damping ratio that corresponds to the resonant stress is not known apriori. Hence an iteration process is used to determine the correct damping and resonant stress by using the nonlinear damping obtained earlier in Fig. 9.

In the first iteration a damping ratio is assumed and the first resonant stress is estimated. With this resonant stress the second iterated damping value is obtained from Fig. 9. For this damping the next estimate of resonant stress is determined and checked against the previous value. This iteration is continued until the desired convergence is obtained. This procedure is automated in *TurboManager*.

The bird hit case however is not the case of crossing a critical speed or operating at or near a critical speed. The bird strike takes place at the designed operating speed during a take-off operation. Here the speed might have reached full speed or it may be still going up to full speed during take-off. Then there are two possibilities.

1. As the speed increases during take-off the bird strike might take place at a critical speed below the operating speed, e.g., at 14302.5 rpm with 8× exciting 1907 Hz third mode frequency. We then need CFD work to be carried out at this speed 14302.5 rpm and obtain the pressure field and carry out determining the resonant stress.
2. If the engine has reached full speed 15000 rpm, there is no resonance and transient vibrations occur at a natural frequency, here the closest one is the third mode 1907 Hz. Note that the bird strike forces act for a few milliseconds. Therefore the major component of response will be at the closest natural frequency, which is akin to resonance at 15000 rpm.

In either case there is a shock load and transient analysis with the excitation pressure field is to be carried out. This calculation is under progress and will be reported subsequently in the next six months period. For the time being the resonant stress and the damping after reaching convergence are obtained at the operating speed from TurboManager as shown in Fig. 11.

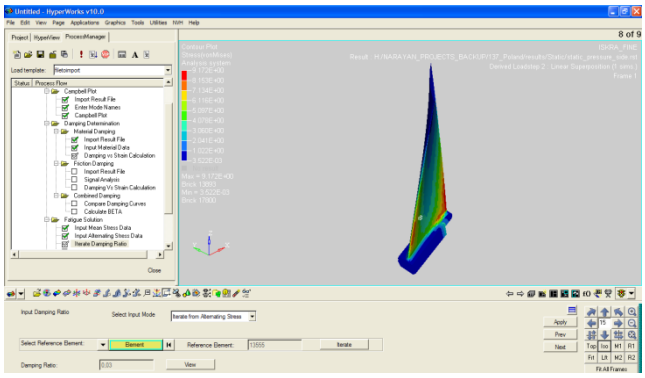

Fig. 11 Resonant stress and damping ratio

The iterated Damping ratio is 0.03 with the maximum alternating stress = 152 MPa. The peak alternating stress occurred at element 13893 as shown in Fig. 12. A zoomed view of this stress is shown in Fig. 13. The mean stress at this location from Fig. 9 is 100 MPa.

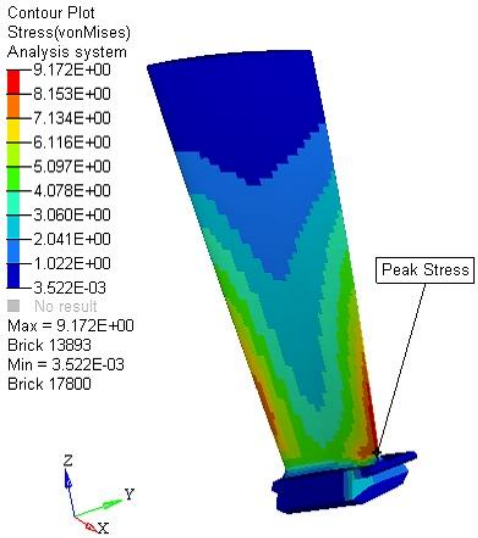

Fig. 12 Resonant stress Location

When resonance occurs the stress rises to resonance and falls rapidly. This rise and fall depends on the acceleration with which the blade is taken through resonance. TurboManager determines the stress - speed variation as shown in Fig. 14.

In determining this quasi-steady stress as a function of speed ratio $r = \omega/p$, the following magnification factor is used in *TurboManager*.

$$H(\omega) = \frac{1}{\sqrt{(1-r^2)^2 + (2\xi r)^2}}$$

This variation can be used to determine the cumulative damage for each crossing at critical.

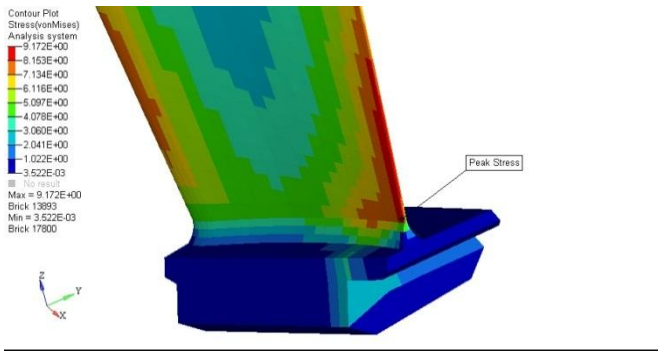

Fig. 13 Zoomed view of Resonant stress Location

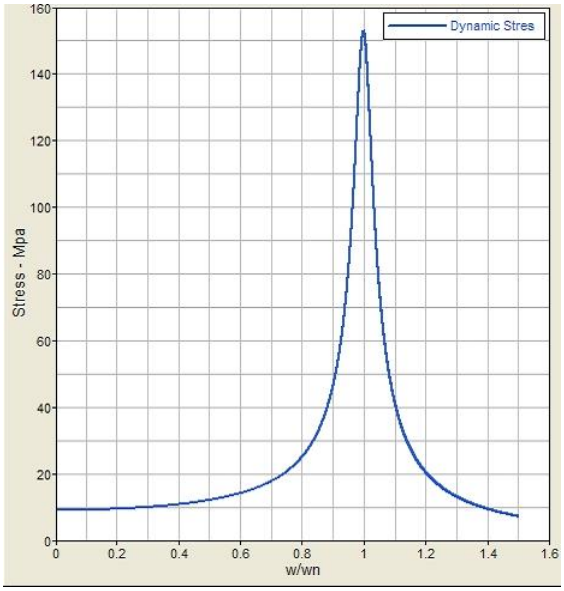

Fig. 14 Resonant stress at critical speed at element 13893

7. Fatigue Modification of the Blade

The endurance limit of the material needs to be updated for the component taking into account various factors. The following fatigue material data is assumed in updating the endurance limit as shown in Fig. 15.

σ_u = 863 MPa

σ_e = 400 MPa

K_t = 1.7

TurboManager evaluates the modification. Fig. 15 shows the panel for this calculation. The fatigue reduction factor is estimated to be 0.588. The surface finish, size effect will pull down this factor further; however it is left conservative in this manner.

Modified endurance limit for the blade then is estimated to be 256 MPa.

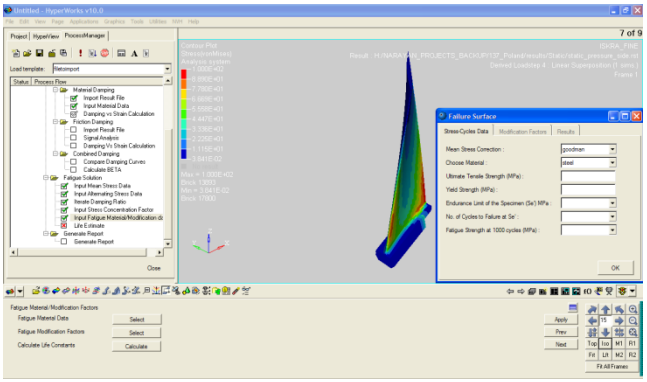

Fig. 15 Fatigue Strength Reduction

8. Life

As the alternating stress magnitude is in the elastic range strain based life estimation was not attempted.

The material properties assumed for the blade are

Fatigue Strength Coefficient $\sigma f' = 1165$ MPa

Fatigue Strength Exponent $b = -0.075$

Fig. 14 gives quasi-steady stress distribution of dynamic stress around the critical speed 15045 rpm. Usually we can calculate the damage suffered by the blade while crossing the critical speed either by a linear Palmgren-Miner damage rule or by nonlinear Marco-Starkey rule (or any other rule for which material data may be available. In the present case the unsteady pressure suffered by the blade is due to bird impact which lasts for a small period of time; however the blade suffers transient impact response at resonance which will last for some time. Therefore a continuous response is assumed with resonant stress to estimate life. Under these conditions, TurboManager estimated life as shown in Fig. 16.

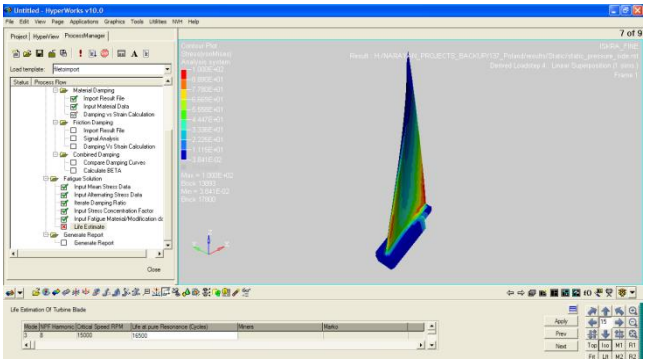

Fig. 16 Life for continuous operation at 15045 rpm

The estimated Life at 15000 RPM is given as 16500 cycles. Under the above circumstance the blade would last for $\frac{16500}{2006.02 \times 60} = 0.137$ sec

9. Conclusion

- A bird impact is modeled as a block in the flow path that generates transient high pressure distribution on the first compressor rotor as a shock for few milliseconds.
- FFT analysis has shown that this pressure distribution has a predominant 8× frequency component at the operating speed.
- For four block segment closure, resonance occurs at 10467 rpm running speed during coast-up condition with the third mode.
- Two cases are identified for life calculation using transient impulse excitation lasting few milliseconds.
- For the present, a simplified case of resonance arising out of free vibrations at the nearest natural frequency i.e., the third mode was considered at the operating speed.
- To determine resonant stress the hysteresis damping alone was considered here, since at high operational speeds, friction can be neglected.
- The material damping is determined in the III mode of vibration as a function of reference strain amplitude at the operating speed. This nonlinear damping model is used by an iteration procedure to obtain the resonant stress.
- The fatigue strength reduction is estimated for the blade and using the material endurance limit the blade fatigue limit stress is obtained.
- As the alternating stress is within the elastic range, stress based life estimation is adopted. Together with the mean stress and the iterated alternating stress the life is determined.

10. Next Work Plans for Fourth Six Months

1. For the two cases identified for life calculation, determine the transient stress field due to the shock excitation from the bird strike lasting few milliseconds.
2. Perform FFT for both the cases and determine the excitation harmonics.
3. Determine the possibility of macro or micro friction damping at the two speeds corresponding to the two cases besides the hysteresis damping.
4. Use the nonlinear damping model with an iteration procedure to obtain the alternating stress field.
5. Estimate the fatigue strength reduction in both the cases.
6. Develop the basics of crack propagation with the element developed before and the code that is to be amalgamated with TurboManager

11. Acknowledgements

The team expresses its gratitude to The Szewalski Institute of Fluid Flow Machinery, Gdansk, Poland, Air Force Institute of Technology, Warsaw, Poland, K L University, Green Fields, Vaddeswaram, India, National Ukrainian Academy of Sciences, Ukraine and Altair Engineering India for their cooperation in carrying out this work. The team is also grateful to European Office of US Aerospace: Research and Development for providing this grant.

12. List of Symbols

b	Fatigue strength exponent
C	Damping coefficient
D	Loss of Energy per cycle
D_0	Total damping energy
E	Young's modulus
F	Factor
$H(\omega)$	Dynamic magnifier
J	Lazan's law coefficient
K	Modal stiffness
K_t	Fatigue stress concentration factor
m	Modal mass
n	Strength exponent and Lazan's law exponent
p	Natural frequency
Q	Quality factor
r	Frequency ratio
S_e	Fatigue strength of the material
W_0	Total strain energy
α	Angular acceleration
ε	Strain
η	Loss Factor
ΔS	Nominal stress range
$\Delta\sigma$	True stress range
σ_e	Endurance limit
σ_m	Mean stress
σ_u	Ultimate tensile strength
σ_r	Resonant stress
σ_f'	Fatigue strength coefficient
ξ	Equivalent viscous damping ratio
ω	Operational speed

List of Figures

List of Tables

References

1. R. Rzadkowski, J.S. Rao and Yu.S. Vorobiev, Crack Propagation in Compressor Rotor Blade, (Grant FA8655-10-1-3062), Report for First Six Months, April – September 2010
2. R. Rzadkowski, J.S. Rao and Yu.S. Vorobiev, Crack Propagation in Compressor Rotor Blade, (Grant FA8655-10-1-3062), Report for Second Six Months, October 2010 – March 2011

Annexure 1
Plan of Work

First year

1. Model and perform Modal stress analysis of one compressor rotor blade of SO-3 to find the possible crack initiation locations.

2. Modelling of different crack depths using a three-dimensional finite element model with the 3D prismatic quarter point Isoparametric elements of Vorobiev et al. (2004) and 20 noded Isoparametric elements.

3. Calculating natural frequencies of blades for different crack lengths.

4. Calculation of unsteady pressures acting on compressor rotor blade in a stage – using transient analysis in Fluent.

5. Determine material and friction damping values as a function of strain amplitude in each mode of vibration interest using process driven approach codes developed on HyperWorks platform.

Actual Work done as against the Plan: There were some deviations from the above as given below.

In the first six months report (*April-September 2010*) *modal stress analysis was carried out on one compressor rotor blade of an SO-3 engine to locate the possible crack initiations. Various crack depths and lengths were created using a three-dimensional finite element model with the 3D prismatic quarter-point isoparametric elements and 20-node isoparametric elements to calculate the natural frequencies and mode shapes of the rotor blades.*

In the second six months report (October 2010 - March 2011), the methodology to analytically determine a nonlinear damping model as a function of strain amplitude at a reference point in a given mode of vibration at a given speed of rotation of bladed-disk is described. Both material and friction damping are included. The friction damping is considered for both macro (Coulomb) and micro (fretting) slip conditions. For the blade under consideration, these damping values are determined and presented. The damping estimation process is developed on HyperWorks platform by calling suitable solvers for determining the mode shapes. The pre-processing is done by using HyperMesh and post-processing is carried out by using HyperView.

Item 4: The CFD analysis was initiated but could be finished only in the current third six months period

Second year

7. Determine resonant stresses at critical speeds.

8. Stress Intensity Factor approach will be used for fatigue crack initiation studies.

9. Stress Intensity Factor approach will be used for fatigue crack propagation studies with the help of Paris law.

10. Determine crack propagation using finite element model under the alternating stress

11. Compare Paris values, FE model values and experiments

Crack Propagation in Compressor Rotor Blade

(Grant FA8655-10-1-3062)

Report for Fourth Six Months

Oktober 2011 – June 2012

R. Rzadkowski[1] J.S. Rao[2],

[1]The Szewalski Institute of Fluid Flow Machinery, Gdansk, Poland

[2]K L University, Green Fields, Vaddeswaram, India

Submitted to
European Office of Aerospace:
Research and Development
86 Blenheim Crescent
Ruislip, Middlesex HA4 7HB
United Kingdom

June, 2012

Investigators

1. Principal Investigator: Professor Romuald Rzadkowski
The Szewalski Institute of Fluid Flow Machinery,
Fiszera 14, 80-952 Gdansk, Poland
Tel: +48502975518
E-mail: z3@imp.gda.pl

2. Senior Investigator and Mentor: Prof. J.S Rao
Protem Chancellor
K L University, Green Fields
Vaddeswaram, India 522502
Tel: +91 98453 46503
E-mail: jsrao@kluniversity.in

5. Investigator: Dr Marcin Drewczyński
Assistant Professor
The Szewalski Institute of Fluid Flow Machinery,
Fiszera 14, 80-952 Gdansk, Poland
E-mail: mdrew@imp.gda.pl

6. Investigator: Prof. Ryszard Szczepanik
Assistant Professor
Air Force Institute of Technology
01-494 Warszawa, Poland
E-mail: ryszard.szczepanik@itwl.pl

7. Investigator: Mr. Narayan Rangarajan
Lead Engineer, Altair Engineering (India)
Tel: +91 80 6629 4500/ 4700 (Fax)
E-mail: narayan.rangarajan@altair.com

8. Investigator: Mr. Rejin Ratnakar
General Motors (India) Bangalore
Tel: +91 99860 15670
E-mail: rejin.ratnakar@gm.com

Table of Contents

Summary

In the first six-month report (*April-September 2010*) *modal stress analysis was carried out on one compressor rotor blade of a jet engine to locate possible crack initiations. Various crack depths and lengths were created using a three-dimensional finite element model with 3D prismatic quarter-point isoparametric elements and 20-node isoparametric elements to calculate the natural frequencies and mode shapes of the rotor blades.*

Described in the second six-month report (October 2010 - March 2011) is the methodology of analytically determining a nonlinear damping model as a function of strain amplitude at a reference point in a given mode of vibration and speed of rotation of bladed-disk. Both material and friction damping were included. Friction damping was considered for both macro (Coulomb) and micro (fretting) slip conditions and these damping values were determined and presented for the blade under consideration,. The damping estimation process was developed on a HyperWorks platform by applying suitable solvers to determine the mode shapes. HyperMesh was used for the pre-processing and HyperView for the post-processing.

In the third six months 2012April – September 2011, the excitation pressure field due to a bird strike was simulated using CFD and unsteady pressure field was determined on the rotor blade pressure and suction surfaces. A bird strike was simulated by two or three blade passage blocks in the incoming flow and the pressure field was obtained from a CFD code. A Campbell diagram was prepared for the blade to identify the critical speeds. The alternating pressures corresponding to the critical speed were obtained from an FFT. A nonlinear damping model was estimated using Lazan's hysteresis law and a previously developed model; the equivalent viscous damping model was determined as a function of reference strain amplitude in the given mode of vibration of a given rotational speed. An iterative solution was developed with the nonlinear damping model and the resonant stress and location were determined for 8EO excitation. The life at this critical speed, 8EO, was determined using a cumulative damage criterion.

In a subsequent eight-month report, October 2011 – June 2012:

1. The material rotor blades data was verified in experiments carried out at the Air Force Institute of Technology in Warsaw.
2. For 2EO and unsteady forces the transient stress field due to the shock excitation from the bird were calculated for four and five block segments.
3. The life at this critical speed, 2EO, was determined using a cumulative damage criterion and a comparison with the experiment was presented.
4. Crack propagation analysis was performed.
5. The Stress Intensity Factor approach was applied for fatigue crack propagation studies with the help of the Paris law and compared with experiments.
6. Crack propagation was determined using a finite element model with singular elements under alternating stress and compared with the experiment results.

1. Introduction

In determining of the life of a turbomachine blade it is essential to accurately assess the unsteady forces and damping that affect the peak stress and strain levels at a critical speed when the engine is started or shut down. Previous reports [1,2,3] discussed and presented the procedures used in developing a nonlinear model for damping dependent on strain in the rotating blade for a given mode of vibration at an operating speed or critical speed.

In this fourth report the material rotor blades data was verified in experiments carried out at the Air Force Institute of Technology in Warsaw. The transient stress field resulting from a bird strike was calculated for 2EO excitation and the first blade mode shape. Nonlinear damping was modelled as an equivalent of viscous damping for the first natural frequencies [3].

This resonant stress together with the mean stress allowed for an accurate determination of damage incurred by a blade while crossing a critical speed. The expected blade life for 2EO was determined using a cumulative damage criterion. A comparison with the experiment was made. The crack propagation analysis was carried out and also compared with the experiment.

2. Numerical and experimental results for rotor blade dynamic

The material rotor blade data obtained experimentally are : σ_u = 1100 MPa, σ_{yiel} =800 MPa, σ_e = 630 MPa [4].

The endurance limit of the material was updated for K_t = 2.1. The fatigue reduction factor was estimated to be 0.476.

The modified endurance limit for the blade was then estimated to be 300 MPa.

The CAD model of the blade for structural analysis is shown in Fig. 1. The natural frequencies calculated numerically and measured at various speeds at the Air Force Institute of Technology [4] are presented in Table 1. The Campbell diagram of the rotor blade is shown in Fig. 2.

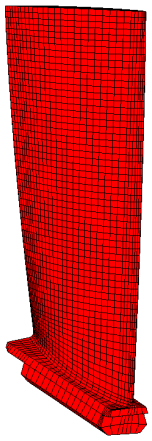

Fig. 1 CAD model of rotor blade

Table 1 Natural frequencies of rotor blades in Hz

	Numerical calculations $n = 0$	Experimental data $n = 0$	Numerical calculations $n = 15\,000$ rpm
	f [Hz]	f [Hz]	f [Hz]
1	337,13	<318 - 385>	501,84
2	1338,9	<1312 - 1408>	1535,3
3	1835,0	<1840 - 1920>	1892,0
4	3170,7	-	3264,4
5	4074,6	<3712 - 3956>	4282,0
6	4688,0	<4544 - 4744>	4784,7
7	7509,2	<7440 - 7616>	7688,3
8	8093,9	-	8298,0
9	10520,0	-	10550,0
10	11470,0	-	11640,0

From the Campbell diagram of the first stage compressor rotor blade (Fig. 2) one can see that 2EO excitation at 15000 rpm can cause blade resonance stress, particularly with a bird strike, modelled here as a partial blocking of the engine inlet [4].

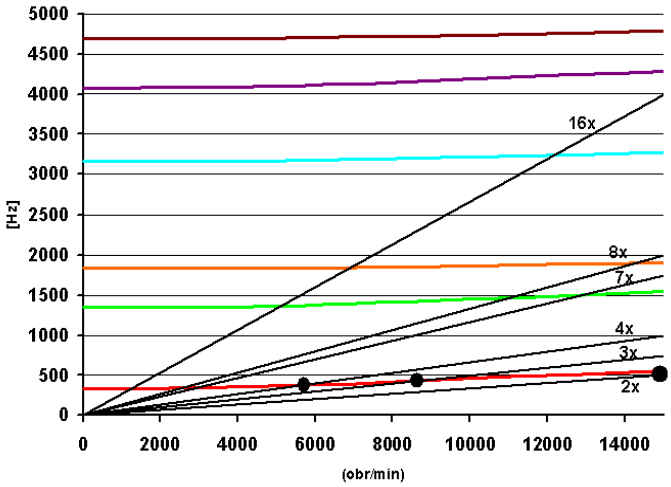

Fig. 2 Campbell diagram for first compressor stage of a jet engine

3. Unsteady forces - one to five block segments

In the experiment the jet engine inlet was blocked by one to five block segments (see Fig.3a).

The blocks simulated a bird strike. The number of blocks corresponded to the size of the bird. One to five blocks ([3], [5]) produced resonance at 15000 rpm in the 1st mode natural frequency. The unsteady amplitude at 500 Hz along the blade length for one block segment is presented in Tab. 2a, two block segment (Tab 2b), two block segments in opposite direction (see Fig. 3b) (Tab. 2c), tree block segments (Tab.2d), four block segments (Tab. 2e) and five block segments (Tab. 2f).

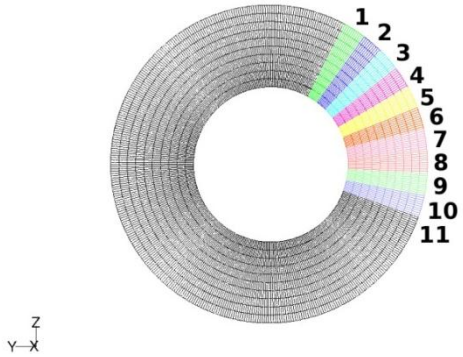

Fig. 3a View of inlet segments

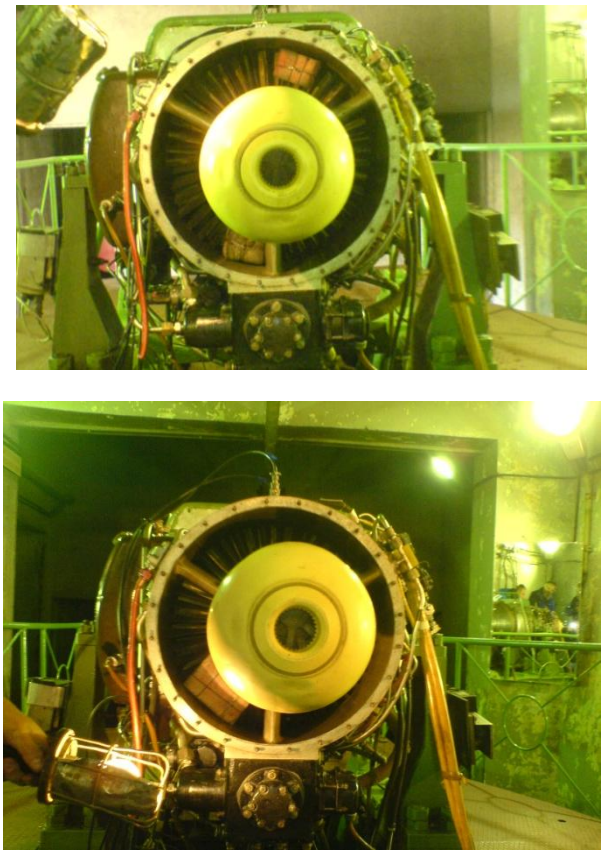

Fig. 3b Block segments in inlet of jet engine

Tab. 2a. Unsteady forces (One Block segment [3], [5]) at 500 Hz acting on rotor blades.

Cross-section	F_x	F_y
	[N]	[N]
1	0,05221	0,11822
2	0,04979	0,09890
3	0,05204	0,09328
4	0,05341	0,08622
5	0,05429	0,07809
6	0,05625	0,07064
7	0,05915	0,06337
8	0,06382	0,05788
9	0,07051	0,05459
10	0,07785	0,05235

Tab. 2b. Unsteady forces (Two Block segment [3], [5]) at 500 Hz acting on rotor blades

Cross-section	F_x	F_y
-	[N]	[N]
1	0,2126	0,4214
2	0,1955	0,3545
3	0,2045	0,3417
4	0,214	0,3272
5	0,2268	0,3209
6	0,2386	0,3214
7	0,2415	0,3058
8	0,2227	0,2606
9	0,224	0,2323
10	0,2357	0,2119

Tab. 2c. Unsteady forces (Two Block segments in opposite direction [3], [5]) at 500 Hz acting on rotor blades

Cross-section	F_x	F_y
-	[N]	[N]
1	0,5683	1,084
2	0,5133	0,8921
3	0,5383	0,8633
4	0,5761	0,8664
5	0,6195	0,8787
6	0,6516	0,8703
7	0,7117	0,9094
8	0,7865	0,9745
9	0,6713	0,8194
10	0,2448	0,3243

Tab. 2d. Unsteady forces (Three Block segment [3], [5]) at 500 Hz acting on rotor blades

Cross-section	F_x	F_y
-	[N]	[N]
1	0,3585	0,8675
2	0,3259	0,7266
3	0,3509	0,721
4	0,3729	0,7029
5	0,372	0,6341
6	0,3596	0,5497
7	0,3585	0,496
8	0,3614	0,4506
9	0,3781	0,4067
10	0,4232	0,3771

Tab. 2e. Unsteady forces (Four Block segment [3], [5]) at 500 Hz acting on rotor blades.

Cross-section	F_x	F_y
-	[N]	[N]
1	0,6006	1,371
2	0,5656	1,302
3	0,5692	1,258
4	0,5228	1,126
5	0,4565	0,944
6	0,4426	0,831
7	0,4318	0,676
8	0,3405	0,440
9	0,0571	0,0283
10	0,4024	0,2913

Tab. 2f. Unsteady forces (Five Block segment [3], [5]) at 500 Hz acting on rotor blades.

Cross-section	F_x	F_y
-	[N]	[N]
1	0,6809	2,2532
2	0,566	1,9475
3	0,4508	1,5147
4	0,3446	1,1499
5	0,2788	0,9324
6	0,3172	0,8339
7	0,429	0,8237
8	0,452	0,7025
9	0,936	0,908
10	1,340	1,169

4. Material (Hysteresis) Damping

The nonlinear model developed gives equivalent viscous damping ratio as a function of reference strain amplitude in a chosen mode of vibration at a given speed of rotation.

A plot of equivalent viscous damping ratio as a function of reference strain amplitude in a chosen mode of vibration defined the nonlinear damping model.

Hysteresis damping [10] was determined for the first mode of vibration (Fig. 5). The chosen reference element ID is 13555, as shown in Fig. 4. The material properties in Lazan's law are taken as $J = 16$, $n = 2.3$

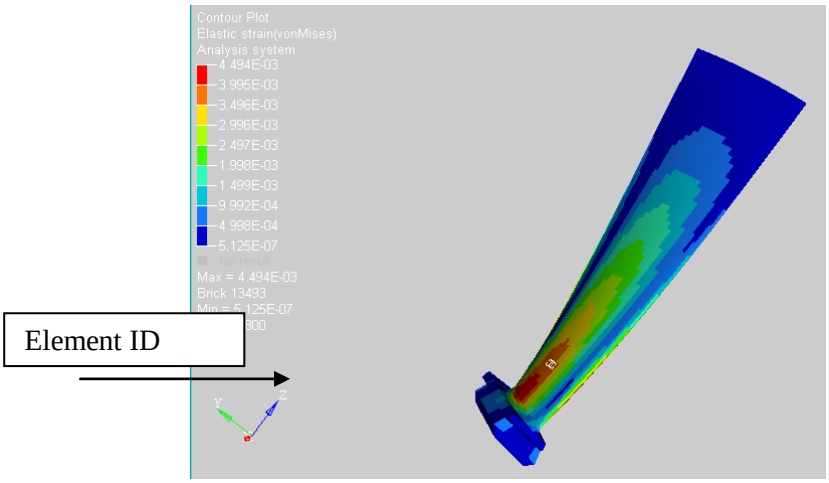

Fig. 4 Reference element of rotor blade

This damping model is used in evaluating the resonant stress in a life estimate.

The Coulomb friction damping and fretting damping were neglected here because of the very high speed of operation.

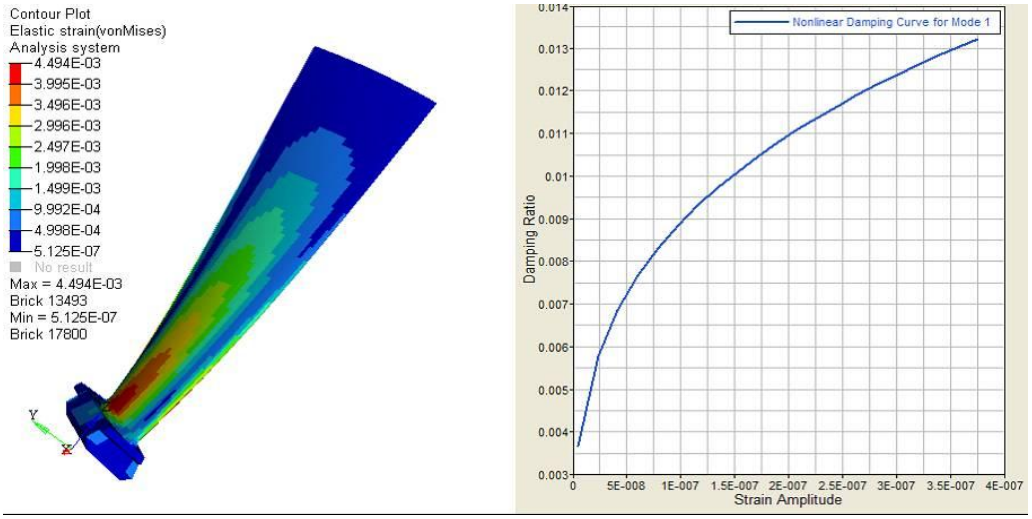

Fig. 5 Nonlinear damping in the first mode of the blade

5. Mean Stress on the Blade

The material Young's modulus *E* was taken as 204000 MPa. At an operating speed of 15000 rpm the peak value of mean stress was 268.7 MPa, see Fig. 6. The mean stress and alternating stress peak occurred at the same location.

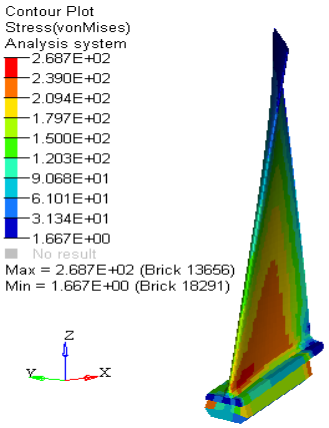

Fig. 6 Mean stress of rotor blade at operating speed

6. Alternating Stress

In order to estimate the alternating stress, the forces acting on the blade were taken from Tables 2a-2f [3]. The resonant stress was then determined by multiplying the average stress by the quality factor $\frac{1}{2\xi}$ [3].

For one block segment the iterated damping ratio was 0.0049 with the maximum alternating stress = 46.7 MPa.

For two block segments the iterated damping ratio was 0.0069 with the maximum alternating stress = 129.6 MPa.

For two block segments in opposite direction in the engine inlet the iterated damping ratio was 0.0087 with the maximum alternating stress = 292.5 MPa.

For three block segments the iterated damping ratio was 0.00754 with the maximum alternating stress = 183.1 MPa.

For four block segments the iterated Damping ratio was 0.0097 with the maximum alternating stress = 342 MPa. The peak alternating stress occurred at element 13893 as shown in Fig. 7. A zoomed view of this stress is shown in Fig. 8.

For five block segments the iterated Damping ratio was 0.00913 with the maximum alternating stress = 337.2 MPa.

The damping ratio obtained from the non-rotating single blade experiment at the Air Force Institute of Technology was in the region of 0.0065-0.0075 [4].

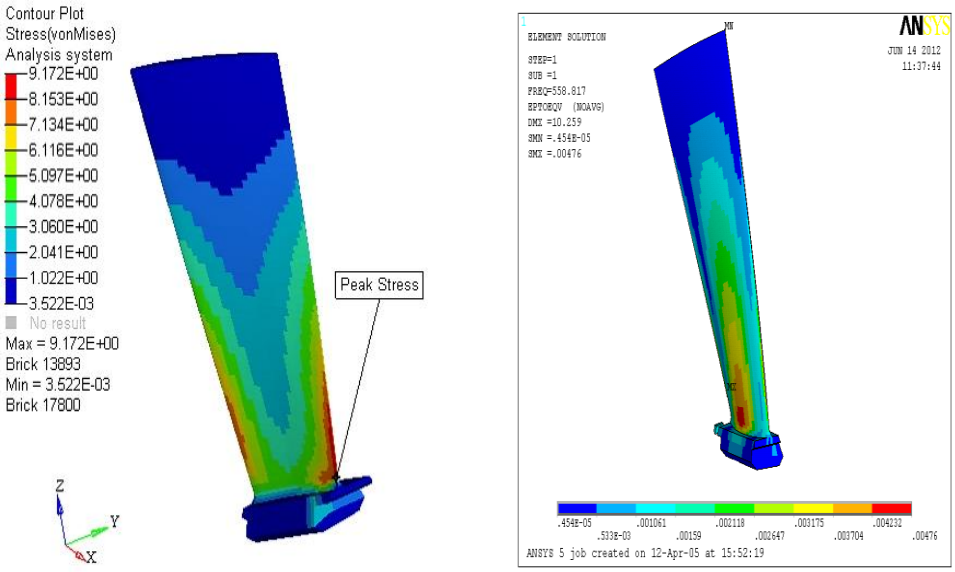

Fig. 7 Resonant stress location in the rotor blade

7. Fatigue calculation of the Blade

The endurance limit of the material was updated to take into account various factors. The following fatigue material data was assumed:

$$\sigma_u = 1100 \text{ MPa}$$

$$\sigma_e = 630 \text{ MPa}$$

$$K_t = 2.1$$

The fatigue reduction factor was estimated to be 0.476. The size effect was not taken into account because the endurance limit was taken from the real blade experiment.

The thus modified endurance limit was 300 MPa.

8. Life

The strain based life estimation was not attempted as the alternating stress magnitude range was elastic.

Usually we can calculate the damage suffered by a blade while crossing the critical speed by using either a linear Palmgren-Miner damage rule or a nonlinear Marco-Starkey rule (or any other rule for which material data may be available) [11]. Here, although the unsteady pressure suffered by the blade was due to a bird strike which lasted a short period of time, the blade suffered a transient impact response at resonance which lasted longer. Therefore a continuous response was assumed to estimate life.

With 4 or 5 block segments (342 MPa), the estimated Life at 15000 RPM was 1.37 min and with three block segments (181 MPa) it was 182 min using Goodman theory [7]:

$$\sigma_a = \sigma_e^{'}(1 - \frac{\sigma_m}{K_t \sigma_u})$$

In the real engine experiment [4] the total time for crack initiations was 124.4 min [4]. From one to five blocks were used. At 15000 rpm the engine inlet was blocked with: 4 block segments for 5.91

min, three block segments for 99.9 min, five block segment for 12.94 min, one block segment for 18 min and two block segments for 5.69min.

In previous report [3], it was reported that any of the blockages produced the transient load to exist for about 2 seconds and then died out. The response due to this sudden loads lasts longer, particularly with low damping. Therefore irrespective of time taken to block the inlets in the experiment as achieved, the response due to individual blockages can be expected to last for about a minute.

In analytical calculations, the estimated life for severe loading is 1.37 minutes. Other lesser load cases provide longer life. In tests too, it is the 4 block segment closure case for 5.91 minutes is the one that will be mainly responsible for the damage, the remaining becoming of less significance. Though 4 block segment closure is for 5.91 minutes, its transient influence will be only for about 2 seconds, which becomes almost steady after the transient period. Thus we can explain the failure in the test of 124.4 minutes.

9. Crack propagation

In the experiment the inlet was blocked with two block segments (129.6 MPa) for 55.7 min to obtain a 5-7 mm crack. Next the block segments were removed (35 MPa) but crack propagation continued for 17,91 min to reach 9-10 mm [4].

Crack propagation was simulated for semi - elliptical crack at the location shown in Fig. 8, with initial crack length: 0.015 mm**.**

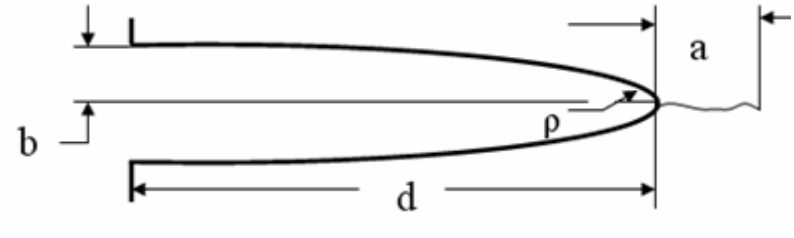

Fig 8. Semi elliptical notch geometry

In the blade model the peak stress region is considered as semi elliptical notch with dimensions as shown below

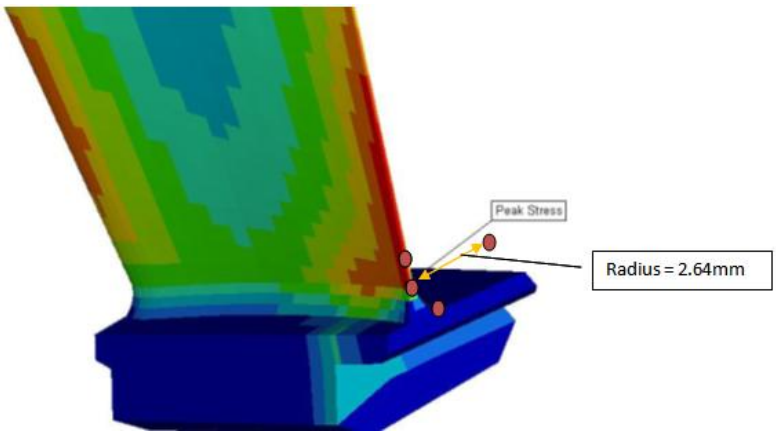

Fig 9. Notch considered in blade model

The methodology followed to calculate the crack propagation is explained below

9.1. Stress range and Stress Intensity Factor range conversion

To determine the stress intensity factor from nominal stress values, the notch geometry is modelled, say by a semi elliptical (b and a_N) notch as shown in Fig. 10. Δa_f is starting crack length, assumed generally as the least count of crack detection machine and a_T is the location of the crack tip, ρ is the radius at the notch [7].

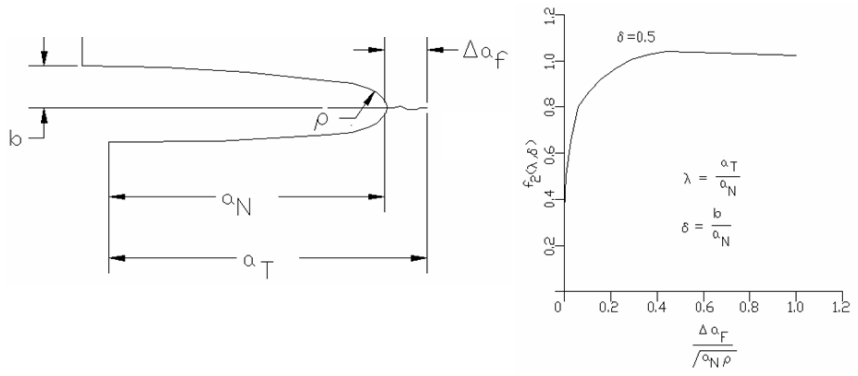

a/b	*k*
0.1	1.03
0.2	1.07
0.3	1.15
0.4	1.22
0.5	1.35
0.6	1.5
0.7	1.69
0.8	1.91
0.9	2.2
1	2.55

Fig. 10 Semi-elliptical notch model [7]

Conversion between stress intensity factor range ΔK and nominal stress range $\Delta\sigma$ is given by ([7] p.282)

$$\Delta K = 1.12\Delta\sigma\sqrt{\pi a_T}\,k\left(\frac{a}{b}\right)f_2(\lambda,\delta)$$

where $f_2(\lambda,\delta)$ and $k(a/b)$ are given in Fig. 10.

The critical crack length is calculated as [7]

$$a_{cr} = \frac{1}{\pi}\left(K_{1c}/\{1.12\sigma_{\max}k\left(\frac{a}{b}\right)f_2(\lambda,\delta)\}\right)^2$$

For a center-cracked panel (Fig. 11-13), conversion between stress intensity factor range ΔK and nominal stress range $\Delta\sigma$ is given by ([8] p. 249)

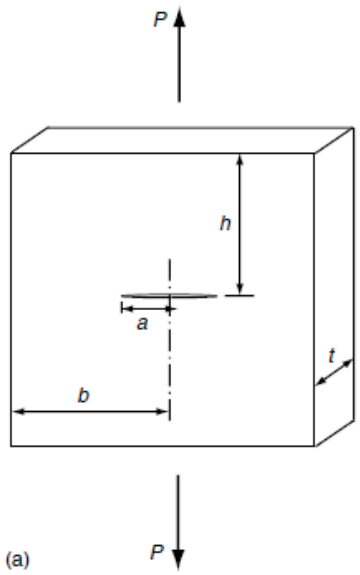

Fig. 11. Center crack plate with finite width

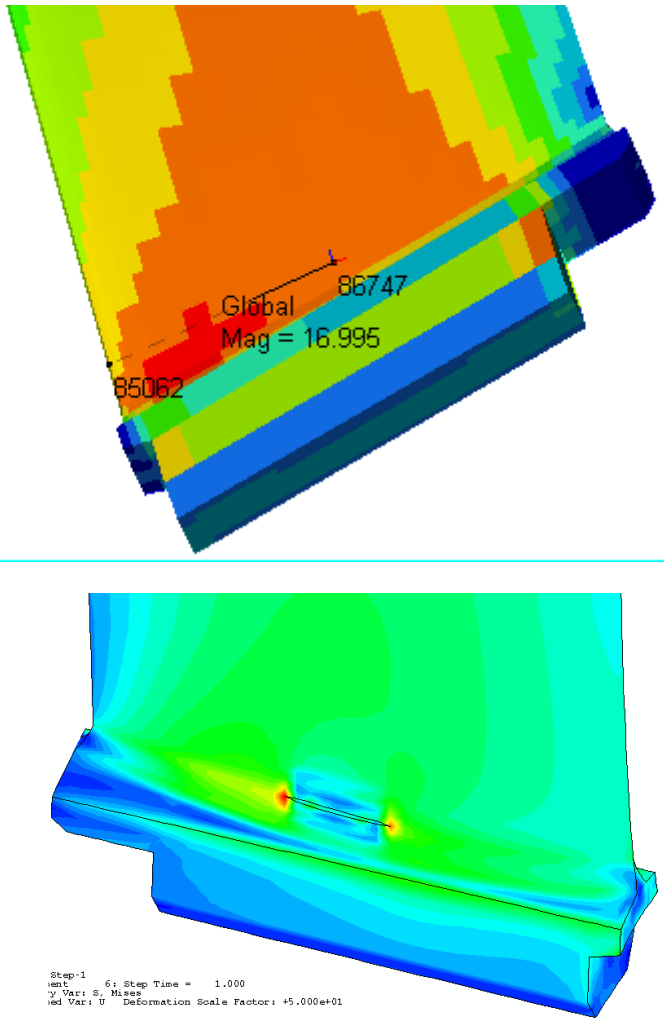

Fig. 12. Center crack in rotor blade

Induced crack areas on the blade cross-section where Peak Stress Occurs

Fig. 13. Center crack in rotor blade-cross-section

$$\Delta K = F(\alpha)\Delta\sigma\sqrt{\pi a}$$

Where $F($ is a geometric function of the normalized crack length **a**. Here, $= a/b$, where b represents the width of the panel [8] (p. 249).

$$F(\alpha) = \frac{1 - 0.5\alpha + 0.326\alpha^2}{\sqrt{1-\alpha}} \text{ for } h/b \geq 1.5$$

Critical crack length is calculated as

$$a_{cr} = \frac{1}{\pi}\left(\frac{\Delta K}{\sigma_{\max} F(\alpha)}\right)^2$$

9.2 Unstable crack length and Crack propagation life

A crack initiated propagates when the stress range exceeds the threshold value given above following Paris law, e.g., for 18H2N4 steels [7]

$$\frac{da}{dN} = C(\Delta K)^m \text{ microns/cy cle}$$

where C = 4.88 x10^{-6} and m=3.2 Paris material constants [9].

Until the stress intensity factor range becomes equal to fracture toughness of the material when it becomes unstable according to Griffith's law.

9.3 Crack propagation Life calculations:

For the initial crack length (semi elliptic crack) Δa_f= 0.015 mm, the notch radius ρ= 2.64 mm measured from model shown in Fig 10. In considered notch geometry *a/b* is taken as 0.5, *K(a/b)* = 1.35 and $f_2(\lambda,\delta)$ = 0.5 from Fig 10. The mean stress is 268 MPa and amplitude of alternating is 129.6 MPa

Life estimation with crack propagation to 1cm at 15000 RPM and a 2EO equalled 111514 cycles.

Thus life for 501.84 Hz : 111514 / (501.84) = 222.32 sec =3.705 min.

For the elliptical crack shown in Figs. 11-13, life estimation was calculated as follows: crack length was 0.19 mm**,** in the blade model *b*= 17 mm, therefore *α= a/b = 0.*19/17 = .01117**,** and *F(α)* = 1.000056.

When $\Delta\sigma = 129.6 \times 2 = 259.2$ MPa and the mean stress is 268 MPa, the estimated life with crack propagation to 5.19 mm at 15000 RPM and 2 EO = 584624 cycles

Thus life for 501.84 Hz : 584624/ (501.84) = 1164.96 sec =19.41 min.

This numerical result is not satisfactory because in experiment crack propagation lasted 55.7 min.

10. Stress in the blade for FE modelled crack

A crack with a length of (2 x 5.8 mm) and a depth of 2,1 mm was modelled using singular elements - [1] near the crack and 20-node isoparametric elements in the remaining area (Fig. 14, 15, 16). The maximum stress calculated numerically in the tip of the crack caused by two block segments in the engine inlet was 166 MPa.

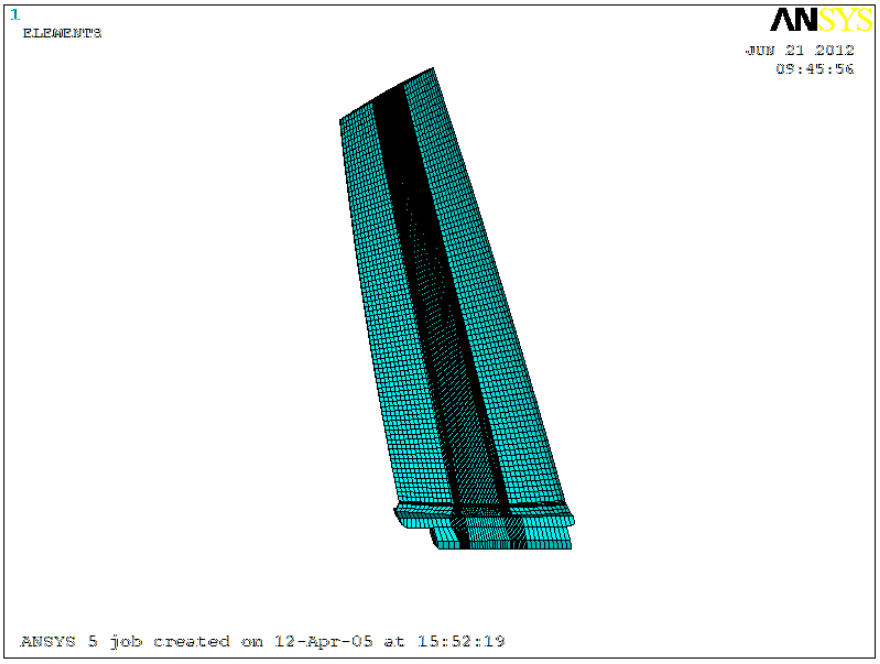

Fig. 14 FE mesh of rotor blade using singular elements in crack area

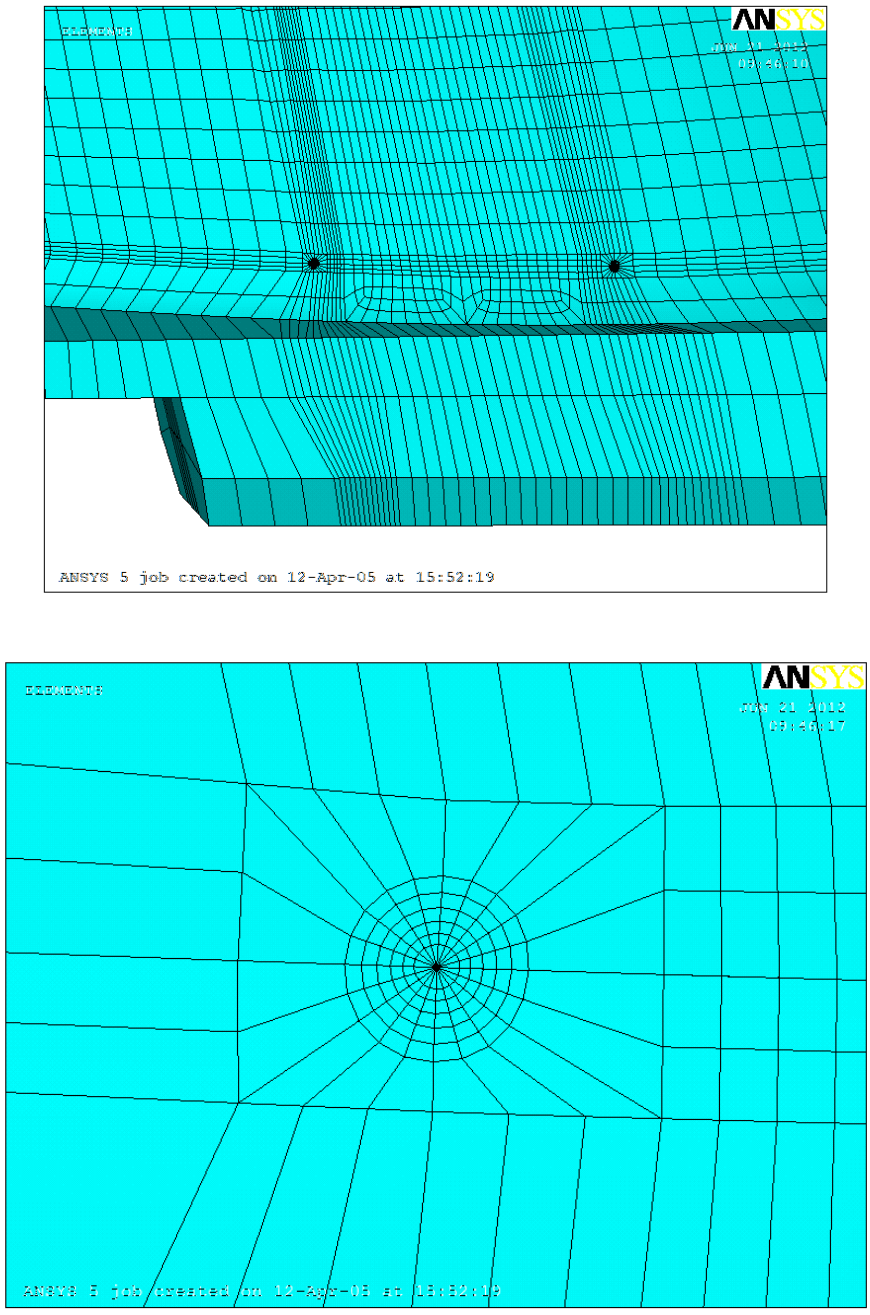

Fig. 15 FE mesh of rotor blade using singular elements in crack area -

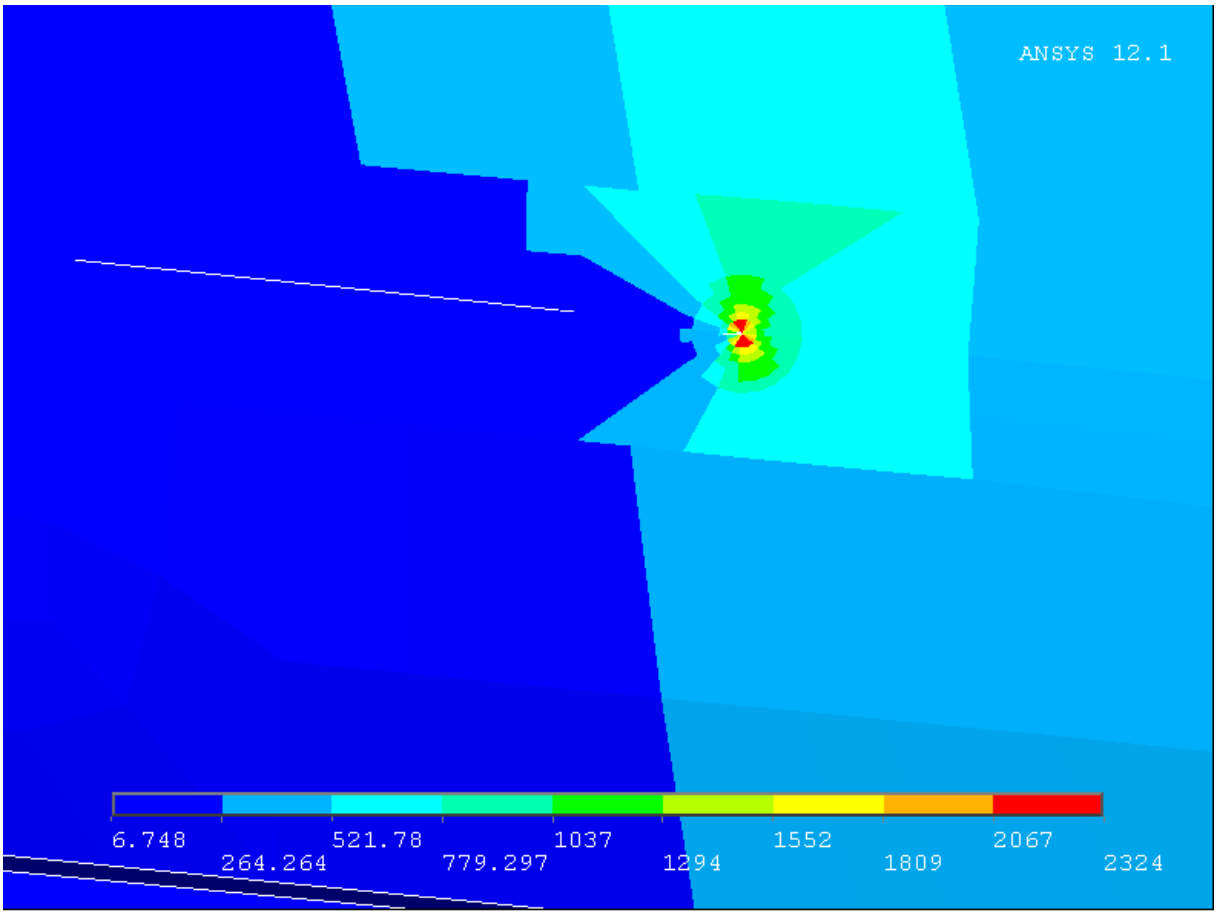

Fig. 16 Resonance stress in the crack area

When $\Delta\sigma = 166*2 = 332$ MPa and the mean stress was 268 MPa, the life estimation with crack propagation up to 5.19 mm, at 15000 RPM in 2X harmonic = 264769.7 cycles

Thus life for 501.84 Hz: 264769.7/ (501.84) = 527.5 sec =8.79 min

Therefore the time of crack propagation decreased in comparison to the 20-node isoparametric element (129.6 MPa and 19.41 min), but in the experiment it lasted 55.7 min.

11. Conclusion

The blade material data was verified experimentally. Several excitation harmonics of unsteady forces acting on a rotor blade (blocked by one to five block segments) were found using the FFT. A nonlinear damping model with an iteration procedure to obtain the alternating stress field was used in five cases.

The life estimation up to crack initiation was calculated numerically and compared with the experiment. The results obtained from numerical analysis were shorter than the experimental ones.

The crack propagation was carried our using Paris law. The crack propagation was shorter in the case of numerical results. Next stress in the blade with a crack was calculated using singular elements. The crack propagation was calculated and the time was shorter than in the case of the FE model blade without a crack.

The general conclusion is that the blade life estimation procedure used here for the initiation and propagation of a crack does not correspond well with experimental results.

A future model should take into account the length and depth of crack propagation.

Therefore a FE model must be used from very beginning and singular elements, instead of stress intensity formulas, should be used to represent crack propagation. Moreover, Paris coefficients C and n should be first verified experimentally.

12. Acknowledgements

The team expresses its gratitude to The Szewalski Institute of Fluid Flow Machinery, Gdansk, Poland, Air Force Institute of Technology, Warsaw, Poland, K L University, Green Fields, Vaddeswaram, India and Altair Engineering India for their cooperation in carrying out this work. The team is also grateful to European Office of US Aerospace: Research and Development for providing this grant.

13. List of Symbols

b	Fatigue strength exponent
C	Damping coefficient
D	Loss of Energy per cycle
D_0	Total damping energy
E	Young's modulus
F	Factor
$H(\omega)$	Dynamic magnifier
J	Lazan's law coefficient
K	Modal stiffness
K_t	Fatigue stress concentration factor
m	Modal mass
n	Strength exponent and Lazan's law exponent
p	Natural frequency
Q	Quality factor
r	Frequency ratio
S_e	Fatigue strength of the material
W_0	Total strain energy
α	Angular acceleration
ε	Strain
η	Loss Factor
ΔS	Nominal stress range
$\Delta\sigma$	True stress range

σ_e	Endurance limit
σ_m	Mean stress
σ_u	Ultimate tensile strength
σ_r	Resonant stress
σ_f'	Fatigue strength coefficient
ξ	Equivalent viscous damping ratio
ω	Operational speed

List of Figures

List of Tables

References

1. R. Rzadkowski, J.S. Rao and Yu.S. Vorobiev, Crack Propagation in Compressor Rotor Blade, (Grant FA8655-10-1-3062), Report for First Six Months, April – September 2010
2. R. Rzadkowski, J.S. Rao and Yu.S. Vorobiev, Crack Propagation in Compressor Rotor Blade, (Grant FA8655-10-1-3062), Report for Second Six Months, October 2010 – March 2011,
3. R. Rzadkowski, J.S. Rao, Crack Propagation in Compressor Rotor Blade, (Grant FA8655-10-1-3062), Report for Second Six Months, April 2011 – September 2011
4. Szczepanik R., Rzadkowski R., Dynamic Analysis of rotor blades of a jet engine in different operating conditions, PIB Radom 2012, (in Polish)
5. Rządkowski R., Soliński M., Szczepanik R.: The Unsteady Low-Frequency Aerodynamic Forces Acting on the Rotor Blade in the First Stage of an Jet Engine Axial Compressor, Advances in Vibration Engineering, 11(2), 171-183, 2012.
6. Szczepanik R., Rządkowski R., Kwapisz L.: Crack Initiation of Rotor Blades in the First Stage of SO-3 Compressor, Advances in Vibration Engineering, 9(4), 357-362, 2010.

7. Rao J.S. Turbine Blade Life Estimation, Narosa 2000.
8. Lee Y., Pan J., Hathaway R., Barkey M.: Fatigue Testing and Analysis (Theory and Practice), Elsevire 2005
9. Kłysz S., Estimation of life of aircraft materials and elements in the region of crack initiations and propagation, Report of Air Force Institute of Technology , No. 5, 1999 (in Polish).
10. Rao, J. S., Rejin Ratnakar, Suresh, S and Narayan, R., A Procedure to Predict Influence of Acceleration and Damping of Blades Passing Through Critical Speeds on Fatigue Life, Proceedings of ASME Turbo Expo 2009: Power for Land, Sea and Air, GT2009-59433 June 8-12, 2009, Orlando, Florida, USA,
11. Rao, J. S., Pathak, A and Chawla, A., Blade Life - A Comparison by Cumulative Damage Theories, Journal of Engineering for Gas Turbines and Power, vol. 123, No. 4, 2001, p. 886

Annexure 1

Plan of Work

First year

1. Model and perform Modal stress analysis of one compressor rotor blade of SO-3 to find the possible crack initiation locations.

2. Modelling of different crack depths using a three-dimensional finite element model with the 3D prismatic quarter point Isoparametric elements of Vorobiev et al. (2004) and 20 noded Isoparametric elements.

3. Calculating natural frequencies of blades for different crack lengths.

4. Calculation of unsteady pressures acting on compressor rotor blade in a stage – using transient analysis in Fluent.

5. Determine material and friction damping values as a function of strain amplitude in each mode of vibration interest using process driven approach codes developed on HyperWorks platform.

Actual Work done as against the Plan: There were some deviations from the above as given below.

In the first six months report (*April-September 2010*) *modal stress analysis was carried out on one compressor rotor blade of an SO-3 engine to locate the possible crack initiations. Various crack depths and lengths were created using a three-dimensional finite element model with the 3D prismatic quarter-point isoparametric elements and 20-node isoparametric elements to calculate the natural frequencies and mode shapes of the rotor blades.*

In the second six months report (October 2010 - March 2011), the methodology to analytically determine a nonlinear damping model as a function of strain amplitude at a reference point in a given mode of vibration at a given speed of rotation of bladed-disk is described. Both material and friction damping are included. The friction damping is considered for both macro (Coulomb) and micro (fretting) slip conditions. For the blade under consideration, these damping values are determined and presented. The damping estimation process is developed on HyperWorks platform by calling suitable solvers for determining the mode shapes. The pre-processing is done by using HyperMesh and post-processing is carried out by using HyperView.

Item 4: The CFD analysis was initiated but could be finished only in the current third six months period

Second year

7. Determine resonant stresses at critical speeds.

8. Life were calculated to crack imitations using Goodman theory and Wohler diagram.

9. Stress Intensity Factor approach will be used for fatigue crack propagation studies with the help of Paris law.

10. Determine crack propagation using finite element model under the alternating stress

11. Compare Paris values, FE model values and experiments